THESIS FOR THE DEGREE OF DOCTOR OF PHILOSOPHY

The axisymmetric turbulent wake

Peter B V Johansson

Department of Thermo and Fluid Dynamics
CHALMERS UNIVERSITY OF TECHNOLOGY
Göteborg, Sweden, 2002

The axisymmetric turbulent wake

PETER B V JOHANSSON

ISBN 91-7291-178-6

Doktorsavhandling vid Chalmers tekniska högskola
Ny serie nr 1860
ISSN 0346-718X

Department of Thermo and Fluid Dynamics
Chalmers University of Technology
SE-412 96
Sweden
Telephone +46 31 7721000

Printed at Chalmers Reproservice
Göteborg, Sweden

This thesis is based on the following papers:

Paper 1

"On the effect of finite Reynolds number and initial conditions on the axisymmetric wake", P. B. V. Johansson and W. K. George. Published in "Proceedings of the Second International Symposium on Turbulence and Shear Flow Phenomena", volume I, pp. 323-328, Stockholm, Sweden, June 27-29, 2001.

Paper 2

"Proper orthogonal decomposition of an axisymmetric turbulent wake behind a disk", P. B. V. Johansson, W. K. George and S. H. Woodward. In press, Physics of Fluids, volume 14, number 6, 2002.

Paper 3

"Further studies of the axisymmetric disk wake using the 'slice POD'", P. B. V. Johansson and W. K. George. To be published in "Proceedings of the ASME Fluids Engineering Division Summer Meeting, FEDSM2002-31411", Montreal, Quebec, Canada, July 14-18, 2002.

Paper 4

"Far downstream development of POD modes in a turbulent disk wake", P. B. V. Johansson and W. K. George. To be published in "Advances in Turbulence IX, Proceedings of the Ninth European turbulence conference", I. P. Castro, P. E. Hancock & T. G. Thomas, editors, Southampton, UK, July 2-5, 2002.

(Continued on next page)

(Continued from previous page)

Paper 5

"Equilibrium similarity, effects of initial conditions and local Reynolds number on the axisymmetric wake", P. B. V. Johansson, W. K. George and M. J. Gourlay. Submitted to Physics of Fluids in revised form.

Paper 6

"How has the study of coherent structures contributed to our understanding of turbulence?", W. K. George, P. B. V. Johansson and S. Gamard. To be published in "Proceedings of the ASME Fluids Engineering Division Summer Meeting, FEDSM2002-31408", Montreal, Quebec, Canada, July 14-18, 2002.

Paper 7

"Another look at the Batchelor and Gill temporal stability analysis of parallel axisymmetric flows", S. Gamard, P. B. V. Johansson and W. K. George. Submitted to the Journal of Fluid Mechanics.

Paper 8

"The far downstream evolution of the high Reynolds number axisymmetric wake behind a disk. Part 1. Single point statistics", P. B. V. Johansson and W. K. George. Prepared for submission to the Journal of Fluid Mechanics.

Paper 9

"The far downstream evolution of the high Reynolds number axisymmetric wake behind a disk. Part 2. Slice POD", P. B. V. Johansson and W. K. George. Prepared for submission to the Journal of Fluid Mechanics.

Abstract

This thesis presents a theoretical and experimental study of the turbulent axisymmetric wake.

In the theoretical part, an equilibrium similarity solution of the far wake was derived that was found to admit to two different solutions for this flow. The high Reynolds number solution predicts that the flow grows as the cube root of the distance downstream, whereas the low Reynolds number solution grows as the square root of the downstream distance. None of these solutions had unambiguously been confirmed in earlier work. The analysis also provided necessary criteria for when to expect either solution.

In the experimental part, data was obtained by hot-wire anemometry using arrays of 13 and 15 probes. For the first time, experimental data was proven to behave like the high Reynolds number equilibrium similarity solution predicted. These multi-point probe rakes were also used to measure cross-spectra in cross-sections of the flow from 10 to 150 disk diameters downstream.

The cross-spectra obtained from the measurements were Fourier transformed in the azimuthal direction and used in the kernel for a proper orthogonal decomposition (POD). The POD was shown to order the energetic structure in a highly organized manner, with approximately 56% of the resolved energy in the first mode. The decomposition revealed that the initial wake region from 10 to 30 diameters downstream was dominated by an azimuthal mode-1 type of motion, but also that the importance of this mode vanishes as the flow evolves. Instead the far wake from 30 diameters downstream on was found to be dominated by a mode-2 type of azimuthal motion. This was found to coincide very well with the position at which the similarity solution became valid. This mode-2 dominance continued throughout the whole range of the investigation, with virtually no change in the modal decomposition. The mode-1 was interpreted as a convected structure associated to the vortex shedding in the near wake that was just swept by the probes and dies off downstream, and the mode-2 was postulated to be associated with a global instability manifested as a slow movement of the whole mean velocity field.

The findings of the experiment triggered new theoretical investigations, and a re-visit of the classical linear temporal stability analysis. It was found that the theory permits unstable solutions of mode-0, 1, and 2 kind, contrary to the previous view that only azimuthal mode-1 can be unstable.

Acknowledgements

First of all I would like to thank my supervisor Professor William K. George for keeping me busy these years. It has been very stimulating, challenging, rewarding, and lots of fun.

I would like to thank Professor Jean Paul Bonnet of Université de Poitiers, France, for serving as the opponent of my defense. Also, I would like to thank the grading committee, Professors Henrik Alfredson of KTH, Sweden, Jens Nørkjær Sørensen, DTU, Denmark, Dan Ewing, McMaster University, Canada, and Lars Larson, CTH, Sweden, for accepting the task.

I would also like to thank Professor Lennart Löfdahl, who with his enthusiasm inspired me to become a PhD student.

Thanks to Docent Gunnar Johansson for the aid throughout the entire period I have been at the department. Thanks also to Dr. Stephan Gamard and Dr. Martin Wosnik for the great company both at work and off duty.

Thanks also to Scott Woodward, whose help incredibly sped up the development of the experimental setup. To Lars Jernqvist for the help with everything, especially anything related to electronics and to Uno Hansson for the construction and manufacturing of all kinds of mechanical devices needed.

Thanks to the former head of the department, Jan Hansson, for supporting me from the start and promoting me to join committees of all sorts to broaden my view.

Financial support from the Department of Thermo and Fluid Dynamics and the Swedish Research Council (VR) is gratefully acknowledged.

Finally, I want to thank my family for the constant support and encouragement and all colleagues and friends at the Department of Thermo and Fluid Dynamics for providing a great atmosphere and making sure that it was never boring.

Contents

Chapter 1

Introduction

This is a thesis about turbulent flow and about the tools used to investigate it. Everyone encounters turbulence almost everywhere, even though most people are usually not aware of it. Turbulence is perhaps most widely known as the hands-on experience onboard an airplane when the plane all of a sudden starts jumping up and down. Most of the time the captain tells the passengers to put on their seat belts "and by the way, always have it on while seated". For most people it does seem strange, living in the twenty-first century and all, that we do not have the tools to know in advance when a flight might get bumpy. Among all those instruments and indicators in a cockpit — is there really not one little light that goes on as a warning? The answer is, well, maybe there is, but it sure is not very reliable. We cannot anticipate exactly when we will encounter turbulence. This is a really big problem — and not only when it comes to passenger comfort and safety in airplanes.

1.1 Turbulence around us

Turbulence is everywhere. In the atmosphere, around vehicles such as cars or planes, inside vehicles, building ventilation systems, hair dryers, dish washers, you name it. It is often the cause of the noise we hear when there is a flow. Next time you are riding a car (not while driving it), try to stick out your head through the side window. You are most likely to find out that the faster the car goes — the more the noise.

Turbulent flow makes a great image. The picture below (figure 1.1) is taken from the Landsat 7 satellite orbiting the earth. It shows an unusually clear image of clouds forming something called a vortex street above Selkirk island (also known as Robinson Crusoe island) off the coast of Chile. The weather was just right for the clouds to form big eddies behind the island. There are a lot more of pictures like this at http://visibleearth.nasa.gov and http://www.efluids.com.

Scientists with some interest in history like to show a picture of a turbulent flow by Leonardo da Vinci made around 1500. He was a man who "wore many

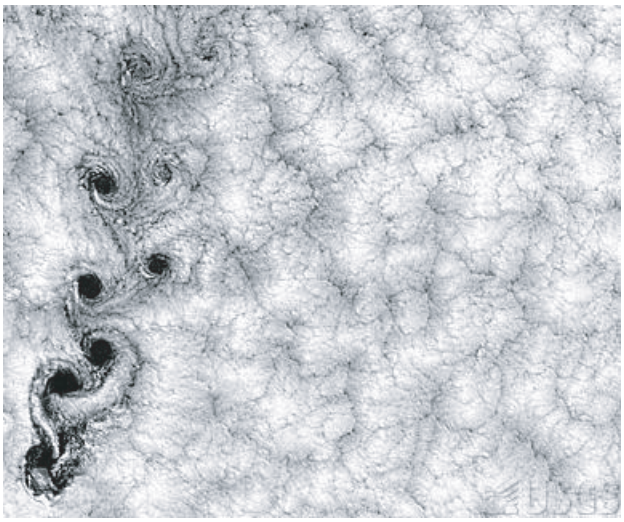

Figure 1.1: Satellite image of clouds above Selkirk Island. Obtained from http://edcwww.cr.usgs.gov/earthshots/slow/Selkirk/Selkirk

hats", with many contributions to science. Some say that he was a couple of hundred years ahead of everyone else, since he is said to have been the first to separate the mean, large scale, motion of a fluid from the small scale, fluctuating part. This is a very common approach, even today, to deal with turbulent flow, and is usually credited to Reynolds (1883). This method is widely known as 'the Reynolds decomposition'.

It is often stated in review articles that 'turbulence is the last great unsolved problem of classical physics'. A famous story about Albert Einstein goes as follows: As he lay dying Einstein said that he would like to ask God two questions: Why relativity, and why turbulence? "I really think," said Einstein, "He may have an answer to the first question."

1.2 What is turbulence?

There is one especially important number to be aware of, that will keep on appearing throughout this thesis: the Reynolds number. It is a non-dimensional number defined as $Re = UL/\nu$ Here, U is a characteristic velocity for the flow, L is a characteristic length, and ν is the kinematic viscosity of the fluid. If this number is 'low', the flow is nice and smooth — laminar. And if this number is 'high', the flow is seemingly chaotic — turbulent. Exactly at which critical Re the transition between laminar and turbulent flow takes place is different for each type of flow. Traditionally, these values were obtained from laboratory experiments. Experiments are quite sensitive to even very small disturbances, so researchers have investigated transition of all kinds of flows for about a century.

There is no precise definition of turbulence. One usually encounters seven

characteristics of it as listed in the textbook by Tennekes and Lumley (1972). A few of them are: turbulent flow is random in its nature, and also three-dimensional. That is, a turbulent flow fluctuates in all directions. Also, it must have (local) rotation or swirl (called vorticity by fluid dynamicists). Another characteristic is that there are different length scales involved. This means that there are eddies of different sizes in the flow all present at the same time. Turbulence enhances mixing, maybe its most useful property. And finally, it dissipates energy — most of the energy dissipation in the flow is due to turbulence, in fact.

A major incentive for studying turbulence in an industrial environment is to make it go away. And if this is managed — problem solved. But most of the time it is not understood why the fix worked. The natural question that arises is: Why is it so difficult?

1.3 Why is turbulence so difficult?

Let us consider an example: Take one cubic meter of fluid and stir it into motion. Let's stir it quite vigorously. The largest eddy is about the same size as the largest scale possible, one meter in this thought experiment. If this cubic meter of fluid is stirred hard enough, the smallest eddy might be a tenth of a millimeter — and this is the scale at which most of the energy dissipation occurs! To be able to compute what happens to these very important dissipative little eddies, we need a computational grid fine enough to capture all the scales. This means we need $10^4 \times 10^4 \times 10^4 = 10^{12}$ cells to resolve this cubic meter of fluid — for each time step! And these time steps have to be small enough to capture fast events, which can have a duration of a millisecond.

One cubic meter of fluid is not much when you want to find out what happens in a hydro power plant — or around an airplane. Today, the best resolved numerical simulations have about 10^{10} cells. Certainly, the computer speed can keep on doubling every 18 months for a long time before we can start talking about *only* doing computations. Nevertheless, the ability to do numerical simulations is a very important tool. Sometimes it is the only tool that can provide an answer. On the other hand, sometimes only a physical experiment can show us what really happens. Exploring turbulence is closely related to choosing the right tool for the problem, and choosing the right problems to study.

This thesis is mostly about experiments on turbulent flows. But it is also about theory, because an experiment without theory is like walking in an unknown forest with neither map nor compass. Sometimes an experiment triggers new developments of the theory, but most of the time it is the theory that suggests what we want to measure in the first place. And it is only a theory that can help us understand what we did and whether it all makes sense.

1.4 The goal

The ultimate goal is to be able to make turbulence go away or come as we please. That is called control. To be able to control something, we have to know what to control. It also helps to have an idea of how it got there — so we can make guesses how to prevent it from doing so, without having to only make blind trial-and-error tests. In this view, the experiments that will be reported in this thesis tell us what is in the flow, and the theory tries to at least give us hints as to how it got there. If we are lucky this will eventually lead us to simplified equations that will allow us to control it.

In summary, the aim of this research was to investigate and advance towards a description of how the turbulent fluctuations extract energy from the mean flow. Insights into this process are invaluable when modelling turbulence, and also when evaluating whether any specific model contains the essential physics. If the process of energy transfer from the mean flow to the fluctuations can be described accurately, it might be one step towards driving a nail into the solid rock that is loosely called 'the turbulence problem'. In the turbulence community, it is heavily debated whether the real problem originates in understanding what happens at the dissipative (small) scale or whether it is more important to understand how the energy got there in the first place. This thesis focus on the latter.

1.5 The axisymmetric wake

The axisymmetric wake is an interesting flow to study from many perspectives. Any three-dimensional object that moves through space creates a wake. If it is self-propelled, it is a momentumless wake, and if it is towed, it creates a wake with a momentum deficit. Wakes in general are extremely complex flows that are not well understood. Therefore, a simplified geometry has to be investigated to understand the physics.

The most basic form of a three-dimensional wake is the axisymmetric flow behind a disk or a sphere. Of course, if the flow is turbulent, it is really only statistically axisymmetric.

1.6 The work of this thesis

This work presented in this thesis mostly concerns the statistically axisymmetric turbulent wake behind a disk. In early experiments, the disk was actually a Swedish 5 kronor coin.

Theory

This study has been theoretical as well as experimental. The theoretical part deals with equilibrium similarity analysis and the background and derivation of

some specific properties of a technique called 'proper orthogonal decomposition' (POD). The study also briefly touches some aspects of linear stability theory. The POD is an essential part in understanding the flow in this sense, because it is an optimal way to describe the large scale energy containing structure in terms of a modal decomposition. This helps understand what really is in the flow, the building blocks if you wish. Now the question is: How did they all get there? To try to answer this, the instability of the mean flow is analyzed since the results are strikingly similar to what is found when the POD is applied to this flow.

Experiments

The axisymmetric wake has puzzled researchers for at least seventy years, since measured results have been very hard to interpret. The results have actually been inconclusive or contradictory. It is a very challenging flow to investigate experimentally (and numerically as well), since it is in some sense very weak. The mean velocity variations one wants to measure are less than 1% of the free stream velocity, and the fluctuating velocities are of the same magnitude as the velocity deficit.

The only measurement technique that is capable of resolving such small fluctuations is hot-wire anemometry. Even this technique has limitations that affect the accuracy, but it will be shown that there are ways to overcome at least part of them. In fact, the far axisymmetric wake is at the threshold of what is possible to measure today using the best wind tunnels and most stable low-noise anemometer equipment.

The theoretical part of this thesis has been carried out all over the world. It began in Buffalo, NY, evolved on boats and airplanes, and from endless discussions and notes on napkins around coffee tables.

The experimental part has been performed at different Swedish institutions; at Chalmers University of Technology in Göteborg as well as at Royal Institute of Technology in Stockholm.

Chapter 2

The history of axisymmetric wake research

The axisymmetric wake has been under investigation for at least seventy years. To make a complete survey of all the investigations of this flow is a task that is overwhelming. In this chapter, the aim is to present a historical review placing the work done in this thesis into perspective. The survey builds the framework that leads to our current level of understanding of this flow. And it concludes by summarizing which important questions are left unanswered.

2.1 Early laboratory experiments

The first published study of the 'structure' of the three-dimensional wake was perhaps that of Marshall and Stanton (1931). They presented photographs of wakes behind circular disks in water. They used dye to trace flow patterns which revealed an unsteadiness when Re exceeded about 200. They also concluded that there was a periodic discharge of a series of rings of vortices.

The sphere wake was studied in a water tank by means of flow visualization by Möller (1938), who found a spiral vortex in the wake in a certain range of Reynolds numbers. He presented Strouhal number versus Reynolds number to quantify the change in frequency of the vortex shedding. The Strouhal number is defined by:

$$St = \frac{fd}{U_\infty} \tag{2.1}$$

where f is the frequency of the vortex shedding, d is the diameter of the body, and U_∞ the free stream velocity.

With the development of hot-wire anemometry, experimentalists were very ambitious and initially focused on the far wake. Each wanted to be recognized for confirming the single universal wake of the 'classical' theory due to von Karman and others. None suceeded, which is why this thesis is still possible. The first complete set of data in the wake of an axisymmetric disk perpendicular to the

flow was presented by Carmody (1964), who measured mean velocity, turbulence intensity, Reynolds stress and wake growth in an axisymmetric disk wake at a Reynolds number (Re) based on the free stream velocity and the disk diameter of 70,000. Based on these measurements, he stated that the wake was self-similar 15 diameters from the disk, meaning that the mean velocity profiles appeared to collapse when normalized by the centreline velocity difference and a lateral length scale determined from the velocity profile itself.

One extensive study was made by Hwang and Baldwin (1966), who measured turbulence intensities and wake growth for a large span of downstream locations, all the way down to 900(!) diameters downstream. One serious problem with both the Carmody (1964) and Hwang and Baldwin (1966) data is that they show a significant scatter. Also in the sixties, Gibson et al. (1968) investigated the sphere wake using hot-wires and Pitot tubes, and reported decay of mean and variance of velocity and temperature down to $x/D = 60$.

In the sixties, the hot-wire technique was not fully developed, and of course there were no computers to handle the large amount of data required to provide undisputable statistics. Hwang and Baldwin (1966) even reported difficulties in reproducing their own results on a day-to-day basis, and Gibson et al. (1968) noted that their errors were as large as $\pm 10\%$. Most, however, covered their uncertainties by simply not showing the important profiles. In fact, these experiments are still very difficult, even with today's technology as will be seen later.

2.2 Higher Reynolds numbers and transition

In parallel, flow visualization experiments were performed on low Reynolds number wakes by Magarvey and Bishop (1961) who studied falling drops up to $Re = 2500$. They used dye visualization techniques to study the eddy (or more properly, vortex) structure of the wake, hoping to describe the mechanisms of transition and to provide limits to when the flow undergoes transition from laminar to turbulent. This study was followed by Magarvey and MacLatchy (1965), who studied falling spheres for $Re < 500$, attempting to describe the manner in which vortices are released to the free stream.

Later experimentalists pushed the Reynolds number higher and higher. They probably considered the transition process explained. Part of the reason for this was the experimental investigation of the stability of the axisymmetric wake by Sato and Okada (1966), who studied a slender axisymmetric body of revolution. This body created a laminar wake which was triggered acoustically. Because of the earlier experimental flow visualization and nearly concurrent theoretical studies, it was very interesting to find out which azimuthal modes that existed in the flow. Analytically, Sato and Okada (1966) applied a criteria of Batchelor and Gill (1962) to their laminar wake velocity profile, and concluded that azimuthal modes 1 and 2 were possibly unstable (Batchelor and Gill (1962) found that only mode 1 can be unstable for their particular choice of mean velocity profile). They were not

able to numerically find a solution for mode 2, and their experimental data was found to be in agreement with mode 1 being the only possible unstable mode. We shall come back to azimuthal modes and the Batchelor and Gill (1962) criteria later in this thesis, especially in paper 7.

The vortex structure for a sphere wake at a substantially higher Re was studied by means of flow visualization by Pao and Kao (1977). They investigated wakes with Re up to 2×10^4. The main finding was that without stratification, vorticity was shed three-dimensionally. Stable stratification resulted in the wake collapsing. They made a model of the vortex configuration in the wake that has been, and still is, heavily cited.

The sphere wake was later studied by Taneda (1978), who used the surface oil-flow method, smoke visualization and a tuft-grid to visualize the flow for Re up to 10^6. He showed evidence of the wake performing a wave motion up to $Re = 3.8 \times 10^5$, and that it forms a pair of streamwise vortices at higher values of Re.

2.3 Higher Reynolds numbers and far wakes

In 1972, Achenbach (1972) studied the high Reynolds number (up to $Re = 6 \times 10^6$) sphere wake, measuring drag, local static pressure, and the skin friction coefficient to find out how these quantities were changing during transition. The same sphere was investigated in Achenbach (1974), where hot-wire data was presented. These data were used to support the model he constructed in the previous paper.

Using hot-wires became more manageable already in the early seventies, and Uberoi and Freymuth (1970) measured the velocity distribution in the far wake of a sphere at a Reynolds number of 8,600. They were very precise in their statement that the wake had become self-similar by 50 diameters downstream, even though they only measured a few more positions downstream. One curious omission in their paper is the fact that the streamwise turbulence intensities were presented for more downstream locations than the mean velocity profiles were shown, indicating that perhaps things weren't as clear as they suggested.

Bevilaqua and Lykoudis (1978) investigated the wakes of a sphere and a porous disk with the same drag and reported that these became self-similar in terms of mean velocity and Reynolds stress profiles within ten diameters of the sphere and within twenty diameter of the porous disk — but not in the same manner. That is, the sphere and the porous disk do not reach the same state of similarity. They concluded that this result was not consistent with the idea that the turbulence forgets how it was created, as commonly believed (c.f. Townsend (1956)). This study was (and still is) largely ignored by those who write textbooks.

A similar, but more extensive experiment was that of Cannon (1991) who investigated the axisymmetric far wake behind five different wake generators (disk, sphere and three porous disks with different porosity, all five with the same drag. The measurements extended over a range of x/D of about 10 to 125. From these

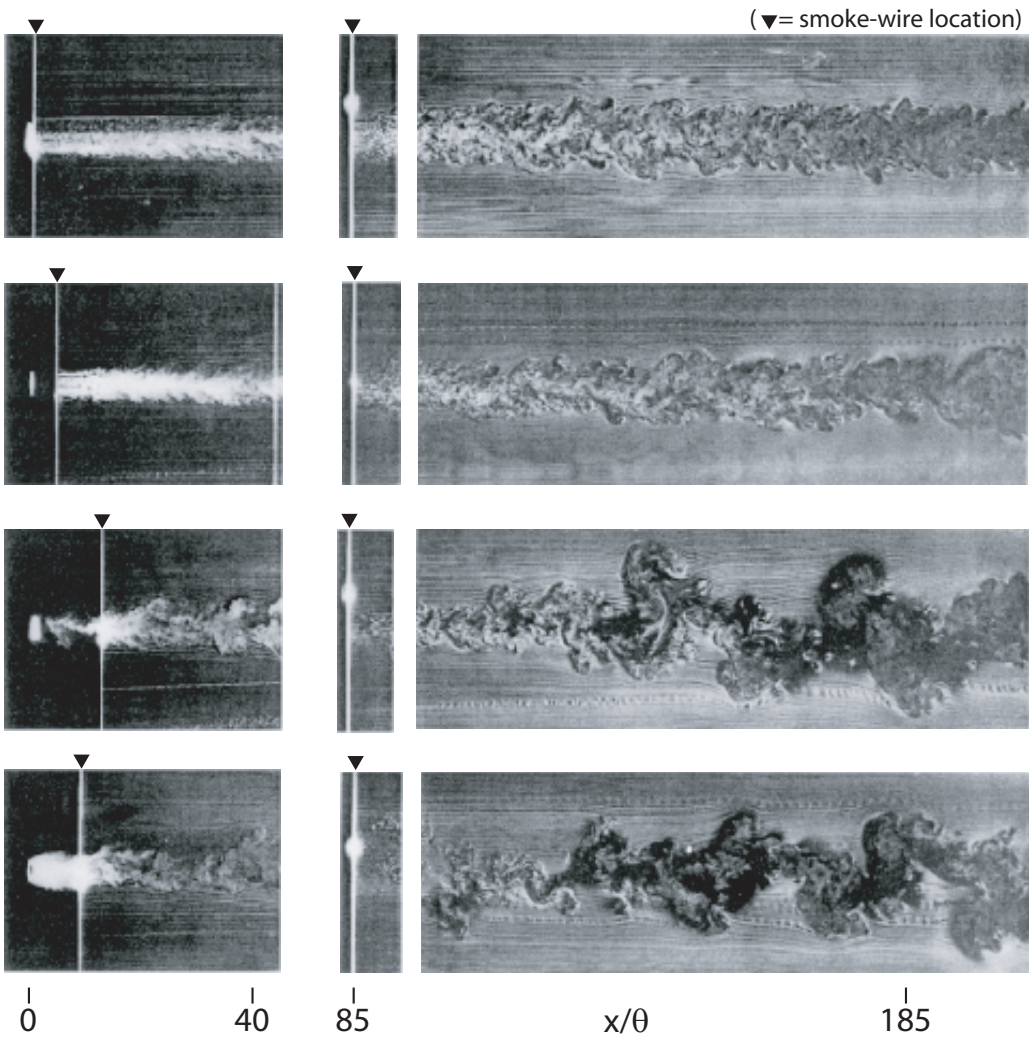

Figure 2.1: Four different wakes, Cannon (1991).

data, it was obvious that there is something more than the drag that dictates the evolution of the flow. Even though all wake generators used had the same drag, the wakes behaved very differently. This is very pronounced in the flow visualization images in Cannon (1991), shown in figure 2.1, where even the turbulence eddies look different. The statistical properties and growth rates of the wakes differ by as much as a factor of four. Even with this data, some insist that we only need to go far enough downstream and they will all look alike. Cannon (1991) also found that it was possible to fit both of the two possible similarity solutions of George (1989) equally well to the data. It was not clear which was the best, or even if either flow had reached equilibrium.

The stability of the axisymmetric wake was investigated theoretically by Monkewitz (1988), who expanded previous studies by investigating a family of wake velocity profiles. He confirmed previous conclusions that azimuthal mode 1 was the

most unstable — in fact the only one that can trigger absolute instability of this flow.

2.4 The computer age - back to low Reynolds numbers

By the nineties, computers had evolved to the point that they started to become really useful for computing turbulent flows. Kim and Pearlstein (1990) made a computational study of the transition range for $Re < 300$ using a spectral method. They claimed that their result compared well to experimental results. The instability of the flow behind spheres and disks was also investigated by Natarajan and Acrivos (1993) using finite-element methods. They disagreed with Kim and Pearlstein (1990) on how the actual transition from laminar to turbulent flow takes place, but both agreed that azimuthal mode 1 was the most dominant feature.

Basu et al. (1992) made a direct numerical simulation (DNS) of the axisymmetric wake for $Re = 1,500$. The authors claimed that the solution approached the self-similar state in a slow manner, and the computation was interrupted before this could be verified.

Johnson and Patel (1999) investigated the flow behind a sphere at low Reynolds number numerically and experimentally. They proposed a symmetry breaking mechanism to advance the basic understanding of the steady, non axisymmetric regime between $Re = 210$ and 270. At $Re = 300$, a highly organized periodic flow was found that was dominated by vortex shedding. Transitional and weak turbulent flow was shortly thereafter studied by Tomboulides and Orszag (2000), who confirmed the results of experiment and linear stability analysis. The conclusion that mode 1 was most important was supported by the non-linear dynamical systems approach by Ghidersa and Dušek (2000).

Very recently, Gourlay et al. (2001), presented the first DNS of the high Reynolds number ($Re = 10{,}000$) 'late' wake (which can be directly compared with the 'far' wake). This work was found to be very interesting in the context of this thesis, and these data are used extensively in paper 5.

2.5 Large scale structures

The large scale, 'coherent' features of this flow have not only been studied using flow visualization, but also by means of phase averaging and conditional sampling techniques, (Lee and Bearman, 1992; Miau et al., 1997; Perry and Lim, 1978; Perry and Watmuff, 1981). Most interestingly in the context of this thesis, Roberts (1973), and later Fuchs et al. (1979) used two hot-wires to measure cross-spectra at a single radius of the near wake. Fuchs et al. (1979) varied the angular separation of the probes and were able to decompose the cross-spectra into Fourier modes.

The azimuthal modal content was then studied at the frequencies that were found to be eventful. At $x/D = 9$, they found a strong azimuthal mode-1 peak at a frequency corresponding to the vortex shedding frequency, but also a peak for mode-2 at very low frequencies. The mode-1 peak was clearly dominant. Berger et al. (1990) also conducted a similar investigation, and reported a dominant mode-1 peak. They did not at all mention mode-2, even though it is clearly present in their results. Subsequently, Cannon et al. (1993) also measured the cross-spectra at a fixed radius of the wake, but further downstream, $x/D = 27$. They confirmed that mode-1 was dominant.

2.6 Proper orthogonal decomposition, POD

Proper orthogonal decomposition is in essence a structured way of organizing the azimuthally transformed cross-spectra. Originally introduced to the field of turbulence by Lumley (1967), it has only recently become heavily utilized, because of the very large amount of data required. The POD has been applied to many flows, such as the plane mixing layer by Bonnet et al. (1998), where different techniques of eddy structure identification methods were compared. This role of the POD was further discussed in detail by Delville et al. (1999).

The POD orders the energetic structures, and also gives an answer to which modes are dominant over a whole plane. Thus it is more general than for instance azimuthal decompositions at a fixed radius. A POD in a plane at a fixed downstream position, called 'slice' POD has been previously applied to the jet mixing layer Glauser (1987); Glauser and George (1987); Citriniti and George (2000) and to the far jet Gamard et al. (2002b). These were followed up by Gamard et al. (2002a) and most recently by Gamard (2002). Much to our surprise, azimuthal mode-2 was found to dominate the far jet, contrary to previous experiments.

2.7 Equilibrium similarity theory

The work in this thesis actually started with the topic of equilibrium similarity theory. The idea is that "nature loves balance". In other words, all the terms in the governing equations of a particular flow go up and down together as the flow evolves. If some term does not follow — it either takes over and new balance is established, or it dies off. The concept was introduced by George (1989), who studied a family of shear flows like the plane and axisymmetric jets and wakes. A continuation was presented in George (1995). Already in the first paper, two possible solutions for the axisymmetric wake were suggested.

The equilibrium similarity has been applied to many flows, such as plane wakes by Ewing (1995) and Moser et al. (1998), and in extended form to boundary layers by George and Castillo (1997), to wall jets by George et al. (2000), and to pipe and channel flow by Wosnik et al. (2000). It is pretty obvious now that flows like to be in equilibrium similarity. The obvious and unanswered question is why?

2.8 Unanswered questions

The research mentioned above has left some questions unanswered, which is why this thesis was possible. Some of the questions are:

1. Does the axisymmetric wake ever become self-similar?
2. Which solution will it go to if it does?
3. Provided the answer to the first question if yes, how far downstream is the wake self-similar?
4. Will azimuthal mode-1 continue to be the most dominant mode far downstream?

In May 2000, these questions were formulated in almost the same way in an application to a no longer existing source of funding of fundamental research in Sweden. The application was turned down. Fortunately we were able to proceed anyway, and all of the questions have been answered in this thesis. Amazingly, enough new fundamental questions about turbulence have been raised that the continuation of this research has been funded by the successor agency.

Chapter 3

Summary of papers

3.1 Papers 1 & 5: Equilibrium similarity

Paper 1 presents the equilibrium similarity theory applied to the turbulent axisymmetric wake. For the first time, it was shown without *ad hoc* assumptions that two solutions are theoretically possible: one for high Reynolds number flows where the wake grows as $x^{1/3}$ and another for low Reynolds number flows with a wake growth as $x^{1/2}$. In this paper, the theory was applied to experimental data available at the time, and it was not clear whether any of the solutions applied anywhere. An intermediate asymptotic solution was presented that provided an excellent fit to the data.

This paper has been superseded by Paper 5, but is left in the thesis to show the evolution of the work. As new experimental data became available, presented in Paper 9, together with the far downstream study of the evolution of the POD, it became clear that the data analyzed in Paper 1 simply had not evolved far enough downstream for the initial transients to die off. Also, high Reynolds number DNS data became available to the authors, which contributed to the final results presented in Paper 5. Here it is shown that the turbulent disk wake at a Reynolds number of 26,400 satisfies the high Reynolds number equilibrium similarity solution, once the flow has had enough downstream distance to evolve. The necessary distance was found to be 30 diameters. This is characterized by the flow approaching a state where u'/U_o is constant, and when the local Reynolds number is high enough (> 500).

The high Reynolds number DNS was found to also satisfy these conditions, but after a certain time, the turbulence intensity ratio diminished, whereafter the flow slowly evolved towards the low Reynolds number state, again characterized by a constant value of u'/U_o.

3.2 Papers 2 & 3: The near wake

A probe consisting of 13 hot-wires arranged in two rakes were used to obtain the first POD of the axisymmetric wake for three different downstream positions, $x/D = 10$, 30, and 50. The results of this study are presented in Paper 2. It was found that azimuthal mode 1 dominates the first position. At $x/D = 30$, it was found that mode 1 and 2 were equally important, and by $x/D = 50$ mode 2 seemed to dominate. This was a very surprising result, contradicting all previously reported.

To ensure that the results were reliable, a sensitivity study was conducted, where the effect of probe coverage and disk suspension configuration was investigated. The results presented in Paper 1 were confirmed.

3.3 Papers 4 ,8, & 9: The far wake

The investigation of Papers 2 & 3 was extended to cover larger downstream distances (to $x/D = 150$). Here, the single-point statistics were obtained to provide a data base of the disk wake evolution. This was used extensively in the study presented in Paper 5. Paper 4 shows preliminary results from this experiment, using the POD to extract the energetic structures. The experiment is thoroughly explained in Paper 9.

The decomposition revealed that the initial wake region from 10 to 30 diameters downstream was indeed dominated by an azimuthal mode-1 type of motion, but also that the importance of this mode vanishes as the flow evolves. Instead the far wake from 30 diameters downstream on was found to be dominated by a mode-2 type of azimuthal motion. This was found to coincide very well with the position at which the similarity solution became valid. This mode-2 dominance continued throughout the whole range of the investigation, with virtually no change in the modal decomposition. The mode-1 was interpreted as a convected structure associated to the vortex shedding in the near wake that was just swept by the probes and dies off downstream, and the mode-2 was postulated to be associated with a global instability manifested as a slow movement of the whole mean velocity field.

3.4 Papers 6 & 7: Connection to stability theory

In light of the acquired results, we decided to re-examine some widespread views regarding coherent structures, linear stability, and the dominant azimuthal behavior of the wake. Especially, we re-examined the temporal linear stability analysis developed by Batchelor and Gill (1962). Their conclusion that mode-1 is the only unstable mode in axisymmetric shear flows is purely a consequence of their postulated 'far jet' profile. More realistic profiles for jets as well as wakes, show that

modes-0, 1, and 2 can be unstable, which is in agreement with our findings in the wake.

Bibliography

E. Achenbach. Experiments on the flow past spheres at very high reynolds numbers. *Journal of Fluid Mechanics*, 54(3):565–575, 1972.

E. Achenbach. Vortex shedding from spheres. *Journal of Fluid Mechanics*, 62(2): 209–221, 1974.

A. J. Basu, R. Narasimha, and U. N. Sinha. Direct numerical simulation of the initial evolution of the axisymmetric wake. *Current Science*, 63(12):734–740, 1992.

G. K. Batchelor and E. A. Gill. Analysis of the instability of axisymmetic jets. *Journal of Fluid Mechanics*, 14:529–551, 1962.

E. Berger, D. Scholz, and M. Schumm. Coherent vortex structures in the wake of a sphere and a circular disk at rest and under forced vibrations. *Journal of Fluids and Structures*, 4:231–257, 1990.

P. M. Bevilaqua and P. S. Lykoudis. Turbulence memory in self-preserving wakes. *Journal of Fluid Mechanics*, 89(3):589–606, 1978.

J. P. Bonnet, J. Delville, M. N. Glauser, R. A. Antonia, D. K. Bisset, D. R. Cole, H. E. Fiedler, J. H. Garem, D. Hilberg, J. Jeong, N. K. R. Kevlahan, L. S. Ukeiley, and E. Vincendeau. Collaborative testing of eddy structure identification methods in free turbulent shear flows. *Experiments in Fluids*, 25:197–225, 1998.

S. Cannon, F. Champagne, and A. Glezer. Observations of large-scale structures in wakes behind axisymmetric bodies. *Experiments in Fluids*, 14:447–450, 1993.

S. C. Cannon. *Large-scale structures and the spatial evolution of wakes behind axisymmetric bluff bodies*. PhD thesis, Dept. of Aerosp. and Mech. Engr., Univ. of Arizona, 1991.

T. Carmody. Establishment of the wake behind a disk. *Journal of Basic Engineering*, 86:869–882, 1964.

J. H. Citriniti and W. K. George. Reconstruction of the global velocity field in the axisymmetric mixing layer utilizing the proper orthogonal decomposition. *Journal of Fluid Mechanics*, 418:137–166, 2000.

J. Delville, L. Ukeiley, L. Cordier, J. P. Bonnet, and M. Glauser. Examination of large-scale structures in a turbulent plane mixing layer. part 1. proper orthogonal decomposition. *Journal of Fluid Mechanics*, 391:91–122, 1999.

D. Ewing. *Utilizing a Two Point Similarity Hypothesis to Determine Optimal Orthogonal Functions in Free Shear Layers*. PhD thesis, State University of New York at Buffalo, 1995.

H. V. Fuchs, E. Mercker, and U. Michel. Large scale coherent structures in the wake of axisymmetric bodies. *Journal of Fluid Mechanics*, 93:189–211, 1979.

S. Gamard. *The axisymmetric turbulent jet*. PhD thesis, Chalmers University of Technology, Göteborg, Sweden, 2002.

S. Gamard, D. Jung, and W. K. George. Downstream evolution of the most energetic modes in a turbulent axisymmetric jet at high reynolds number. Part 2. The far jet. *Submitted to Journal of Fluid Mechanics*, 2002a.

S. Gamard, D. Jung, S. Woodward, and W. K. George. Application of a 'slice' POD to the far field of an axisymmetric turbulent jet. *Accepted for publication in Physics of Fluids*, 14(6), 2002b.

W. K. George. The self-preservation of turbulent flows and its relation to initial conditions and coherent structures. In *Advances in Turbulence*, pages 39–73. Hemisphere Press, 1989.

W. K. George. Some new ideas for similarity of turbulent shear flows. In K. Hanjalic and J. C. F. Pereira, editors, *Proc. ICHMT Symposium on Turbulence, Heat and Mass Transfer, Lisbon, Portugal (1994)*. Begell House, 1995.

W. K. George, H. Abrahamsson, J. Eriksson, R. I. Karlsson, L. Lfdahl, and M. Wosnik. A similarity theory for the turbulent plane wall jet without external stream. *Journal of Fluid Mechanics*, 425:367–411, 2000.

W. K. George and L. Castillo. Zero-pressure-gradient turbulent boundary layer. *Applied Mech. Rev.*, 50(12):689–729, 1997.

B. Ghidersa and J. Dušek. Breaking of axisymmetry and onset of unsteadiness in the wake of a sphere. *Journal of Fluid Mechanics*, 423:33–69, 2000.

C. H. Gibson, C. C. Chen, and S. C. Lin. Measurements of turbulent velocity and temperature fluctuations in the wake of a sphere. *AIAA Journal*, 6:642–649, 1968.

M. N. Glauser. *Coherent Structures in the Axisymmetric Turbulent Jet Mixing Layer*. PhD thesis, State University of New York at Buffalo, 1987.

M.N. Glauser and W.K. George. Orthogonal decomposition of the axisymmetric jet mixing layer including azimuthal dependence. In G. Comte-Bellot and J. Mathieu, editors, *Advances in Turbulence*, pages 357–366. Spring-Verlag, 1987.

M. J. Gourlay, S. C. Arendt, D. C. Fritts, and J. Werne. Numerical modeling of initially turbulent wakes with net momentum. *Phys. Fluids*, 13:3783–3802, 2001.

N. C. H. Hwang and L. V. Baldwin. Decay of turbulence in axisymmetric wakes. *Journal of Basic Engineering*, 88:261–268, 1966.

T. A. Johnson and V. C. Patel. Flow past a sphere up to a reynolds number of 300. *Journal of Fluid Mechanics*, 378:19–70, 1999.

I. Kim and A. J. Pearlstein. Stability of the flow past a sphere. *Journal of Fluid Mechanics*, 211:73–93, 1990.

S. I. Lee and P. W. Bearman. An experimental investigation of the wake structure behind a disk. *Journal of Fluids and Structures*, 6:437–450, 1992.

J. L. Lumley. The inertial subrange in nonequilibrium turbulence. In A. M. Yaglom and V. I. Tatarsky, editors, *Atmospheric Turbulence and Radio Wave Propagation*, pages 157–164, Moscow, USSR, 1967. Nauka.

R. H. Magarvey and R. L. Bishop. Transition ranges for three-dimensional wakes. *Canadian Journal of Physics*, 39:1418–1422, 1961.

R. H. Magarvey and C. S. MacLatchy. Vortices in sphere wakes. *Canadian Journal of Physics*, 43:1649–1656, 1965.

D. Marshall and T. E. Stanton. On the eddy system in the wake of flat circular plates in three dimensional flow. *Proc. Roy. Soc. London A*, 130:295–301, 1931.

J. J. Miau, T. S. Leu, T. W. Liu, and J. H. Chou. On vortex shedding behind a circular disk. *Experiments in Fluids*, 23:225–233, 1997.

W. Möller. Experimentelle untersuchengen zur hydrodynamik der kugel. *Phys. Z.*, 39:57–80, 1938.

P. A. Monkewitz. A note on vortex shedding from axisymmetric bluff bodies. *Journal of Fluid Mechanics*, 192:561–575, 1988.

R. D. Moser, M. M. Rogers, and D. W. Ewing. Self-similarity of time-evolving plane wakes. *Journal of Fluid Mechanics*, 367:255–289, 1998.

R. Natarajan and A. Acrivos. The instability of the steady flow past spheres and disks. *Journal of Fluid Mechanics*, 254:323–344, 1993.

H.-P. Pao and T. W. Kao. Vortex structure in the wake of a sphere. *The Physics of Fluids*, 20(2):187–191, 1977.

A. E. Perry and T. T. Lim. Coherent structures in coflowing jets and wakes. *Journal of Fluid Mechanics*, 88:451–463, 1978.

A. E. Perry and J. H. Watmuff. The phase-averaged large-scale structures in three-dimensional turbulent wakes. *Journal of Fluid Mechanics*, 103:33–51, 1981.

O. Reynolds. *Phil. Trans. Roy. Soc.*, 174:935–982, 1883.

J. B. Roberts. Coherence measurements in an axisymmetric wake. *AIAA Journal*, 11, no. 1:1569–1571, 1973.

H. Sato and O. Okada. The stability and transition of an axisymmetric wake. *Journal of Fluid Mechanics*, 26:237–253, 1966.

S. Taneda. Visual observations of the flow past a sphere at reynolds numbers between 10^4 and 10^6. *Journal of Fluid Mechanics*, 85(1), 1978.

H. Tennekes and J. L. Lumley. *A First Course in Turbulence*. MIT Press, Cambridge,MA, 1972.

A. G. Tomboulides and S. A. Orszag. Numerical investigation of transitional and weak turbulent flow past a sphere. *Journal of Fluid Mechanics*, 416:45–73, 2000.

A. A. Townsend. *The Structure of Turbulent Shear Flow*. Cambridge University Press, Cambridge, UK, 1956.

M. S. Uberoi and P. Freymuth. Turbulent energy balance and spectra of the axisymmetric wake. *Phys. Fluids*, 13(9):2205–2210, 1970.

M. Wosnik, L. Castillo, and W. K. George. A theory for turbulent pipe and channel flows. *Journal of Fluid Mechanics*, 421:115–145, 2000.

Paper 1

On the effect of finite Reynolds number and initial conditions on the axisymmetric wake

Proceedings of the Second International Symposium on Turbulence and Shear Flow Phenomena, volume I, pp. 323-328, Stockholm, Sweden, June 27-29, 2001

P. B. V. Johansson
W. K. George

ON THE EFFECT OF FINITE REYNOLDS NUMBER AND INITIAL CONDITIONS ON THE AXISYMMETRIC WAKE

Peter Johansson
Department of Thermo and Fluid Dynamics, CTH
S-412 96 Göteborg, Sweden
jope@tfd.chalmers.se

William K. George
Department of Thermo and Fluid Dynamics, CTH
S-412 96 Göteborg, Sweden
wkgeorge@tfd.chalmers.se

ABSTRACT

Equilibrium similarity considerations are applied to the axisymmetric turbulent wake. Two solutions are found; one for infinite Reynolds number, one for small Reynolds number, and both dependent on the upstream conditions. Neither agrees particularly well with the data. For both solutions, the local Reynolds number of the flow diminishes with increasing downstream distance. As a consequence, even when the initial Reynolds number is large, the flow evolves from one state to the other. Intermediate asymptotics is used to provide a bridge between the two solutions, which is in excellent agreement with the experimental data.

INTRODUCTION

The axisymmetric wake is of fundamental importance since it is one of few flows where the local Reynolds number decreases as the flow evolves. Also, the equations of motion governing the axisymmetric wake contain all of the important dynamical terms for turbulent flow away from surfaces. Hence the data from this flow form an important data base for developing turbulence models of all types, as well as for validating DNS and LES simulations.

The following observations can be made from various experiments:

- Different initial conditions affect the growth rates, contrary to the classical theory which states that all wakes should depend only on the downstream distance, x, and the drag, $\pi U_\infty^2 \theta^2$. This is most strikingly illustrated by the photographs of Cannon et al. (1993). Data from Cannon (1991) (for several different wake generators that all have the same drag) and Menut et al. (2000) are plotted in Figure 1. These show the variation with x of the transverse length scale defined by

$$\delta_*^2 = \lim_{r\to\infty} \frac{1}{U_o} \int_0^r (U_\infty - U)\, r\, dr \qquad (1)$$

where U_o is the centerline velocity deficit. The data do not collapse to a single curve, nor do these source dependent effects vanish, even for large Reynolds numbers or large downstream distance. The curves denoted "model" will be explained in a later section.

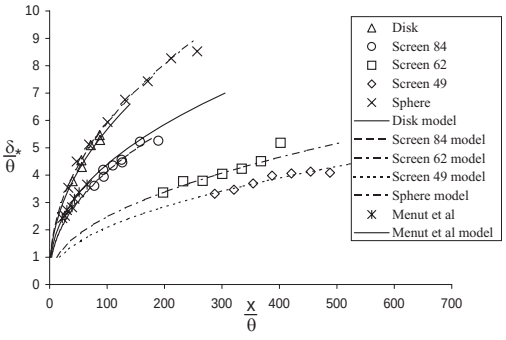

Figure 1: Cross-stream length scale, δ_*/θ versus x/θ, Cannon (1991) and Menut et al. (2000).

- The wake does not in general grow as the 1/3-power of downstream distance, x, as predicted by the classical similarity theory (c. f., Tennekes and Lumley, 1972). As noted previously by Cannon, curve fits to the data agree equally well with both a cube root and a square root variation, and not particularly well with either.
- In apparent contradiction, the mean velocity profiles from all experiments collapse

on a single curve when scaled with centerline velocity deficit and δ_*, as illustrated in Figure 2a.

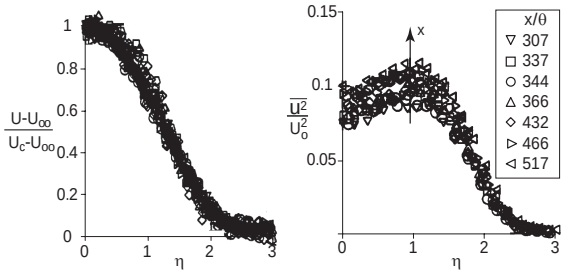

Figure 2: a) Mean velocities, b) Turbulence intensities, Cannon (1991)

- And to further confuse the issue, the turbulence intensities do not appear to collapse at all, even for fixed upstream conditions. Figure 2b shows profiles of $\overline{u^2}/U_o^2$ for various downstream distances for one of the screen wakes (the most porous) in Cannon (1991). In fact, it seems like the there are two branches; one for the near wake and one for the far wake.

These observations cannot be explained by classical similarity analysis, which argues that the asymptotic wake is independent of its initial conditions and depends only on the distance downstream and the drag. Nor can they be explained by measurement errors. While the low turbulence intensities of the axisymmetric wake make measurements far downstream difficult, they also insure that the hot-wire techniques utilized are highly accurate. At very least the problems presented by wake measurements are no more difficult than for grid turbulence, for which hot-wire measurements have long been accepted.

The classical self-preservation approach to free shear flows was questioned by George (1989) and (1995), who argued that it was based on assumptions that were not in general valid. He proposed a new methodology called *equilibrium similarity analysis*, and demonstrated with it that solutions were possible which depended *uniquely* on the upstream conditions. The new theory was in striking agreement with the nearly concurrent experiments of Wygnanski et al. (1986) for two-dimensional wakes. These showed dramatic differences between spreading rates and eddy structure which depended on the wake generator.

George (1989) also argued that the axisymmetric wake would behave similarly. He predicted that the mean velocity profiles from the different experiments would be the same, if scaled by the centerline deficit velocity and velocity deficit half-width, even if the wakes grew at different rates. This is consistent with the observations shown in Figure 2a. This result is very important, since previous researchers have often used such collapse to argue that wakes are independent of upstream conditions. The whole point of George's analysis, however, is that the source-dependent differences only show up in the spreading rate, and the higher turbulence moments.

In this paper, the analysis of George (1989) is re-visited, corrected, and extended. It will be shown that two different equilibrium similarity solutions for the axisymmetric wake are possible: one for very high local Reynolds numbers, and another for very low. Most importantly, because the local Reynolds number decreases with distance downstream, the flow will evolve from one state to the other, no matter how high the initial Reynolds number of the flow. The available experimental data is analyzed, especially addressing the particular points listed above. Not surprisingly (given the state of confusion regarding it), most of the experiments are shown to take place in the evolution region where neither limit applies exactly. An intermediate asymptotics solution for this region is shown to be in excellent agreement with the data.

GOVERNING EQUATIONS

The Reynolds averaged x-momentum equation for the axisymmetric far wake without swirl reduces to second order to:

$$U_\infty \frac{\partial}{\partial x}\left(U - U_\infty\right) = -\frac{1}{r}\frac{\partial}{\partial r}\left(r\overline{uv}\right) + \left\{ \frac{\partial}{\partial x}\left(\overline{v^2} - \overline{u^2}\right) + \nu\frac{1}{r}\frac{\partial}{\partial r}\left(r\frac{\partial}{\partial r}\left(U - U_\infty\right)\right)\right\} \tag{2}$$

Here, the r-momentum equation has been used to integrate out the pressure. The terms in curly brackets are usually neglected, but are retained here.

The momentum equation can be integrated over a cross-section to yield an integral constraint for the conservation of momentum:

$$U_\infty \int_0^\infty \left(U_\infty - U\right)\, 2\pi r\, dr \cong \pi\theta^2 U_\infty^2 \tag{3}$$

where θ is the momentum thickness.

As noted by George (1995), the momentum equation alone is not sufficient to determine

the similarity constraints. Even the inclusion of the kinetic energy equation is not enough to close the system so that the x-dependence can be determined. Instead, the individual Reynolds stress equations have to be investigated. These, together with the constraint of continuity on the pressure-strain rate terms provide the necessary conditions. The component Reynolds stress equations for the far wake are:

$\overline{u^2}$ balance

$$U_\infty \frac{\partial}{\partial x}\left(\frac{1}{2}\overline{u^2}\right) = -\overline{uv}\frac{\partial}{\partial r}\left(U - U_\infty\right) - \frac{1}{r}\frac{\partial}{\partial r}\left(r\frac{1}{2}\overline{u^2 v}\right) + \overline{\frac{p}{\rho}\frac{\partial u}{\partial x}} - \frac{1}{\rho}\frac{\partial}{\partial x}\overline{pu} + \nu\frac{1}{r}\frac{\partial}{\partial r}\left\{r\frac{\partial}{\partial r}\left(\frac{1}{2}\overline{u^2}\right)\right\} - \varepsilon_u \quad (4)$$

$\overline{v^2}$ balance

$$U_\infty \frac{\partial}{\partial x}\left(\frac{1}{2}\overline{v^2}\right) = -\frac{1}{r}\frac{\partial}{\partial r}\left(r\frac{1}{2}\overline{v^3}\right) + \frac{\overline{vw^2}}{r} + \overline{\frac{p}{\rho}\frac{\partial v}{\partial r}} - \frac{1}{\rho}\frac{\partial}{\partial r}\overline{pv} + \nu\frac{\partial}{\partial r}\left\{\frac{1}{r}\frac{\partial}{\partial r}\left(r\frac{1}{2}\overline{v^2}\right)\right\} - \varepsilon_v \quad (5)$$

$\overline{w^2}$ balance

$$U_\infty \frac{\partial}{\partial x}\left(\frac{1}{2}\overline{w^2}\right) = -\frac{1}{r}\frac{\partial}{\partial r}\left(r\frac{1}{2}\overline{uw^2}\right) - \frac{\overline{vw^2}}{r} + \nu\frac{\partial}{\partial r}\left\{\frac{1}{r}\frac{\partial}{\partial r}\left(r\frac{1}{2}\overline{w^2}\right)\right\} - \varepsilon_w \quad (6)$$

$\overline{uv}$ balance

$$U_\infty \frac{\partial}{\partial x}\left(\overline{uv}\right) = -\overline{v^2}\frac{\partial}{\partial r}\left(U - U_\infty\right) - \frac{1}{r}\frac{\partial}{\partial r}\left(r\overline{uv^2}\right) + \frac{\overline{uw^2}}{r} + \overline{\frac{p}{\rho}\left(\frac{\partial u}{\partial r} + \frac{\partial v}{\partial x}\right)} - \frac{1}{\rho}\left(\frac{\partial}{\partial r}\overline{pu} + \frac{\partial}{\partial x}\overline{pv}\right) + \nu\frac{\partial}{\partial r}\left\{\frac{1}{r}\frac{\partial}{\partial r}\left(r\frac{1}{2}\overline{uv}\right)\right\} - \varepsilon_{uv} \quad (7)$$

where ε_u, ε_v, ε_w, and ε_{uv} are the components of the homogenous dissipation.

The Similarity Transformations

We seek solutions on the form (written here for the momentum equation and $\overline{u^2}$ equations only — the others are treated similarly):

$$U - U_\infty = U_s(x) f(\eta, *) \quad (8a)$$
$$-\overline{uv} = R_s(x) g(\eta, *) \quad (8b)$$
$$\frac{1}{2}\overline{u^2} = K_u(x) k_u(\eta, *) \quad (8c)$$
$$\frac{1}{2}\overline{u^2 v} = T_{u^2 v}(x) t_{u^2 v}(\eta, *) \quad (8d)$$
$$\overline{\frac{p}{\rho}\frac{\partial u}{\partial x}} = P_u(x) p_u(\eta, *) \quad (8e)$$
$$\frac{1}{\rho}\overline{pu} = P_u^D(x) p_u^D(\eta, *) \quad (8f)$$
$$\varepsilon_u = D_u(x) d_u(\eta, *) \quad (8g)$$

where $\eta = r/\delta(x)$ and $*$ denotes a possible (unknown) dependence on initial conditions.

The Momentum Integral

Substitution of eq. (8) into eq. (3) yields:

$$U_s \delta^2 \int_0^\infty 2 f \eta \, d\eta = U_\infty \theta^2 \quad (9)$$

It follows immediately that if $\delta \equiv \delta_*$ and $U_s \equiv U_o$:

$$\frac{U_s}{U_\infty} = \left[\frac{\theta}{\delta_*}\right]^2 \quad (10)$$

The Transformed Mean Momentum Equation

Substituting eq. (8) into the momentum equation, eq. (2), and rearranging the terms yields:

$$\left[\frac{\delta}{U_s}\frac{dU_s}{dx}\right] f - \left[\frac{d\delta}{dx}\right] \eta f' = \left[\frac{R_s}{U_\infty U_s}\right] \frac{(\eta g)'}{\eta} + \left[\frac{\nu}{U_\infty \delta}\right] \frac{(\eta f')'}{\eta} \quad (11)$$

where $'$ denotes derivation with respect to η. Note that the second order term could have been retained. To this point the mean momentum equations have simply been transformed by the separation of variables in eq. (8) so that all of the explicit x-dependence is in the bracketed terms. Thus the results are completely general and no similarity assumptions have been made (although the form of the solutions has been restricted).

The Transformed Reynolds Stress Equations

Substituting eq. (8) into the transport equations for Reynolds stresses yields:

$\overline{u^2}$-equation

$$\left[U_\infty \frac{dK_u}{dx}\right] k_u - \left[\frac{U_\infty K_u}{\delta}\frac{d\delta}{dx}\right]\eta k_u' = - \left[\frac{R_s U_s}{\delta}\right] f' - \left[\frac{T_{u^2v}}{\delta}\right]\frac{(\eta t_{u^2v})'}{\eta} + [P_u]\, p_u + \left[\frac{dP_u^D}{dx}\right] p_u^D - \left[\frac{P_u^D}{\delta}\frac{d\delta}{dx}\right]\eta (p_u^D)' + \left[\frac{\nu K_u}{\delta^2}\right]\frac{(\eta k_u')'}{\eta} - [D_u]\, d_u \quad (12)$$

$\overline{v^2}$-equation

$$\left[U_\infty \frac{dK_v}{dx}\right] k_v - \left[\frac{U_\infty K_v}{\delta}\frac{d\delta}{dx}\right]\eta k_v' = - \left[\frac{T_{v^3}}{\delta}\right]\frac{(\eta t_{v^3})'}{\eta} + \left[\frac{T_{vw^2}}{\delta}\right]\frac{t_{vw^2}}{\eta} + [P_v]\, p_v + \left[\frac{P_v^D}{\delta}\right](p_v^D)' + \left[\frac{\nu K_v}{\delta^2}\right]\frac{(\eta k_v')'}{\eta} - [D_v]\, d_v \quad (13)$$

$\overline{w^2}$-equation

$$\left[U_\infty \frac{dK_w}{dx}\right] k_w - \left[\frac{U_\infty K_w}{\delta}\frac{d\delta}{dx}\right]\eta k_w' = - \left[\frac{T_{uw^2}}{\delta}\right]\frac{(\eta t_{uw^2})'}{\eta} - \left[\frac{T_{vw^2}}{\delta}\right]\frac{t_{vw^2}}{\eta} + \left[\frac{\nu K_w}{\delta^2}\right]\frac{(\eta k_w')'}{\eta} - [D_w]\, d_w \quad (14)$$

$\overline{uv}$-equation

$$- \left[U_\infty \frac{dR_s}{dx}\right] g - \left[\frac{U_\infty R_s}{\delta}\frac{d\delta}{dx}\right]\eta g' = \left[\frac{K_v U_s}{\delta}\right] f' k_v - \left[\frac{T_{uv^2}}{\delta}\right]\frac{(\eta t_{uv^2})'}{\eta} + \left[\frac{T_{uw^2}}{\delta}\right]\frac{t_{uw^2}}{\eta} + [P_{uv}]\, p_{uv} - \left[\frac{P_u^D}{\delta}\right](p_u^D)' - \left[\frac{dP_v^D}{dx}\right](p_v^D) - \left[\frac{P_v^D}{\delta}\frac{d\delta}{dx}\right]\eta (p_v^D)' - \left[\frac{\nu R_s}{\delta^2}\right]\left(\frac{(\eta g)'}{\eta}\right)' - [D_{uv}]\, d_{uv} \quad (15)$$

As before, the equations have simply been transformed by the similarity transformations so that all the explicit x-dependence is in the bracketed terms.

EQUILIBRIUM SIMILARITY SOLUTIONS TO THE TRANSFORMED EQUATIONS

For the particular type of "equilibrium" similarity solutions suggested in George (1995), *the terms in the governing equations must maintain the same relative balance as the flow evolves.* These "equilibrium" similarity solutions exist only if the terms within square brackets have the same x-dependence, and are independent of the similarity variable, η. Thus, the bracketed terms must remain proportional to each other as the flow evolves. This is denoted by the symbol $\sim$ which should be interpreted as "has the same x-dependence as"[1].

For the mean momentum equation, these equilibrium similarity constraints can be written as:

$$\left[\frac{\delta}{U_s}\frac{dU_s}{dx}\right] \sim \left[\frac{d\delta}{dx}\right] \sim \left[\frac{R_s}{U_\infty U_S}\right] \sim \left[\frac{\nu}{U_\infty \delta}\right] \quad (16)$$

Note that there is nothing in the equations or the theory which suggests that the constants of proportionality are independent of source conditions, nor in fact do they appear to be. This is contrary to the usual assumptions in self-preservation analysis (c. f., Tennekes and Lumley, 1972). It is trivial to show that the relation between the first and second terms of eq. (16) is satisfied by the momentum integral result of eq. (10).

The proper scale for $-\overline{uv}$ is obtained by using the second and third terms, which yields:

$$R_s \sim U_\infty U_s \frac{d\delta}{dx} \quad (17)$$

It is immediately obvious how the equilibrium similarity approach yields a different and more general result than the classical approach, where it is *assumed* without justification that $R_s = U_s^2$ (c. f., Tennekes and Lumley, 1972).

The same equilibrium similarity hypothesis can be applied to the component Reynolds stress equations; namely that all of the bracketed terms should remain proportional (i.e., have the same x-dependence). For example, inserting eq. (8) into eq. (4) yields after some elementary calculus that equilibrium similarity can be maintained only if:

$$\frac{\delta}{K_u}\frac{dK_u}{dx} \sim \frac{d\delta}{dx} \sim \frac{T_u \delta}{U_\infty K_u} \sim \frac{D_u \delta}{U_\infty K_u} \sim \frac{\nu}{U_\infty \delta} \quad (18)$$

Similar relations arise from the other component equations.

All of these relations *cannot* simultaneously be satisfied given the constraints already placed on U_s, δ, and R_s from the mean momentum equation. On the other hand a solution is

[1] Note that the symbol $\sim$ has nothing to do with order of magnitude in this paper.

possible if the viscosity is identically zero, since then all terms involving the viscosity fall out of the problem. And also a solution for finite viscosity is possible if it can be shown that the production term in the Reynolds shear stress equation, $\overline{v^2}\partial U/\partial y$, is negligible relative to the leading terms in the equation.

It will be demonstrated below that these are in fact limiting solutions for very large turbulence Reynolds number, and for very low turbulence Reynolds number. Note that the latter solution should *not* be confused with the laminar solution, but instead identified with turbulent flow for which the velocity spectra do not have a developed $k^{-5/3}$ range. And by contrast, the high Reynolds number limit will be a flow which does have an easily apparent inertial subrange in the spectra. Further it will be demonstrated that no matter how high the Reynolds number of the drag-producing device, say $R_\theta = U_\infty\theta/\nu$, the diminishing local Reynolds number will move the equations (and the solutions as well) from one regime to the other.

The Infinite Reynolds Number Solution and its Limitations

A solution having the same x-variation as the classical solution can be derived by setting the viscous terms in eq. (11) to (15) exactly equal to zero, which corresponds to the limiting solutions at infinite Reynolds numbers. It is straightforward to show (in the same manner as George, 1995) that all of the remaining constraints can be satisfied. Of particular interest are the following:

$$\frac{d\delta}{dx} \sim \frac{D_u\delta}{U_\infty K_u} \tag{19}$$

$$K_u \sim K_v \sim K_w \sim U_s^2 \tag{20}$$

$$D_u \sim D_v \sim D_w \sim U_s^3/\delta \tag{21}$$

The scaling for the dissipation is just what one should expect for an infinite Reynolds number solution where the dissipation is completely controlled by the energetic turbulence (i. e., $\epsilon \propto u^3/l$ in the usual notation of texts).

It follows immediately after some manipulation that:

$$\frac{\delta_*}{\theta} = a\left[\frac{x-x_o}{\theta}\right]^{1/3} \tag{22}$$

$$\frac{U_s}{U_\infty} = b\left[\frac{x-x_o}{\theta}\right]^{-2/3} \tag{23}$$

where $a = a(*)$, $b = b(*)$, and $x_o = x_o(*)$ is a virtual origin. This is, of course, the classical solution with but a single difference – the dependence of the coefficients on upstream conditions, $*$. This possible dependence must be acknowledged, since there is nothing in the equations themselves to suggest independence of upstream conditions. The mean velocity profile, on the other hand, can be shown to be independent of upstream conditions. This is achieved by incorporating a factor of $[R_s/(U_\infty U_s)\, d\delta/dx]$ into the definition of g so that there are no parameters at all in eq. (11).

Now it was noted in the introduction that the cube root solutions simply do not account for most of the data, and especially the careful data of Cannon (1991). So where might the problem be? It is easy to show that, unlike most other free shear flows, this infinite Reynolds number solution contains the seeds of its own destruction. The *local* Reynolds number, $R = U_s\delta/\nu$, controls the relative importance of the viscous terms in the mean moment and Reynolds shear stress equations. Substitution of eq. (22) and (23) into the definition of R yields:

$$R = \frac{U_s\delta_*}{\nu} = \frac{U_\infty\theta}{\nu}\left[\frac{x-x_o}{\theta}\right]^{-1/3} \tag{24}$$

Thus, no matter how large the initial Reynolds number, R_θ, eventually far enough downstream it is diminished until the viscous terms can no longer be neglected. And if the viscous terms are not negligible, the infinite Reynolds number similarity solution cannot be even approximately true.

The Low Re Solution

As noted above, there is another equilbrium similarity solution to the same set of equations. The difference is that this time the terms involving viscosity are kept. This produces one additional constraint:

$$\frac{d\delta}{dx} \sim \frac{\nu}{U_\infty\delta} \tag{25}$$

It is extremely important to note that even though some of the relations are the same (e.g., K_u/U_s^2 = constant), the constants of proportionality (or more properly, the parameters of proportionality since they all depend on $*$) are most likely different from those governing the infinite Reynolds number solution.

There is one problem which at first glance appears to be quite serious. All of the constraints in the Reynolds shear stress equation cannot be met, in particular the one arising from the production term, $\overline{v^2}\partial U/\partial y$. These offending terms in fact die off with distance downstream faster than the remaining terms in the equation. Therefore, they can also be neglected in the analysis.

It is straightforward to show that eq. (25) can be integrated to obtain:

$$\frac{\delta_*}{\theta} = c\, R_\theta^{1/2} \left[\frac{x - x_{oo}}{\theta}\right]^{1/2} \tag{26}$$

$$\frac{U_s}{U_\infty} = d\, R_\theta \left[\frac{x - x_{oo}}{\theta}\right]^{-1} \tag{27}$$

where as before $c = c(*)$, $d = d(*)$, and $x_{oo} = x_{oo}(*)$ is a virtual origin which may be different than the one obtained above. And as for the infinite Reynolds number solutions, the mean velocity profile can be shown to be independent of upstream conditions. It is easy to show that the local Reynolds number continues to fall with increasing distance downstream; hence the approximations improve with distance downstream.

A solution for moderate Reynolds numbers

Unfortunately, as is clear from the data presented earlier, most of the experimental data is between the two limiting solutions. Hence neither alone describes the data well. Intermediate asympotics, however, offers the possibility of bridging the gap. The easiest way to understand what is required is to note the appearance of the similarity scaling functions for the dissipation; namely D_u, D_v and D_w. As noted above, for the high Reynolds number solutions, $D_u \sim U_s^3/\delta \sim U_s K_u/\delta$, while for the low Reynolds number solutions, $D_u \sim \nu U_s^2/\delta^2 \sim \nu K_u/\delta^2$. This is exactly the kind of behavior that has long been accounted for by turbulence modelers.

The simplest intermediate asymptotics solution which accounts for both the high and low Reynolds number dissipation limits is simply their sum. Assume then that:

$$D_u = \alpha \frac{U_s K_s}{\delta} + \beta \frac{\nu K_u}{\delta^2} \tag{28}$$

Then applying the similarity constraints yields:

$$\frac{d\delta}{dx} = \left\{ \alpha \frac{U_s K_s}{\delta} + \beta \frac{\nu K_u}{\delta} \right\} \frac{\delta}{U_\infty K_u} \tag{29}$$

After some manipulation this reduces to:

$$\frac{d\delta}{dx} = \alpha \left(\frac{\theta}{\delta}\right)^{-2} + \beta \left(\frac{\theta}{\delta}\right)^{-1} \tag{30}$$

This can be integrated directly to obtain δ/θ as a function of x/θ.

Figure 1 shows the Cannon (1991) and Menut et al. (2000) data and the integral of eq. (30) where the coeffients have been determined by optimization techniques. The theory describes the data remarkably well, and also makes understandable Cannon's difficulties in making sense of it.

CONCLUSIONS

The conclusions that can be drawn are that the initial conditions dominate the axisymmetric wake. The effect of initial conditions shows up in growth rate and higher moments, see George (1989). Local Reynolds number effects are also very important since it goes down as the flow evolves. This accounts for deviations from simple power law behaviour of the growth rate. Simple power laws are only reached in the limits $Re \to \infty$ and $Re \to 0$.

REFERENCES

Cannon, S. C., 1991, "Large-scale structures and the spatial evolution of wakes behind axisymmetric bluff bodies," Ph.D. Thesis, Dept. of Aerosp. and Mech. Engr., Univ. of Arizona.

Cannon, S., Champagne, F., and Glezer, A., 1993, "Observations of large-scale structures in wakes behind axisymmetric bodies," *Experiments in Fluids*, Vol. 14, pp. 447–450.

George, W. K., 1989, "The self-preservation of turbulent flows and its relation to initial conditions and coherent structures," *Advances in Turbulence*, George, W. K. and Arndt, R., ed., pp. 39–73.

George, W. K., 1995, "Some new ideas for similarity of turbulent shear flows," *Turbulence, Heat and Mass Transfer* Hanjalic, K. and Pereira, J. C. F., ed., Begell House, N.Y.

Menut, P., Delville, J., and Charnay, G., 2000, "Drag transition effect on the turbulent wake of an axisymmetric bluff body," *Submitted for publication.*

Tennekes, H. and Lumley, J. L., 1972, *"A First Course in Turbulence,"* The MIT Press.

Wygnanski, I. J., Champagne, F. H., and Marasli, B., 1986, "On the large scale structures in two-dimensional, small-deficit, turbulent wakes," *Journal of Fluid Mechanics*, Vol. 168, pp. 31–71, 1986.

Paper 2

Proper orthogonal decomposition of an axisymmetric turbulent wake behind a disk

In press, Physics of Fluids,
volume 14, number 6, 2002.

P. B. V. Johansson
W. K. George
S. H. Woodward

Proper orthogonal decomposition of an axisymmetric turbulent wake behind a disk

Peter B.V. Johansson and William K. George
Dept. of Thermo and Fluid Dynamics
Chalmers University of Technology
SE-412 96 Gothenburg, Sweden

Scott H. Woodward
Dept. of Mechanical and Aerospace Engineering
University at Buffalo
Buffalo, NY 14260, USA
(Dated: February 6, 2002)

A Proper Orthogonal Decomposition (POD) study of the axisymmetric turbulent wake behind a disk has been performed using multi-point hot-wire data. The Reynolds number based on the free stream velocity and disk diameter was kept constant at 28,000. The investigated region spanned from 10 to 50 disk diameters downstream. The hot-wire data was obtained using two rakes: a seven wire fixed array and a six wire array azimuthally traversable to span the cross-section of the flow in increments of 15°. The instantaneous streamwise velocity component data was Fourier transformed in time and decomposed in Fourier series in the azimuthal direction to form the kernel for the POD.

For all downstream positions, two distinct peaks were found in the first eigenspectrum: one at azimuthal mode-2 at near zero frequency, and another at azimuthal mode-1 at a fixed Strouhal number (fd/U_∞) of 0.126. Both peaks decrease in magnitude as the flow evolves downstream, but the peak at the Strouhal number 0.126 decreases more rapidly then the one at near-zero frequency, leaving the latter to eventually dominate. Because of this evolution, the eigenvalues integrated over frequency show an azimuthal mode-1 dominance at $x/D = 10$ and a mode-2 dominance by $x/D = 50$. The results are compared to those recently obtained in the axisymmetric far jet, and the results of previous wake investigations.

I. INTRODUCTION

The turbulent wake behind an axisymmetric object such as a disk or a sphere has been under investigation for almost a century. This flow is of considerable practical importance because of its close relation to many aero- and hydrodynamic applications. In addition, it is of fundamental importance since it is one of the few shear flows where the local turbulence Reynolds number decreases as the flow evolves. Also, the equations of motion governing the axisymmetric wake contain all of the important dynamical terms for turbulent flow away from surfaces. Hence the data from this flow form an important data base for developing turbulence models of all types.

Early experiments on the fundamental features of this flow focused on the far wake. One pioneering study was made by Hwang and Baldwin[1], who measured turbulence intensities and wake growth for a large span of downstream locations, $x/d = 5$ to $x/d \approx 900$. Because the high demands on equipment could not be met at this time, there was severe scatter in their data; and they even reported difficulties in reproducing their own results on a day-to-day basis. More recently, researchers have primarily focused on the early development of the wake or on its stability[2–5]. An exception was the careful far wake measurements of Cannon[6] and Cannon, Champagne and Glezer[7], who found very different results depending on the wake generator used. Intriguingly, they were unable to resolve satisfactorily whether the classical similarity theory applied, a subject addressed in detail by Johansson and George[8].

The large scale, 'coherent' features of this flow have been investigated by means of flow visualization, multi-point, phase averaging and conditional sampling techniques[7,9–15]. These findings have contributed to our understanding of the process of vortex formation behind the generator. There have also been discussions about the randomness and anti-phase characteristics of vortex structures behind axisymmetric bodies. Most interestingly in context of the present work, Fuchs *et al.*[10] used two hot-wires to measure cross-spectra at a single radius of the near wake. This radius varied from $r/D = 0.75$ at $x/D = 3$ to $r/D = 0.83$ at $x/D = 9$. The angular separation of the probes was varied in steps of 30°, and the measured cross-spectra were decomposed into Fourier series in the azimuthal direction. The azimuthal modal content was then studied at the frequencies that were found to be eventful. At $x/D = 9$, Fuchs *et al.*[10] found a strong azimuthal mode $m = 1$ peak in the coherence spectrum at the natural Strouhal number $S_n = f_n D/U_\infty = 0.135$. They also found a distinct peak at azimuthal mode $m = 2$ at a near-zero frequency ($S_2 = 0.005$; Figs. 9–11 of their paper). There was no suggestion, however, that $m = 2$ was the dominant mode, nor is it found to be so in our study until much further downstream (Fig. 7 in this paper).

The first of these results was confirmed by Berger *et al.*[11], who also found the $m = 1$ peak, but they did not

report any $m = 2$ peak. This was a curious omission, since it is clearly present at low frequency in their coherence spectra, Fig. 4 ($x/D = 9$, $r/D = 0.83$, disk at rest) and Fig. 6 ($x/D = 6$, $r/D = 0.83$, nutating disk) of their paper, exactly as noted by Fuchs *et al.*[10]. Instead, they focus on the $m = 1$, $S_n = 0.135$ peak, and interpret this near wake result as a helical vortex structure. From here on, nothing is mentioned in the literature about the occurrence of azimuthal mode $m = 2$, and it has been presumed until now that azimuthal mode $m = 1$ is the most dominant. This is also the result obtained from the linear parallel stability analysis of Monkewitz[4], and the non-linear dynamical systems approach by Ghidersa and Dušek[5].

Because of the small velocity deficit, the very low turbulence intensities, and the slow decay of the velocity deficit downstream, the far axisymmetric wake still is at the threshold of what is possible to measure using even the best wind tunnels and the most stable low-noise anemometer equipment. The work reported here is part of a continuing effort to measure and understand this flow. In the present work, the evolution of the wake is studied using a so-called 'slice' version of the Proper Orthogonal Decomposition (POD) technique. The term 'slice POD' refers to decomposing the flow field at fixed downstream locations in the remaining cross-stream coordinates. This method has been previously applied to the jet mixing layer[16–18] and far jet[19] to quantify the energetics of the POD modes.

II. EXPERIMENTAL SETUP

The experiments were performed in the low-turbulence wind tunnel at Chalmers University of Technology, Gothenburg, Sweden. The free-stream streamwise turbulence intensity over the span of velocities related to this work was less than 0.03%. The measuring cross-section in the tunnel is 1.80×1.25 m^2 and the downstream length is 3.00 m. Special attention was made to avoid flow blockage by the wake generator. The disk used had a diameter of 28 mm, and was suspended with four pairs of wires, each with the diameter 0.2 mm. The total area ratio between the object and tunnel cross-section was less then 0.03%. The tunnel velocity was kept constant at 15 m/s during the experiment, resulting in a Reynolds number based on the free stream velocity and disk diameter of 28,000.

A total number of 13 hot-wires were used in the two arrays as shown in Fig. 1. The arrays were used in the same manner as Glauser and George[17] to obtain the two-point velocity cross-spectra for all combinations of locations shown in Fig. 2. The measurement grid was chosen following Glauser and George[20], so as to provide an optimum resolution to apply the POD. The upper array of probes was movable, and traversed from a 15° separation up to 180° with 15° increments in $\Delta\theta$, see Fig. 2. Each hot-wire probe is numbered and marked by a circle. The

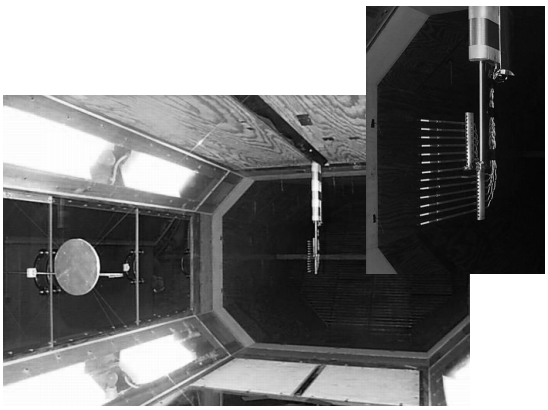

FIG. 1: The probe array and disk in the Chalmers wind tunnel.

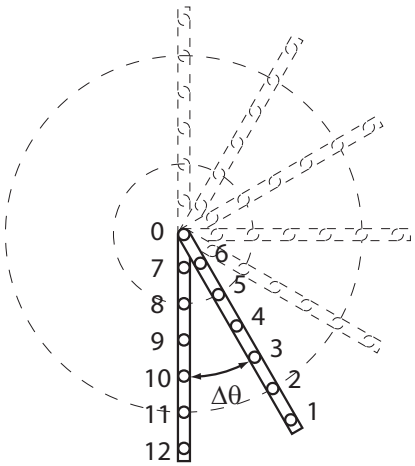

FIG. 2: The traversing scheme, shown in 30° increments in $\Delta\theta$ for simplicity.

angle separation $\Delta\theta = 135°$ could not be measured directly, since the movable probe rake caught the wake of the suspending wires. Instead, measurements at the angles 130° and 140° were used to estimate this position. In all, half the cross-section of the wake at a fixed downstream position was scanned, and pairs of instantaneous velocity cross-spectra for a fixed angle separation computed. Note that the cross-spectra corresponding to the remaining half-plane were available from the azimuthal symmetry of the flow.

Each single hot-wire, 3 mm long and made of unplated 5 μm tungsten wire, was oriented to measure the streamwise component of the velocity. The probes were connected to an AN2000 Constant Temperature Anemometer (CTA) system, and sampled with an IO Tech Wavebook 516 16 bit sample and hold A/D converter. The data was low-pass filtered at 2 kHz and sampled at 6 kHz for all configurations, substantially higher than required by the temporal Nyquist criterion. Measurements were made simultaneously at all 13 positions. Each block

had 8192 samples, and a total of 300 blocks of data was taken per probe for each angular probe location, ensuring a variability of less than 6% for the cross-spectra used in the POD.

III. PROPER ORTHOGONAL DECOMPOSITION

The POD, a well-known mathematical technique which appears under several other names as well (e.g., Singular Value Decomposition, Karhunen-Loève Decomposition, Principal Value Analysis), was introduced to the study of turbulence by Lumley[21]. The mathematical aspects are very well described elsewhere (e.g.,[18,19,22,23]), so we will very briefly point out only the most essential features and focus on the actual procedure used in this work to analyze the data.

The core of the POD is a projection of the velocity field, u_i, into a coordinate system, ϕ_i, optimal in terms of energy; i. e., maximizing

$$\frac{< (u_i, \phi_i)^2 >}{||\phi_i||} = \lambda \tag{1}$$

This can be shown by calculus of variations to result in the following integral equation:

$$\int_D R_{i,j}(\cdot, \cdot')\phi_j(\cdot')r'\, d(\cdot') = \lambda\phi_i(\cdot) \tag{2}$$

where the kernel, $R_{i,j} =< u_i(\cdot)u_j(\cdot') >$, is the two-point velocity correlation tensor and $(\cdot)$ represents the spatial coordinates and time, or a subset of these.

If the field has finite total energy, Hilbert-Schmidt theory assures that the solution exists and consists of a denumerable, infinite, set of eigenvalues, $\lambda^{(n)}$, and corresponding eigenfunctions, $\phi_i^{(n)}$. For an axisymmetric shear flow such as a jet or a wake, this is true in the radial direction at a single downstream location, hence the term 'slice POD'.

The modes are ordered so that the first mode contains most of the energy, and the relation between the kinetic energy and the eigenvalues is given by:

$$E = \int_D u_i(\cdot)u_i^*(\cdot)\, d(\cdot) = \sum \lambda^{(n)} \tag{3}$$

The axisymmetric wake in question is *stationary* in time and *periodic* in the azimuthal direction. Therefore, the Hilbert-Schmidt theory does not apply, but the POD-modes in these directions can be shown to be Fourier modes, see George[24].

If only the streamwise velocity component at a fixed downstream location is considered (i. e., $i = j = 1$), the following integral equation(s) must be solved:

$$\int_0^\infty B_{1,1}(m, f, r, r'; x)\psi_1^{(n)}(m, f, r'; x)r'\, dr' = \lambda^{(n)}(m, f; x)\psi_1^{(n)}(m, f, r; x) \tag{4}$$

where $B_{1,1}(m, f, r, r'; x)$ is the two-point velocity correlation Fourier transformed in time and expanded in Fourier series in the azimuthal direction, the $\psi_1^{(n)}(m, f, r; x)$ are the eigenfunctions, and $\lambda^{(n)}(m, f; x)$ the corresponding eigenspectra.

In practice, the following steps are taken (following Glauser and George[17]):

1. Measurement of the instantaneous velocity at two points.
2. Fourier transformation in time and computation of the cross-spectrum.
3. Repetition of 1. and 2. for many pairs of points.
4. Expansion of the cross-spectra obtained in 2. in Fourier series in the azimuthal direction.
5. Solution of the remaining eigenvalue problem (in the radial direction), equation 4 for each frequency and azimuthal mode number.

Note that this procedure is different than that implemented by Citriniti and George[18] and Gamard *et al.*[19], since in their experiments the velocity at all grid points was obtained simultaneously using a 138-wire probe. Here, only pairs of points were available for the given rake positions, so the procedure had to be repeated as the movable rake was rotated through the entire 180°. This is exactly the procedure used by Glauser and George[17] in an earlier jet mixing layer study.

IV. STATISTICAL RESULTS

In order to ensure the reliability of the data before performing the POD, first and second order statistical properties were analyzed. Mean velocity profiles, scaled by the tunnel velocity, U_∞, for the three downstream locations are shown in Fig. 3. The velocity deficit ranges from around 9% of the free-stream velocity at $x/D = 10$, to about 2% at $x/D = 50$. The left hand side of the plot (negative r) corresponds to the fixed array of probes, and the right hand side (positive r) the movable. These clearly show one of the main difficulties measuring this flow using hot-wires: the velocity deficit is very small, and thus extremely sensitive to the accuracy of the measuring device. These multi-point measurements extended typically over 8-10 hours because of the many cross-spectra needed ($7 \times 7 \times 13$), thus the data are very much affected by any drift in the anemometers (primarily associated with thermal instability of the D.C. offset amplifier). The thermal drift problems with the CTA usually shows up as a calibration error, and is probably the reason most previous researchers interested in the mean profiles have used Pitot-tubes. A separate contribution to the systematic variation in the data is the problem

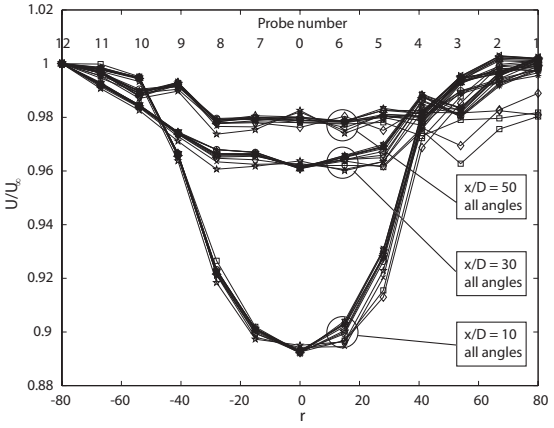

FIG. 3: Mean velocity profiles, U/U_∞, x/D = 10, 30 and 50. $\Delta\theta$ = 15,30,...,180°.

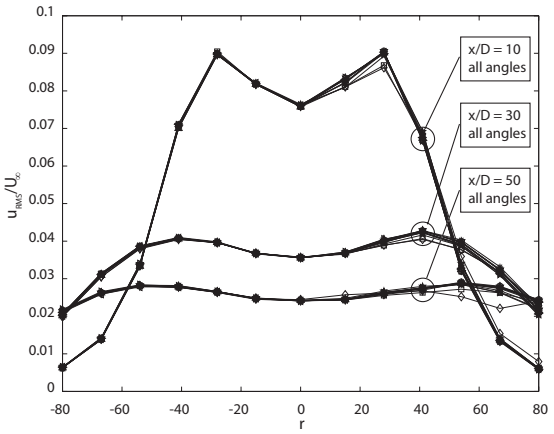

FIG. 4: Turbulence intensity profiles, x/D = 10, 30 and 50. $\Delta\theta$ = 15,30,...,180°.

of aligning the arrays of probes to the wake center. Unlike earlier investigations which used only at most a single linear rake, these errors are more obvious here because of the movable array of probes (i.e., positive r), and show up as an increased spread of data. Nevertheless, the overall quality of the data compare favorably with those of Cannon[6], for example. The mean velocity profile at $x/D = 50$ around the angle 135° is also clearly affected by interference from the wakes of the wires supporting the disk. This data was replaced in the POD calculations by the average of the spectral values at 130° and 140°.

Root mean square velocity profiles were computed and a plot covering all angles and downstream positions is reproduced in Fig. 4. The turbulence intensities, $\sqrt{\overline{u^2}}/U_\infty$, are very small, from 9% at $x/D = 10$ to below 3% at $x/D = 50$. But here, the situation is entirely different from that for the mean velocity; the thermal drift in the anemometers is clearly not affecting the fluctuating velocities. This is because even though the anemometer output voltage was drifting slowly (due to the D.C. offset amplifier), the slope of the calibration curve near the tunnel velocity at which the data was obtained remained nearly constant. (This was confirmed by repeated recalibrations during the experiment.) Thus the fluctuating velocities for these very low turbulence intensities are correctly measured. The consequence of not being able to exactly center the probe rake can still be seen in the right hand side of the plots. As with the mean velocity profiles at $x/D = 50$, the support wire wake has grown enough so that the results from angle 135° are affected by it.

Power spectral densities were computed for all downstream positions as well as rotations of the movable rake. Fig. 5 shows the PSD's at x/D = 10, 30, and 50, respectively, for the probe rake separation $\Delta\theta = 180°$. All PSD's off the center of the wake show a prominent peak at 67 Hz, corresponding to a Strouhal number ($St = fd/U_\infty$) of 0.126. This is consistent with Strouhal number measured by Miau *et al.*[13] in the near wake. The magnitude of this peak decreases with increased downstream position, but is still clearly visible at $x/D = 50$. From the absence of this peak in the center of the wake, one can immediately infer that this type of motion, a very dominant feature of the PSD, can not be related to an azimuthal mode-0 motion.

V. POD RESULTS

A. Eigenspectra, $\lambda^{(n)}(m, f; x)$

Eigenspectra were computed for the three downstream locations by solving Eq. 4 to obtain the distribution $\lambda^{(n)}(m, f; x)$. Even this simple result from the POD provides a large amount of information regarding the overall energy distribution in the flow, and the results can be viewed from many perspectives. Several of these will be presented below.

The eigenspectra, $\lambda^{(n)}(m, f; x)$, are representations of how the energy is distributed as function of azimuthal mode number, m, and frequency, f, at a given downstream position, x. Therefore their evolution show how the main characteristics of the flow evolve. Three-dimensional and contour plots of the eigenspectra for the first POD mode ($n = 1$) are presented in Fig. 6 for the three downstream positions covered in this study. The three pictures are strikingly similar and the general features do not evolve with downstream distance. The energy is concentrated around two separate peaks in the f-m plane. One is at near-zero frequency for azimuthal mode $m = 2$ and the other for azimuthal mode $m = 1$ at a higher frequency, 67 Hz. This second peak for $m = 1$ corresponds to a Strouhal number of 0.126. This Strouhal number does not change with downstream position, and is exactly the same as the one detected in the PSD's off the wake center described in the previous

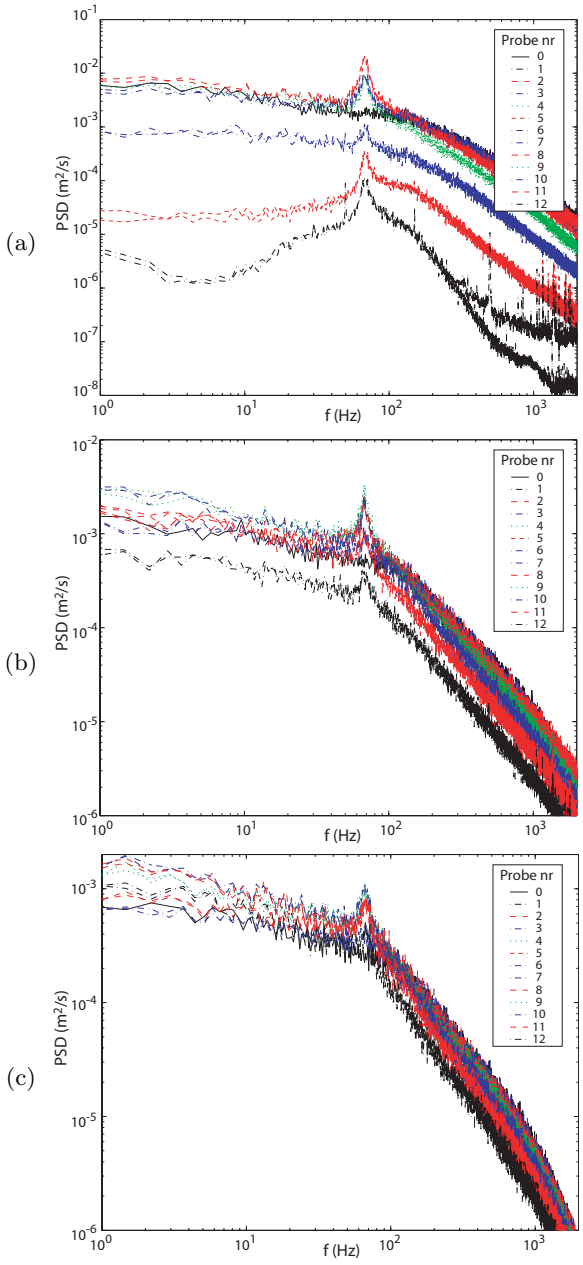

FIG. 5: Power spectral densities, $\Delta\theta = 180^\circ$ for all probes at different downstream positions: (a) $x/D = 10$, and (b) 30, (c) 50.

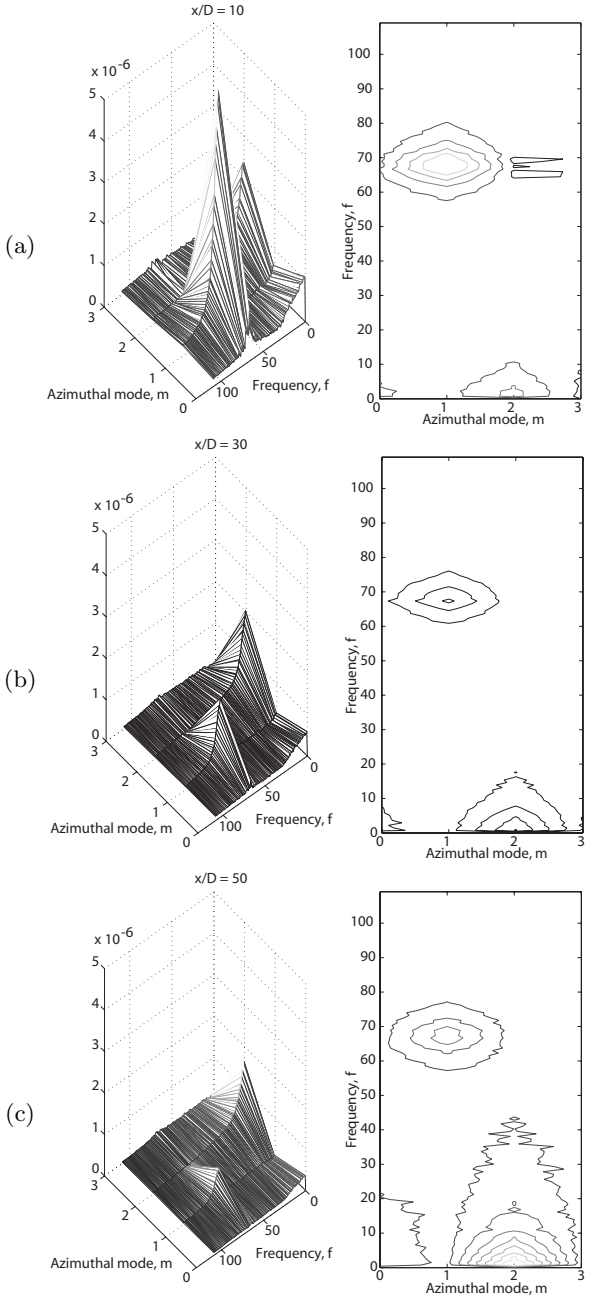

FIG. 6: Eigenspectrum function of azimuthal mode number (m) and frequency (f) at different downstream positions: (a) $x/D = 10$, and (b) 30, (c) 50.

section. The magnitude of these peaks decreases as the flow evolves. It is also clear that the peak at $m = 1$ is largest at $x/D = 10$, but decreases more rapidly than the $m = 2$ peak, leaving the latter the largest by $x/D = 50$. From these pictures, it is not at all clear what role $m = 0$ plays. It does not seem to be directly connected to a specific frequency.

Our results at $x/D = 10$ can be compared to those of Fuchs *et al.*[10]. They did not use the POD, but measured cross-spectra only at a single radius of the near wake as noted in the introduction. At $x/D = 3$, they found a strong azimuthal mode $m = 1$ peak in the coherence spectrum at the natural Strouhal number $S_1 = f_n D/U_\infty = 0.135$. Their Reynolds number was 50,000, which explains the higher Strouhal number than in the present work where $Re = 28,000$, but fully consistent with the results of Miau *et al.*[13] Higher azimuthal modes were all of the same order and small compared to the dominating one. At $x/D = 9$, however, the $m = 1$

peak was still dominant (at $S_1 = 0.135$), but they also found a distinct peak at azimuthal mode $m = 2$ at a near-zero frequency ($S_2 = 0.005$; Figs. 9–11 of their paper). Their Fig. 9 also contains data of Roberts[9], which agrees very well. These results are consistent with our findings at $x/D = 10$ as seen in Fig. 6a; namely that the largest peak in $\lambda^{(1)}$ is at $m = 1$, $f = 67$ Hz, whereas the peak at $m = 2$, $f \approx 1$ Hz is smaller.

Our findings that mode 2 comes to dominate farther downstream appear to be new. These cannot yet be corroborated by the measurements of others, since none exist beyond those cited earlier. And none exist at all beyond $x/D = 10$.

B. Eigenspectra integrated over frequency, $\xi^{(n)}(m;x)$

The eigenspectra can be integrated over frequency to illustrate another key property of the POD, its ability to show how the kinetic energy of the flow is distributed among the various azimuthal modes. To visualize the energy distribution per azimuthal mode number, m, we computed for each downstream position the quantity $\xi^{(n)}(m;x)$ where:

$$\xi^{(n)}(m;x) = \frac{\int_f \lambda(m,f;x)\,df}{\sum_m \int_f \lambda(m,f;x)\,df} \tag{5}$$

Here, the denominator is the total kinetic energy, as defined in Eq. 3. The resulting normalized eigenspectra, $\xi^{(n)}(m;x)$ are plotted in Fig. 7. Since the flow field is homogenous in time (stationary) as well as in the azimuthal direction (periodic), this immediately imposes that the eigenspectrum, $\lambda^{(n)}(m,f;x)$, is symmetric with respect to these directions; i.e. $\lambda^{(n)}(m,f;x) = \lambda^{(n)}(-m,-f;x)$ (see Lumley[21]). When integrating over frequency, to obtain $\xi^{(n)}(m;x)$ according to Eq. 5, it is easy to show that $\xi^{(n)}(m;x)$ are also symmetric in m. Therefore, only positive m are shown in Fig. 7. From these, it is clear that at $x/D = 10$, most of the energy lies in the azimuthal mode $m = 1$, while at $x/D = 50$, the most energetic azimuthal mode is $m = 2$. At the intermediate position, both modes contain roughly the same fraction of the total energy. It is also clear that $m = 0$ is the third most important azimuthal mode.

The overall behavior is strikingly similar to the results of Gamard *et al.*[19] in the axisymmetric jet. In the jet, however, mode 2 becomes dominant by the end of the potential core ($x/D = 6$), whereas here mode 2 does not dominate until $x/D = 50$. This is, perhaps, related to the much higher turbulence intensity in the jet and its faster spreading rate. It might be noted that since $m = 2$ also dominates at low frequencies at large enough distance downstream in the jet of Gamard *et al.*[19], suggesting strongly that this is a natural feature of these very different flows, and not related to the facility.

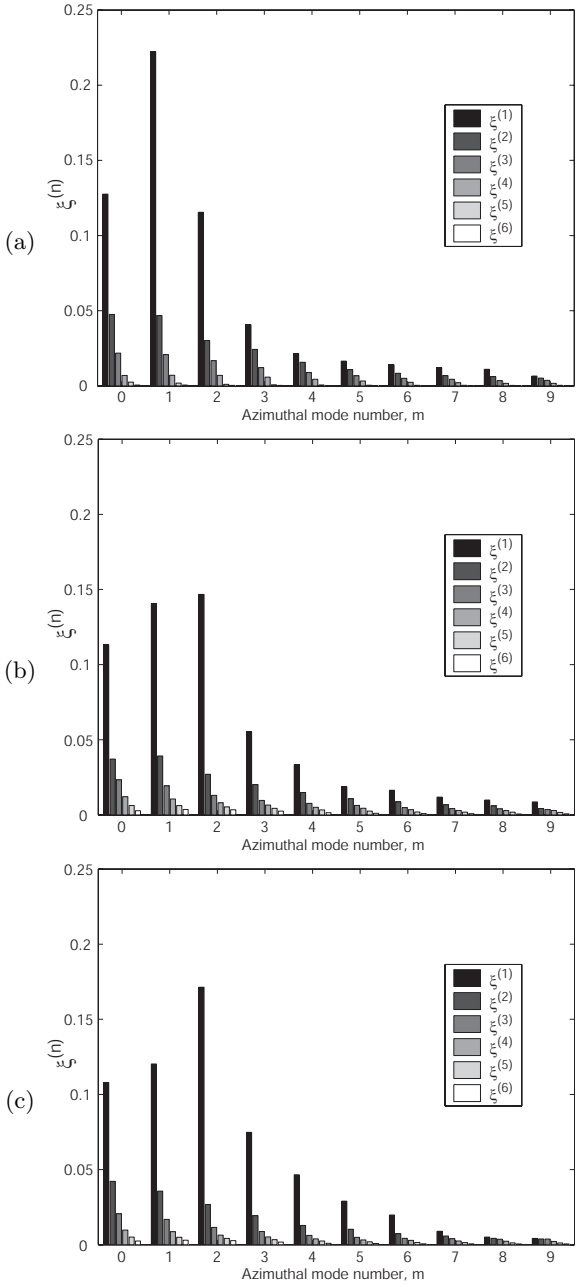

FIG. 7: Eigenspectra integrated over frequency as function of azimuthal mode number (m) at different downstream positions: (a) $x/D = 10$, and (b) 30, (c) 50.

VI. TAYLOR'S HYPOTHESIS AND INTERPRETATION OF FREQUENCY

So far in this paper, we have used the commonly adapted notation and presented our results concerning spectral content as a function of frequency, exactly as measured. In order to physically interpret the results, however, it is necessary to distinguish between spatial and temporal structures. In other words, we must sort

out whether the observed 'frequency' represents a true unsteadiness, or should be interpreted as a 'wavenumber' using Taylor's frozen field hypothesis[25]. In the far axisymmetric wake, the mean velocity deficit between the free stream and the center of the wake is small, varying from 10% at $x/D = 10$ to 2% at $x/D = 50$ as depicted in Fig. 3. Thus the mean velocity gradient is also very small, as is the turbulence intensity which is of the same order as the mean velocity differences (see Fig. 4). Thus the convection velocity can be approximated by the free stream (or equally well, the centreline) velocity.

These together, according to all the criteria in Lumley[25], imply that for all but the very lowest frequencies, Taylor's hypothesis is valid. Thus, the peak at 67 Hz must be interpreted as a frozen turbulence field that is convected by with the wavelength $\lambda = U_c/f = 0.22$ m. Even so, this 'wavelength' can still arise from vortex shedding at the wake generator, since the disturbances generated there will be swept by the probe at approximately the free stream velocity, thereby yielding the same Strouhal frequency.

The situation is much less clear for mode 2 which has a near-zero frequency peak at approximately 1 Hz, since all the fundamental criteria for Taylor's hypothesis are violated. Interpretation as a convected disturbance would suggest a disturbance 15 m long! This is clearly unphysical, and consistent with the breakdown of Taylor's hypothesis at this low frequency. It is thus more likely that the mode 2 disturbance is related to a temporal variation of the wake itself. For example, one possibility might be a mode 2 distortion of the mean velocity, which itself precesses slowly. Clearly, multipoint measurements in the downstream and cross-stream directions simultaneously are required to sort this out.

VII. SUMMARY AND CONCLUSIONS

The axisymmetric turbulent wake behind a disk was studied using a 'slice POD' for three fixed downstream cross-sections of the flow. For all downstream positions, two distinct peaks were found in the first eigenspectrum: one at azimuthal mode $m = 1$ at at a fixed Strouhal number (fd/U_∞) of 0.126, and another at azimuthal mode $m = 1$ at near-zero frequency. Both peaks decrease in magnitude as the flow evolves downstream, but the peak at $m = 1$ decreases more rapidly then the one at $m = 2$, leaving the latter to eventually dominate. Because of this evolution, the eigenvalues integrated over frequency show an azimuthal mode-1 dominance at $x/D = 10$ and a mode-2 dominance by $x/D = 50$. The $m = 1$ peak can be associated with a 'structure' of frozen turbulence that is convected downstream. The $m = 2$ peak clearly is not a convected disturbance.

Despite being two different flows, the axisymmetric wake and the jet share many common features, in particular the mode 2 dominance asymptotically. It is reasonable to expect that the modes in these two flows can behave the same only if they are governed by similar equations, whatever they might be. By projecting the Navier-Stokes equations onto the POD basis functions, Lumley[21] showed that the linearized leading order equations reduce to the Orr-Sommerfeld equations (for the appropriate coordinate system). Thus it is reasonable to anticipate similarities between the POD decomposed measurements and linear stability analyses. Linear parallel stability analysis by Monkewitz[4] as well as the non-linear dynamical systems approach by Ghidersa and Dušek[5] have shown that azimuthal mode $m = 1$ is the fastest growing. At this stage, no analysis has suggested that mode 2 might be the most important. It still might be possible, however, that a non-linear and/or non-parallel stability analysis can predict the eventual dominance of mode-2, and as well explain the similarity between the eigenspectra presented here and those taken in the axisymmetric jet by Gamard *et al.*[19].

VIII. ACKNOWLEDGEMENTS

One of us (WKG) in 1968 joined John L. Lumley at the Pennsylvania State University, with the hope of initiating a POD study of the axisymmetric wake. Fate led our joint work there in other directions, but a fascination for Lumley's POD remained. Now, thirty-three years later, it is with no small measure of satisfaction that these results are presented for the first time at a symposium honoring John L. Lumley. They are offered both as tribute and thank you for his inspiration, as well as for his many contributions to science.

This work was initially supported by the US Air Force Office of Scientific Research, grant number F49620-98-1-0143 and Chalmers University of Technology. It continues with the support of the Swedish Research Council, grant number 2641.

[1] N. C. H. Hwang and L. V. Baldwin. Decay of turbulence inaxisymmetric wakes. *Journal of Basic Engineering*, 88:261–268, 1966.

[2] E. Achenbach. Vortex shedding from spheres. *Journal of Fluid Mechanics*, 62:209–221, 1974.

[3] A. I. Sirviente and V. C. Patel. Experiment in the turbulent near wake of an axisymmetric body. *AIAA Journal*, 37(12):1670–1673, 1999.

[4] P. A. Monkewitz. A note on vortex shedding from axisymmetric bluff bodies. *Journal of Fluid Mechanics*, 192:561, 1988.

[5] B. Ghidersa and J. Dušek. Breaking of axisymmetry and onset of unsteadiness in the wake of a sphere. *Journal of Fluid Mechanics*, 423:33–69, 2000.

[6] S. C. Cannon. *Large-scale structures and the spatial evolution of wakes behind axisymmetric bluff bodies*. PhD thesis, Dept. of Aerosp. and Mech. Engr., Univ. of Arizona, 1991.

[7] S. Cannon, F. Champagne, and A. Glezer. Observations of large-scale structures in wakes behind axisymmetric bodies. *Experiments in Fluids*, 14:447–450, 1993.

[8] P. Johansson and W. K. George. On the effect of finite reynolds number and initial conditions on the axisymmetric wake. In *Turbulent Shear Flow Phenomena II*, Stockholm, June 27-29, 2001.

[9] J. B. Roberts. Coherence measurements in an axisymmetric wake. *AIAA Journal*, 11, no. 1:1569–1571, 1973.

[10] H. V. Fuchs, E. Mercker, and U. Michel. Large scale coherent structures in the wake of axisymmetric bodies. *Journal of Fluid Mechanics*, 93:189–211, 1979.

[11] E. Berger, D. Scholz, and M. Schumm. Coherent vortex structures in the wake of a sphere and a circular disk at rest and under forced vibrations. *Journal of Fluids and Structures*, 4:231–257, 1990.

[12] S. I. Lee and P. W. Bearman. An experimental investigation of the wake structure behind a disk. *Journal of Fluids and Structures*, 6:437–450, 1992.

[13] J. J. Miau, T. S. Leu, T. W. Liu, and J. H. Chou. On vortex shedding behind a circular disk. *Experiments in Fluids*, 23:225–233, 1997.

[14] A. E. Perry and T. T. Lim. Coherent structures in coflowing jets and wakes. *Journal of Fluid Mechanics*, 88:451–463, 1978.

[15] A. E. Perry and J. H. Watmuff. The phase-averaged large-scale structures in three-dimensional turbulent wakes. *Journal of Fluid Mechanics*, 103:33–51, 1981.

[16] M. N. Glauser. *Coherent Structures in the Axisymmetric Turbulent Jet Mixing Layer*. PhD thesis, State University of New York at Buffalo, 1987.

[17] M.N. Glauser and W.K. George. Orthogonal decomposition of the axisymmetric jet mixing layer including azimuthal dependence. In *Advances in Turbulence*, G. Comte-Bellot and J. Mathieu, editors, pages 357–366. Spring-Verlag, 1987.

[18] J. H. Citriniti and W. K. George. Reconstruction of the global velocity field in the axisymmetric mixing layer utilizing the proper orthogonal decomposition. *Journal of Fluid Mechanics*, 418:137–166, 2000.

[19] S. Gamard, D. Jung, S. Woodward, and W. K. George. Application of a 'slice' POD to the far field of an axisymmetric turbulent jet. *submitted to Physics of Fluids*, 2001.

[20] M. N. Glauser and W. K. George. Application of multipoint measurements for flow characterization. *Experimental Thermal and Fluid Science*, 5:617–632, 1992.

[21] J. L. Lumley. The structure of inhomogeneous turbulent flows. In *Atmospheric Turbulence and Radio Wave Propagation*, A. M. Yaglom and V. I. Tatarsky, editors, Moscow, USSR, 1967. Nauka.

[22] W. K. George. Insight into the dynamics of coherent structures from a proper orthogonal decomposition. In *Symposium on Near Wall Turbulence*, Dubrovnik, Yugoslavia, May 16-20 1988.

[23] P. Holmes, J. L. Lumley, and G. Berkooz. *Turbulence, Coherent Structures, Symmetry and Dynamical Systems*. Cambridge, 1996.

[24] W. K. George. Some thoughts on similarity, the POD, and finite boundaries. In *Trends in Mathematics*, Gyr and Tsinobe, editors, pages 117–128, Birkhauser, Sw, 1999.

[25] J. L. Lumley. On the interpretation of time spectra in high intensity shear flows. *Physics of Fluids*, 8:1056–1062, 1965.

Paper 3

Further studies of the axisymmetric disk wake
using the `slice POD'

Proceedings of the ASME Fluids Engineering Division
Summer Meeting, FEDSM2002-31411,
Montreal, Quebec, Canada, July 14-18, 2002.

P. B. V. Johansson
W. K. George

Proceedings of FEDSM'02
2002 ASME Fluid Engineering Division Summer Meeting
July 14-18, 2002, Montreal, Quebec, Canada

FEDSM2002-31411

FURTHER STUDIES OF THE AXISYMMETRIC DISK WAKE USING THE 'SLICE POD'

Peter B.V. Johansson
Turbulence Research Laboratory
Department of Thermo and Fluid Dynamics
Chalmers University of Technology
Gothenburg, SE-41296, SWEDEN
Email: jope@tfd.chalmers.se

William K. George
Turbulence Research Laboratory
Department of Thermo and Fluid Dynamics
Chalmers University of Technology
Gothenburg, SE-41296, SWEDEN
Email: wkgeorge@tfd.chalmers.se

ABSTRACT

This paper presents the findings of three experiments using multi-point hot-wire arrays in the high Reynolds number axisymmetric turbulent wake behind a disk. The purpose of the multiple experiments was to validate earlier and less extensive experiments. The 'slice POD' was applied to all sets to examine the effects of array coverage and the disk support system. The Reynolds number based on the free stream velocity and disk diameter was kept constant at 28,000. The investigated region spanned from 10 to 60 disk diameters downstream.

These results confirm the earlier findings. In particular, the eigenvalues integrated over frequency show a azimuthal mode-1 dominance at $x/D = 10$ which evolves to a mode-2 dominance by $x/D = 50$. For all downstream positions, two distinct peaks were found in the first eigenspectrum: one for azimuthal mode-2 at near zero frequency, and another for azimuthal mode-1 at a Strouhal number (fd/U_∞) of 0.126. Both peaks decrease in magnitude as the flow evolves downstream, but the peak at the Strouhal number 0.126 decrease more rapidly then the one at near-zero frequency, leaving the latter to eventually dominate.

INTRODUCTION

This is the second in a series of papers on the application of 'slice' POD techniques to the axisymmetric wake behind a circular disk. In the first paper (Johansson et al., 2002) the axisymmetric turbulent wake behind a disk was studied using a 'slice POD' for three fixed downstream cross-sections of the flow ($x/D = 10$, 30, and 50). For all downstream positions, two distinct peaks were found in the eigenspectrum of the lowest (and most dominant) radial POD mode: one for azimuthal mode-2 at near zero frequency, and another for azimuthal mode-1 at a fixed Strouhal number ($St = fd/U_\infty$) of 0.126. (Note that measured frequency should be interpreted as a streamwise wavenumber using $k_1 = 2\pi f/U_\infty$ for all frequencies except the very low ones to properly apply Taylor's hypothesis according to the criteria of Lumley, 1965.) Both peaks decreased in magnitude as the flow evolved downstream, but the peak at the Strouhal number 0.126 decreased more rapidly so the latter eventually dominated. The authors did deliberately not associate a Strouhal number with the 'near-zero' frequency, since it was found to be the lowest resolved non-zero frequency (0.73 Hz). When integrated over frequency and normalized by the total kinetic energy, it was seen that the first eigenspectrum accounted for more than 60% of the energy.

These were surprising findings, especially the evolution to azimuthal mode-2 far downstream which had not been previously observed. Fuchs et al. (1979) computed azimuthal cross-spectra using two hot-wires at a fixed radius in the wake, and found an azimuthal mode-2 peak at low frequency (St = 0.005). The investigation was limited to two positions downstream, x/D = 3 and 9, and mode-1 was found to be dominant at these positions. Brücker (2001) investigated the wakes behind a sphere and an axially oriented cylinder with an elliptic nose and a blunt base at low Reynolds numbers (up to Re = 1000), and stated that the results indicated a simultaneous existence of the primary instability causing the vortex shedding together with a long-wave instability (St = 0.05 for the sphere, and St = 0.03 for the cylin-

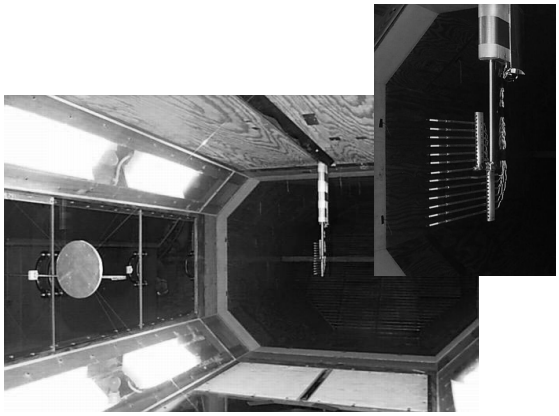

Figure 1. The probe array and disk in the Chalmers wind tunnel

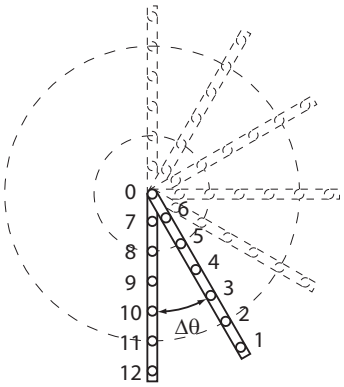

Figure 2. The traversing scheme, shown in 30° increments in $\Delta\theta$ for simplicity

der). He assumed that both of these were associated with an azimuthal mode-1 type of motion. It has long been suspected that there might be a connection between the theory for instability of laminar wakes (see e.g., Monkewitz, 1988) and the behavior of fully turbulent high Reynolds number wakes. The stability results are usually based on the Orr-Sommerfeld equations which are in turn derived from the linearized Navier-Stokes equations with parallel flow approximations. The results of such efforts suggest the emergence of azimuthal mode-1 as dominant, since it is the fastest growing disturbance. Therefore the emergence of mode-2 was quite unexpected. If true, it would seem to imply either that non-linearities must dominate, or non-parallel effects, or simply that such theories may not be relevant to turbulence at all. Regardless, the implications of the experimental POD results are so important that it is of paramount importance that they be confirmed to be true beyond all reasonable doubt, before significant effort is expended trying to explain them. This paper attempts to do that by:

1. Increasing the number of measuring locations.
2. Examining the influence of measurement locations with respect to the wake width.
3. Changing the support structure of the disk to alter any modal excitation by them.

EXPERIMENTAL SETUP

The experiments were performed in the low-turbulence wind tunnel at Chalmers University of Technology, Gothenburg, Sweden. The free-stream streamwise turbulence intensity over the span of velocities related to this work was less than 0.03%. The measuring cross-section in the tunnel is $1.80 \times 1.25\ \mathrm{m}^2$ and the downstream length is 3.00 m. The tunnel velocity was kept constant at 15 m/s during the experiment. The disk was a Swedish five kronor coin with a diameter of 28 mm. The total area ratio between disk and tunnel cross-section was less then 0.03%. The Reynolds number based on the free stream velocity and disk diameter was 28,000.

For the earlier experiments and most of the present work the disk was suspended with four pairs of wires, each with the diameter 0.2 mm and placed at 90°. The photograph shown in Fig. 1 shows the experimental setup. Results are also reported for an alternative suspension arrangement that uses only three pairs of support wires positioned at 120°.

Two different rakes were used for the present experiments: the original 13 hot-wire rake used in Johansson et al. (2002), and a 15 hot-wire rake obtained by extending the same rake to include two additional wires. The two arrays hot-wires were used in the manner of Glauser and George (1987) as shown in Fig. 1. The arrays were used to obtain the two-point velocity cross-spectra for all combinations of locations shown in Fig. 2. The measurement grid was chosen following the guidelines of Glauser and George (1992) to avoid as much spatial aliasing as possible when making the azimuthal Fourier decompositions to obtain the cross-spectra. Of primary concern in this investigation was to determine whether the previous results were influenced by the grid, hence the extra probes.

Half the array of probes was movable, and traversed from a 15° separation up to 180° with 15° increments in $\Delta\theta$, see Fig. 2. Each hot-wire probe is numbered and marked by a circle. Using this scheme, half the cross-section of the wake at a fixed downstream position was scanned, and pairs of instantaneous velocity correlations for a fixed angle separation computed. Note that the cross-spectra corresponding to the remaining half-plane were available from the azimuthal symmetry of the flow. This was justified by an initial test where cross-spectra were obtained on both sides of the wake center plane ($\Delta\theta = 180°$ in Fig. 2). These cross-spectra were impossible to distinguish from each other when the probe rake was properly centered behind the disk. For the partic-

ular angle for which the movable probe rake caught the wake of the suspending wires, the measurements on either side were used to estimate this position.

Each single hot-wire, 3 mm long and made of unplated 5μm tungsten wire, was oriented to measure the downstream component of the velocity. The probes were connected to an AN2000 Constant Temperature Anemometer (CTA) system, and sampled with an IO Tech Wavebook 516 16 bit sample and hold A/D converter. The data was low-pass filtered at 1 kHz and sampled at 4 kHz for all configurations, substantially higher than the temporal Nyquist criterion. Measurements were made simultaneously at all positions. Each block had 4096 samples, and a total of 360 blocks of data was taken per probe for each angular probe location, ensuring a variability of less than 4% for the cross-spectra used in the POD.

PROPER ORTHOGONAL DECOMPOSITION

The POD and the manner in which it is used in this investigation was described in detail in Johansson et al. (2002), so only the most essential features will be reviewed here. Note that the experimental setup is only capable of providing the necessary information to obtain the POD modes, but not the information to project them back on the instantaneous flow. This is because the latter requires measurement at all positions simultaneously in the manner of Citriniti and George (2000).

The POD results from a projection of the velocity field, u_i, into a coordinate system, ϕ_i, optimal in terms of kinetic energy. If the field has finite total energy, Hilbert-Schmidt theory assures that the solution exists and consists of a denumerable, infinite, set of eigenvalues, $\lambda^{(n)}$, and corresponding eigenfunctions, $\phi_i^{(n)}$. For an axisymmetric shear flow such as a jet or a wake, this is true in the radial direction at a single downstream location, hence the term 'slice POD'.

For the axisymmetric wake considered here, the turbulent velocity field is *stationary* in time and *periodic* in the azimuthal direction. Therefore, the Hilbert-Schmidt theory does not apply to them, but instead Fourier modes are appropriate. If only the streamwise velocity component is considered (i. e., $i = j = 1$), the following integral equation(s) must be solved:

$$\int_0^\infty B_{1,1}(m, f, r, r'; x)\psi_1^{(n)}(m, f, r'; x)r'\,dr' = \lambda^{(n)}(m, f; x)\psi_1(m, f, r; x) \quad (1)$$

where $B_{1,1}(m, f, r, r'; x)$ is the two-point velocity correlation Fourier transformed in time and expanded in Fourier series in the azimuthal direction and ψ is the corresponding eigenfunction. Note that ψ and λ are now functions of frequency, f, and azimuthal mode number, m,

In practice, the following steps are taken (following Glauser and George (1987)):

1. Measurement of the instantaneous velocity at two points.
2. Fourier transformation in time and computation of the cross-spectrum.
3. Repetition of 1. and 2. for many pairs of points.
4. Expansion of the cross-spectra obtained in 2. in Fourier series in the azimuthal direction
5. Solution of the remaining eigenvalue problem in the radial direction, Eq. 1, for each frequency and azimuthal mode number.

STATISTICAL RESULTS

The earlier paper of Johansson et al. (2002) details the first order statistics for this flow, and the difficulties in obtaining them. The primary problem is that the velocity deficit is very small (less than 2% of free stream velocity by the last measuring position), and thus extremely sensitive to hot-wire drift and calibration errors. Unlike many other free shear flows, the turbulence intensities, u_{RMS}/U_∞, are very small, from 9% at $x/D = 10$ to below 3% at $x/D = 50$. As a consequence, the hot-wire anemometer is clearly the instrument of choice, since virtually no other technique can resolve these very weak fluctuations.

Power spectral densities were computed for all downstream positions as well as rotations of the movable rake. These are not shown, but are identical to those in Johansson et al. (2002). All PSD's off the center of the wake show a prominent peak at 67 Hz, corresponding to a Strouhal number ($St = fd/U_\infty$) of 0.126. This is consistent with Strouhal number measured by Miau et al. (1997) in the near wake. The magnitude of this peak decreases with increased downstream position, but is still clearly visible at $x/D = 60$. From the absence of this peak in the center of the wake, one can immediately infer that this dominant feature of the PSD can not be related to an azimuthal mode-0 motion.

POD RESULTS

Eigenspectra were computed for the three downstream locations by solving Eq. 1 to obtain the distribution $\lambda(m, f; x)$. Even this simple result from the POD provides a large amount of information regarding the energy distribution in the flow.

The eigenspectra, $\lambda(m, f; x)$, are representations of how the energy is distributed as function of azimuthal mode number, m, and frequency, f, at a given downstream position, x. Therefore their evolution show how the main characteristics of the flow evolve. Three-dimensional plots of the eigenspectra for the first POD mode for the four wire supported wake are presented in Figs. 3 and 4. Here, also the spectral content in each azimuthal mode is shown for the first three azimuthal modes (m = 0, 1, and 2) for all the downstream distances together with the full spec-

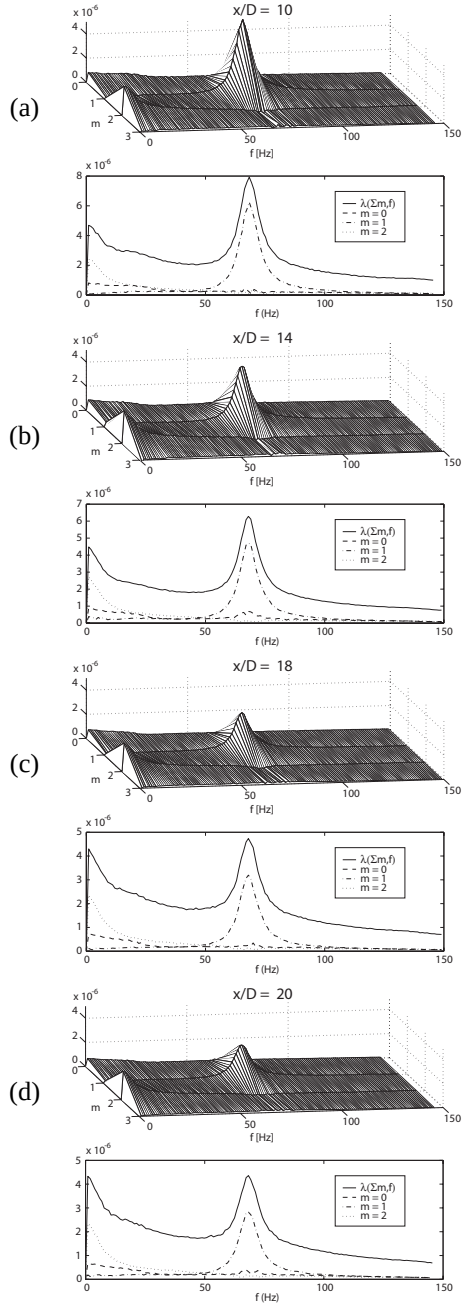

Figure 3. Eigenspectrum function of azimuthal mode number (m) and frequency (f) at different positions: (a) $x/D = 10$, (b) 14, (c) 18, and (d) 20.

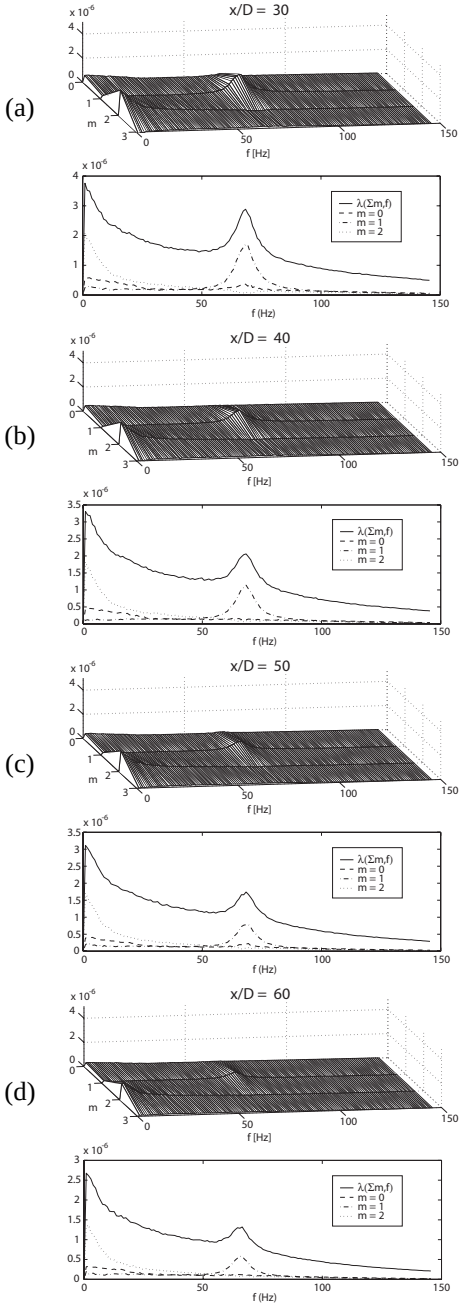

Figure 4. Eigenspectrum as function of azimuthal mode number (m) and frequency (f) at different positions: (a) x/D = 30, (b) 40, (c) 50, and (d) 60.

trum to illustrate the portion of the total energy that is captured by each mode.

As for the earlier results 13-wire results, the pictures are strikingly similar, showing two dominating events. The energy is concentrated around two separate peaks in the f-m plane. One is at near-zero frequency for azimuthal mode-2 and the other for mode-1 at a higher frequency, 67 Hz. This second peak for mode-1 corresponds to a Strouhal number of 0.126. This Strouhal number does not change with downstream position, and is exactly the same as the one detected in the PSD's off the wake

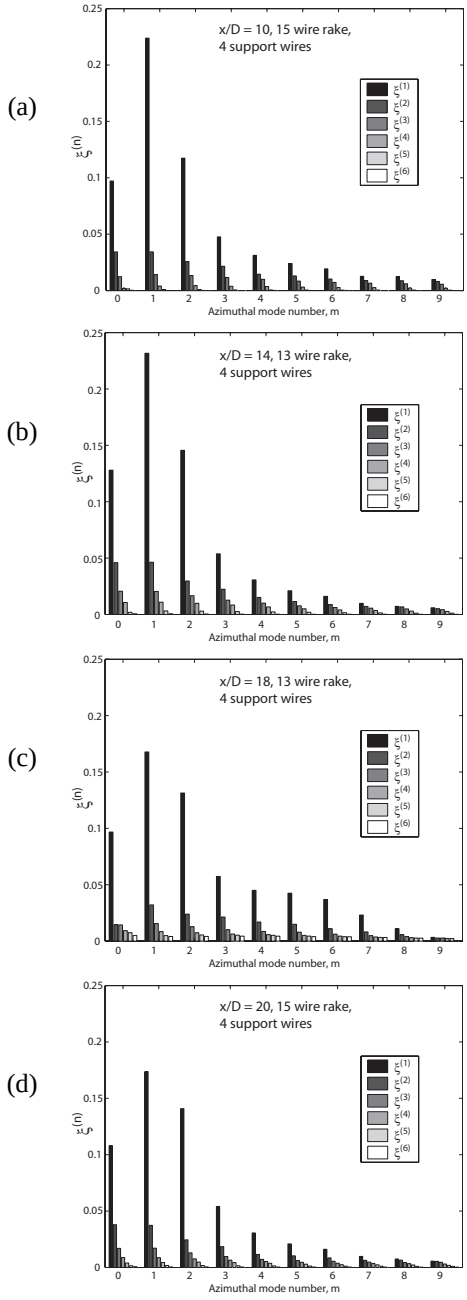

Figure 5. Eigenspectrum integrated over frequency (as defined in equation 2) as function of azimuthal mode number (m) at different positions: (a) x/D = 10, (b) 14, (c) 18, and (d) 20.

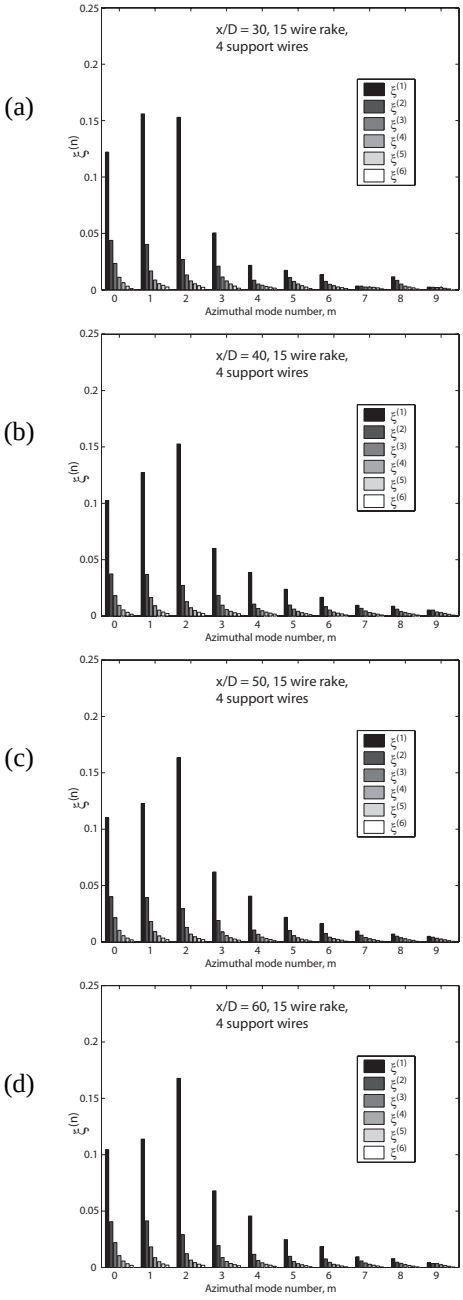

Figure 6. Eigenspectrum integrated over frequency (as defined in equation 2) as function of azimuthal mode number (m) at different positions: (a) x/D = 30, (b) 40, (c) 50, and (d) 60.

center described in the previous section. The peak at 'near-zero' frequency does not either seem to change with downstream distance, even though this has to be investigated further. This is because the 'near-zero' peak lies at the lowest measurable frequency in this experiment, 0.98 Hz.

The eigenspectra can be integrated over frequency to illustrate another key property of the POD, its ability to show how the kinetic energy of the flow is distributed among the various azimuthal modes. To visualize the energy distribution per azimuthal mode number, m, we computed for each downstream

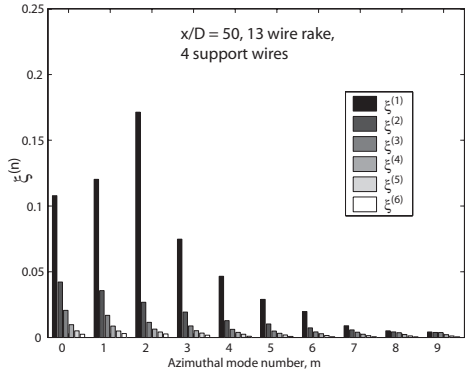

Figure 7.

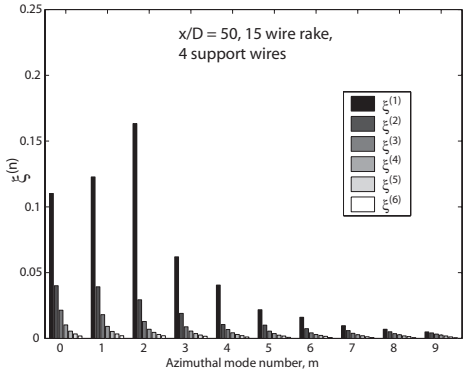

Figure 8.

position the quantity $\xi(m;x)$ where:

$$\xi(m;x) = \frac{\int_f \lambda(m,f;x)\,df}{\sum_m \int_f \lambda(m,f;x)\,df} \qquad (2)$$

Here, the denominator is the total kinetic energy in the field. The resulting normalized eigenspectra, $\xi(m;x)$ for the four-wire supported wake using the 15 hot-wire rake are plotted in Fig. 5 and 6. It is clear that at $x/D = 10$, most of the energy lies in the azimuthal mode-1, while by $x/D = 50$, the most energetic azimuthal mode is number 2.

Figure 7 shows same wake at $x/D = 50$, but using the data obtained with the 13-wire rake presented in Johansson et al. (2002). There are only very small differences, one being that mode 0 is slightly larger for the 15-wire rake. This can be explained by the fact that this rake covers a larger portion of the wake. Certainly, this effect is very small.

Figures 8 and 9 shows the same plots for the four and three wire supported rakes, also obtained using the 15 hot-wire rake at $x/D = 50$. The results are virtually indistinguishable, suggesting strongly that the whatever the physical cause of the observations, it is not a consequence of how the disk is supported in the wind tunnel.

Figure 10 shows plots of ru^2 versus r for all downstream positions. The total energy in the POD is the integral under these curves. Clearly as the rake is traversed downstream, progressively more and more of the total energy is not included in the decomposition (since the hot-wire rake is fixed). (This was one of the primary reasons for expanding from 13 to 15 wires.) The lost energy is less than 1% at $x/D = 10$ but perhaps as much as 20% at $x/D = 60$. As Fig. 6 makes clear, the evolution from azimuthal mode-1 peak to a peak at mode-2 takes place between $x/D = 30$ and 40. Beyond $x/D = 40$ there is virtually no change in the eigenspectra, even though progressively more of the energy is lost. This suggests strongly that the outside energy does not affect the eigenspectra (at least in the lower modes). This is consistent with the lack of observed differences between the 13 and 15-wire arrays.

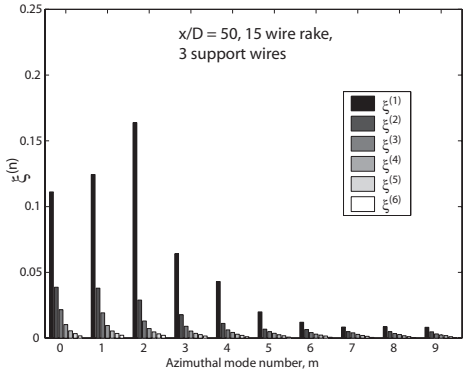

Figure 9.

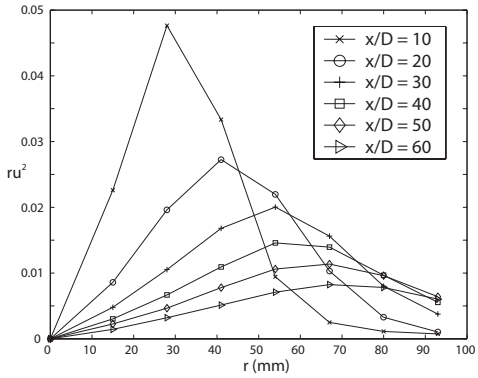

Figure 10.

The investigation was very recently expanded to further

downstream distances and is presented in Johansson and George (2002). In this paper, experiments in a different wind tunnel using different anemometers, with the coin replaced with a disk machined in acrylic with the diameter 20 mm is presented. To maintain a constant Reynolds number with this smaller disk, the velocity was increased. The eigenspectra integrated over frequency, $\xi^{(n)}$, are in perfect agreement to those presented in this paper, ensuring that an eventual asymmetry of the coin is not the cause of the mode-2 dominance.

CONCLUDING REMARKS

Three different 'slice POD' investigations are reported of the axisymmetric turbulent wake behind a disk. Two different hot-wire rake configurations were used: a 13 hot-wire rake and a 15 hot-wire rake covering a larger area of the flow. Also two different supporting methods were used: one a four wire support system, the other a three wire support system. The results were essentially independent of rake, flow coverage or wake support system. The results confirm the earlier observations of Johansson et al. (2001), but with a much more extensive data base.

For all downstream positions, two distinct peaks were found in the eigenspectrum of the lowest (and most dominant) radial POD mode: one for azimuthal mode-2 at near zero frequency, and another for azimuthal mode-1 at a fixed Strouhal number (fd/U_∞) of 0.126. Both peaks decrease in magnitude as the flow evolves downstream, but the peak at the Strouhal number 0.126 decreased more rapidly so the latter eventually dominated. When integrated over frequency and normalized by the total kinetic energy, it was seen that the first eigenspectrum accounts for more than 60% of the energy.

As noted by Johansson et al. (2002), the results are strikingly similar to recent POD results for the far axisymmetric jet obtained with 138 hot-wires presented in Gamard et al. (2002). In particular, azimuthal mode-2 dominates the far downstream development. The main difference from the jet results are that peak at the non-zero frequency scales with the local Strouhal number for the jet, but remains fixed in frequency for the wake.

ACKNOWLEDGMENT

The authors gratefully acknowledge the assistance of Scott Woodward throughout this investigation. This work was initially supported by the US Air Force Office of Scientific Research, grant number F49620-98-1-0143 and Chalmers University of Technology. It continues with the support of the Swedish Research Council, grant number 2641.

REFERENCES

C. Brücker. Spatio-temporal reconstruction of vortex dynamics in axisymmetric wakes. *Journal of Fluids and Structures*, 15: 543–554, 2001.

J. H. Citriniti and W. K. George. Reconstruction of the global velocity field in the axisymmetric mixing layer utilizing the proper orthogonal decomposition. *Journal of Fluid Mechanics*, 418:137–166, 2000.

H. V. Fuchs, E. Mercker, and U. Michel. Large scale coherent structures in the wake of axisymmetric bodies. *Journal of Fluid Mechanics*, 93:189–211, 1979.

S. Gamard, D. Jung, S. Woodward, and W. K. George. Application of a 'slice' POD to the far field of an axisymmetric turbulent jet. *Accepted for publication in Physics of Fluids*, June 2002.

M. N. Glauser and W. K. George. Application of multipoint measurements for flow characterization. *Experimental Thermal and Fluid Science*, 5:617–632, 1992.

M.N. Glauser and W.K. George. Orthogonal decomposition of the axisymmetric jet mixing layer including azimuthal dependence. In G. Comte-Bellot and J. Mathieu, editors, *Advances in Turbulence*, pages 357–366. Spring-Verlag, 1987.

P. B. V. Johansson and W. K. George. Far downstream development of POD modes in a turbulent disk wake. In *Ninth European Turbulence Conference*, Southampton, July 2-5, 2002.

P. B. V. Johansson, W. K. George, and S. H. Woodward. Proper orthogonal decomposition of an axisymmetric turbulent wake behind a disk. *Accepted for publication in Physics of Fluids*, June 2002.

J. L. Lumley. On the interpretation of time spectra in high intensity shear flows. *Physics of Fluids*, 8:1056–1062, 1965.

J. J. Miau, T. S. Leu, T. W. Liu, and J. H. Chou. On vortex shedding behind a circular disk. *Experiments in Fluids*, 23: 225–233, 1997.

P. A. Monkewitz. A note on vortex shedding from axisymmetric bluff bodies. *Journal of Fluid Mechanics*, 192:561–575, 1988.

Paper 4

Far downstream development of POD modes
in a turbulent disk wake

Advances in Turbulence IX, Proceedings of the Ninth European
turbulence conference", I. P. Castro, P. E. Hancock &
T. G. Thomas, editors, Southampton, UK, July 2-5, 2002.

P. B. V. Johansson
W. K. George

[id:261,1]

Advances in Turbulence IX
Proceedings of the Ninth European Turbulence Conference
I.P. Castro, P.E. Hancock & T.G.Thomas (Eds.)

Far downstream development of POD modes in a turbulent disk wake

P.B.V Johansson[1], W.K. George[1]

[1]Turbulence Research Laboratory, Dept. of Thermo and Fluid Dynamics,
Chalmers University of Technology, SE-412 96 Gothenburg, Sweden

Contact address: *jope@tfd.chalmers.se*

1 Introduction

The Proper Orthogonal Decomposition (POD) technique has recently become very popular for investigating the energetic structures of turbulent free shear flows. This is because the POD can describe the energetic structures of such flows with only a few modes. It has become popular only recently because of the development of high-speed computers that can handle massive amounts of data; in particular the large quantity of two-point velocity correlations required to produce the kernel for the POD.

This paper is part of an ongoing investigation of the disk wake using a 'slice' version of this technique. The developing region $x/D = 10$ to 50 was presented in Johansson *et al.* [4]. This was followed up with a sensitivity study of the POD by Johansson and George [5] where the influence of wake generator support and spatial resolution was evaluated. The POD was proven to be extremely robust and insensitive to external disturbances (such as the wakes of supporting wires). In this paper, the investigation is extended to cover downstream distances all the way to $x/D = 150$ to study the far downstream development of the POD modes.

2 Experimental Setup

Unlike the earlier experiments which were conducted at Chalmers University of Technology, these experiments were conducted in the Minimum Turbulence Level (MTL) wind tunnel at Royal Institute of Technology, Stockholm, Sweden. The free-stream streamwise turbulence intensity over the span of velocities related to this work was less than 0.02%. The measuring cross-section in the tunnel is 0.8×1.2 m^2 and the downstream length is 7.0 m. The tunnel velocity was kept constant at 20.5 m/s during the experiment.

The disk was made of plastic with a diameter of 20 mm, and the Reynolds number based on the free stream velocity and disk diameter was 27,000. The investigated region spanned from 30 to 150 disk diameters downstream. A total number of 15 hot-wires were used in two arrays. The probes were used to obtain the two-point velocity cross-spectra in the manner of Glauser and George [3] for all possible combinations of probe locations. The upper array of probes was movable, and traversed from a 15° separation up to 180° with 15° increments in $\Delta\theta$. Half the cross-section of the wake at a fixed downstream position was scanned, and pairs of instantaneous velocity correlations for a fixed angle separation computed. The measurement grid was chosen following the guidelines of Glauser and George [2] to avoid as much spatial aliasing as possible when making the azimuthal Fourier decompositions to obtain the cross-spectra. The cross-spectra corresponding to the remaining half-plane were available from the azimuthal symmetry of the flow.

3 POD

The POD results from a projection of the velocity field, u_i, into a coordinate system, ϕ_i, optimal in terms of energy. If the field has finite total energy, Hilbert-Schmidt theory assures that the solution exists and consists of a denumerable, infinite, set of eigenvalues, $\lambda^{(n)}$, and corresponding eigenfunctions, $\phi_i^{(n)}$. For an axisymmetric shear flow such as a jet or a wake, this is true in the radial direction at a single downstream location, hence the term 'slice POD'.

For the axisymmetric wake considered here, the turbulent velocity field is *stationary* in time and *periodic* in the azimuthal direction. Therefore, the Hilbert-Schmidt theory does not apply to them, but instead Fourier modes are appropriate. If only the streamwise velocity component is considered, the following integral equation(s) must be solved:

$$\int_0^\infty B_{1,1}(m,f,r,r';x)\psi_1^{(n)}(m,f,r';x)r'\,dr' = \lambda^{(n)}(m,f;x)\psi_1(m,f,r;x) \quad (1)$$

where $B_{1,1}(m,f,r,r';x)$ is the two-point velocity correlation Fourier transformed in time and expanded in Fourier series in the azimuthal direction, and ψ is the corresponding eigenfunction. Note that ψ and λ are now functions of frequency, f, and azimuthal mode number, m, More detailed descriptions of the POD and the actual computational procedure can be found in Johansson *et al.* [4].

4 Results

The eigenspectra can be integrated over frequency to illustrate a key property of the POD, its ability to show how the kinetic energy of the flow is distributed among the various azimuthal modes. To visualize the energy distribution per

azimuthal mode number, m, we computed for each downstream position the quantity $\xi(m;x)$ where:

$$\xi(m;x) = \frac{\int_f \lambda(m,f;x)\,df}{\sum_m \int_f \lambda(m,f;x)\,df} \tag{2}$$

Here, the denominator is the total kinetic energy in the field. The resulting normalized eigenspectra, $\xi(m;x)$ are plotted in Fig. 1.

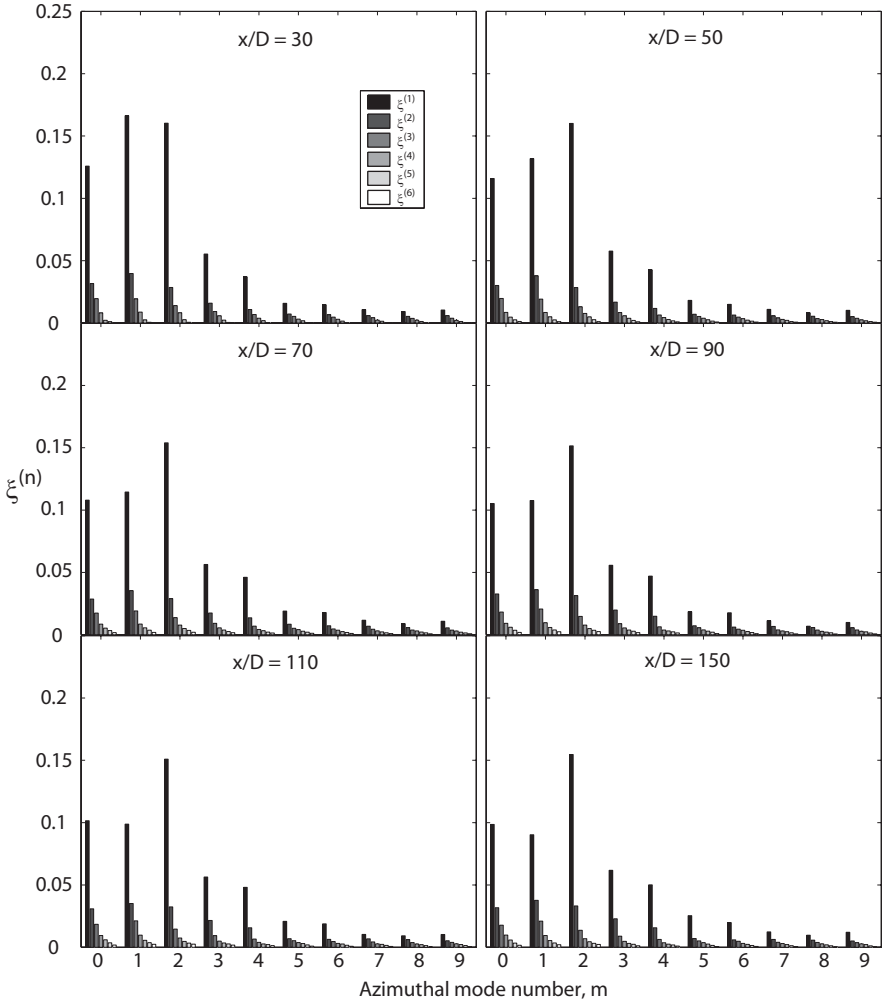

Figure 1: Eigenspectrum integrated over frequency as function of azimuthal mode number (m) at different downstream positions.

It is clear from this picture that the most dominating azimuthal mode at $x/D = 30$ is azimuthal mode number 1. But the importance of azimuthal mode 1 decreases as the flow evolves downstream, and it becomes the third most important mode behind mode 2 and mode 0 by $x/D = 110$. The picture hardly changes at all beyond $x/D = 110$. Note that mode 0 stays nearly constant and the slight decrease is due to the fact that the hot-wire probes do not cover as much of the wake at the farthest downstream position, a matter that is addressed in Johansson and George [5].

5 Summary and Conclusions

This study confirms the earlier results of Johansson *et al.* [4]. In particular, it makes clear that mode 1 does not dominate the energy of the far downstream wake. Instead, mode 2 does. In fact, it is the evolution of the eigenspectrum from mode 1 to mode 2 dominance that characterizes the evolution from near wake to far wake.

The present results are also strikingly similar to results obtained recently in the axisymmetric jet by Gamard *et al.* [1]. Despite being two different flows, the axisymmetric wake and the jet share many common features. It is reasonable to expect that the modes in these two flows can behave the same only if they are governed by similar equations, whatever they might be.

References

[1] S. Gamard, D. Jung, S. Woodward, and W. K. George. Application of a 'slice' POD to the far field of an axisymmetric turbulent jet. *Accepted for publication in Physics of Fluids*, 2002.

[2] M. N. Glauser and W. K. George. Application of multipoint measurements for flow characterization. *Experimental Thermal and Fluid Science*, 5:617–632, 1992.

[3] M.N. Glauser and W.K. George. Orthogonal decomposition of the axisymmetric jet mixing layer including azimuthal dependence. In G. Comte-Bellot and J. Mathieu, editors, *Advances in Turbulence*, pages 357–366. Spring-Verlag, 1987.

[4] P. B. V. Johansson, S. H. Woodward, and W. K. George. Proper orthogonal decomposition of an axisymmetric turbulent wake behind a disk. *Accepted for publication in Phys. Fluids*, June 2002.

[5] P. B. V. Johansson and W. K. George. Further Studies of the Axisymmetric Disk Wake Using the 'Slice POD'. Proceedings of 2002 ASME Fluid Engineering Division Summer Meeting, Montreal, Canada, July 14-18, 2002.

Paper 5

Equilibrium similarity, effects of initial conditions and local Reynolds number on the axisymmetric wake

Submitted to Physics of Fluids
In revised form

P. B. V. Johansson
W. K. George
M. J. Gourlay

Equilibrium similarity, effects of initial conditions and local Reynolds number on the axisymmetric wake

Peter B.V. Johansson and William K. George
Dept. of Thermo and Fluid Dynamics
Chalmers University of Technology
SE-412 96 Gothenburg, Sweden

Michael J. Gourlay
Colorado Research Associates Division/Northwest Research Associates, Inc., 3380 Mitchell Lane. Boulder, Colorado 80302
(Dated: May 12, 2002)

Equilibrium similarity considerations are applied to the axisymmetric turbulent wake, without the arbitrary assumptions of earlier theoretical studies. Two solutions for the turbulent flow are found: one for infinite *local* Reynolds number which grows spatially as $x^{1/3}$; and another for small *local* Reynolds number, which grows as $x^{1/2}$. Both solutions can be dependent on the upstream conditions. Also, the *local* Reynolds number diminishes with increasing downstream distance, so that even when the initial Reynolds number is large, the flow evolves downstream from one state to the other.

Most of the available experimental data are at too low an initial Reynolds number and/or are measured too near the wake generator to provide evidence for the $x^{1/3}$ solution. New results, however, from a laboratory experiment on a disk wake and direct numerical simulations (DNS) are in excellent agreement with this solution, once the flow has had large enough downstream distance to evolve. Beyond this, the ratio of turbulence intensity to centreline velocity deficit is constant until the flow unlocks itself from this behavior when the *local* Reynolds number goes below about 500, and the viscous terms become important. When this happens the turbulence intensity ratio falls slowly until the $x^{1/2}$ region is reached.

No experimental data is available far enough downstream to provide unambiguous evidence for the $x^{1/2}$ solution. The prediction that the flow should evolve into such a state, however, is confirmed by recent DNS results which reach the $x^{1/2}$ at about 200,000 momentum thicknesses downstream After this the turbulence intensity ratio is again constant, until box-size affects the calculation and the energy decays exponentially.

I. INTRODUCTION

The axisymmetric turbulent wake is a flow that has puzzled researchers for more than a half-century, since measured results have been either inconclusive or contradictive. In order to evaluate experimental data in the context of similarity analysis, a "complete" set of measured data is needed. Here, the term "complete" refers to the following necessary set of quantities: at least mean velocity and turbulence intensity distributions across the flow and the wake width. Fig. 1 shows a sketch of the axisymmetric wake together with the coordinate system. U_∞ denotes the free stream velocity, $U_o = U_\infty - U_{cl}$ the centreline velocity deficit, and δ a measure of the wake width.

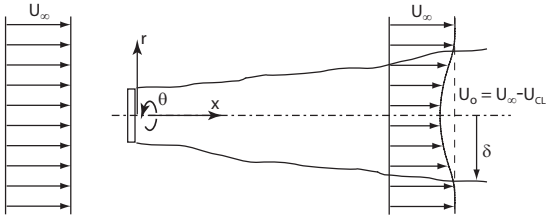

FIG. 1: Axisymmetric wake coordinates and definitions.

The axisymmetric wake is a challenging flow to measure because of the small velocity deficit, the slow decay of the velocity deficit downstream and a turbulence intensity of the same order as the deficit. In fact, the far axisymmetric wake still is at the threshold of what is possible to measure today using even the best wind tunnels and the most stable low-noise anemometer equipment. Also, unlike many other free shear flows for which the *local* Reynolds number remains constant or increases downstream, in the axisymmetric wake it drops slowly. Thus viscous effects continuously become more important until eventually they may dominate (if the flow extends far enough downstream). These varying viscous effects, together with the many very different possibilities for the structure of the near wake from different generators, considerably complicates interpretation of the data. The goal of this study is to use equilibrium similarity theory to sort out these different effects and isolate the regions in which they dominate or in which they can be ignored.

II. HISTORICAL REVIEW

The first complete set of data in the wake of an axisymmetric disk perpendicular to the flow was presented by Carmody[1], who measured mean velocity, turbulence

intensity, Reynolds stress and wake growth in an axisymmetric disk wake at a Reynolds number (R_D) based on the free stream velocity and the disk diameter of 70,000. Based on these measurements, the wake appeared to be self-similar 15 diameters from the disk, meaning that the mean velocity profiles appeared to collapse when normalized by the centreline deficit and a lateral length scale determined from the profile itself. The disk wake was also investigated by Hwang and Baldwin[2], who measured turbulence intensity and wake growth rate at up to 900 diameters downstream distance from the body. They did not, however, present centreline mean velocity decay. Both the Carmody[1] and Hwang and Baldwin[2] data show a significant scatter, presumably due to the limitations of the anemometers used at that time. Uberoi and Freymuth[3] measured the sphere wake at $R_D = 8,600$ and stated that the wake achieved self-similar behavior at 50 diameters downstream, although they only measured a few more points further downstream. Bevilaqua and Lykoudis[4] investigated the wakes of a sphere and a porous disk at $R_D = 10,000$ with the same momentum deficit (drag), and reported that these become self-similar in terms of mean velocity and Reynolds stress profiles within ten diameters of the sphere and within twenty diameter of the porous disk — but not in the same manner; i.e., the sphere and the porous disk do not reach the same state of similarity. They concluded that this result was *not* consistent with the idea that the turbulence forgets how it was created, as commonly believed (c.f. Townsend[5]).

A recent extensive experiment was reported by Cannon[6] who investigated the axisymmetric far wake behind different five different wake generators (disk, sphere and three porous disks with different porosity), all having the same drag and Reynolds number based on the momentum thickness of $R_\theta = U_\infty\theta/\nu \approx 3,500$, where U_∞ is the free stream velocity, ν is the kinematic viscosity, and θ is the momentum thickness defined by:

$$\theta^2 = \lim_{r\to\infty} \frac{1}{U_\infty^2} \int_0^r U(U_\infty - U)\, r\, dr \qquad (1)$$

This corresponds to values of R_D of 13,000 for the solid disk, 14,000—17,000 for the screens, and 21,500 for the sphere. The measurements extended over a range of x/θ of about 35 to 500. There were no conclusions about when the flow achieved self-similar behavior, and in fact it was not obvious that the turbulence intensities ever did.

During the last decade, researchers have primarily focused on the early development of the wake behind differently shaped axisymmetric bluff bodies, among them, İlday *e*l al.[7], Ostowari and Page[8], Portiero and Perez-Villar[9] and Sirviente and Patel[10]. All conclude that the wake becomes similar in *mean* velocity but the turbulence intensity profiles do not collapse. The initial evolution has also been studied numerically by Basu *et al.*[11], who made a Direct Numerical Simulation (DNS) of the axisymmetric wake for $R_D = 1500$. The authors claimed that the solution approached the self-similar state in a slow manner, but the computation was interrupted before this could be verified. From all the data referred to above, it is impossible to conclude whether the axisymmetric wake in general becomes self-similar at all, and if it does, when.

Very recently, Gourlay *et al.*[12], presented the first DNS of the high Reynolds number ($R_D = 10,000$) 'late' wake (which can be directly compared with the 'far' wake). The simulation did not resolve a wake generator, but started from a Gaussian velocity profile consistent with a laminar wake (c.f. Townsend[5] or Schlichting[13]) with superimposed random noise. The simulation ran to very large times which corresponded to very large downstream distances, about $x/D \approx 4 \times 10^5$ or $x/\theta \approx 3 \times 10^6$! This is almost three orders of magnitude larger than any existing laboratory experiment. The accuracy of the statistics is limited, however, since only an azimuthal average for each time (or position downstream) can be computed from the simulation. Gourlay *et al.*[12] did not either make any statements on when or if the wake became self-similar. There was a brief comparison to the results of classical similarity analysis to check the reliability of the numerical data. These DNS results will be used extensively below.

Even more recently, the axisymmetric disk wake from $x/D = 10$ to 60 was studied with the proper orthogonal decomposition (POD) technique by Johansson *et al.*[14]. This work was extended to cover downstream distances up to $x/D = 150$ by Johansson[15,16]. The latter provided values of the mean velocity, streamwise velocity fluctuation profiles, and wake width that will be cited below.

The following observations can be made from all the experiments listed above:

- Different initial conditions affect the growth rates, contrary to the classical theory which states that all wakes should depend only on the downstream distance, x, and the drag, $2\pi\rho U_\infty^2\theta^2$ (Townsend[5], Tennekes and Lumley[17]). Here, ρ is the fluid density, U_∞ the free stream velocity, and θ the momentum thickness defined in Eq. (1). This is most strikingly illustrated by the flow visualization photographs of Cannon *et al.*[18]. Data from Carmody[1], Uberoi and Freymuth[3], Bevilaqua and Lykoudis[4], Cannon[6], Gourlay *et al.*[12], and Johansson[15,16] are plotted in Fig. 2. (The data of Gourlay *et al.*[12] cover much larger x/θ than shown here, and will be discussed later.) These show the variation with x of the transverse length scale (wake width) defined by;

  $$\delta_*^2 = \lim_{r\to\infty} \frac{1}{U_o} \int_0^r (U_\infty - U)\, r\, dr \qquad (2)$$

  where U_o is the centerline velocity deficit. The data shown clearly do not collapse to a single curve independent of the wake generator. Note that the data by Bevilaqua and Lykoudis[4] are for two generators

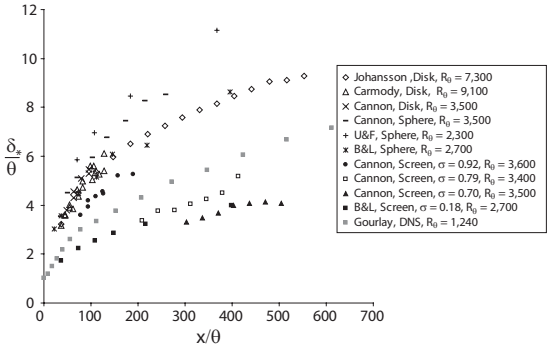

FIG. 2: Cross-stream length scale, δ_*/θ versus x/θ. For the screen wakes, the porosity, σ, is defined as σ = (solid area)/(total area).

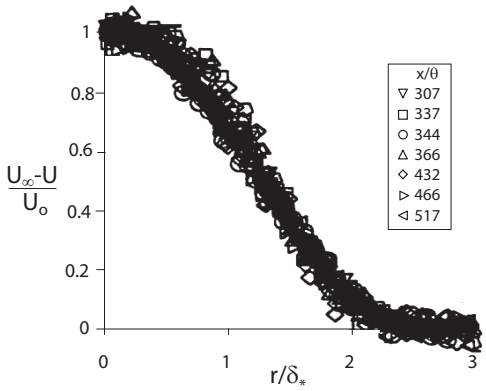

FIG. 3: Mean velocity profiles for the porous disk with σ = 0.70, data from Cannon[6].

with the same drag, and that the data by Cannon[6] is for five generators with approximately the same drag. These source dependent effects do not seem to vanish, even for large Reynolds numbers or large downstream distance.

- In apparent contradiction, the mean velocity profiles from all experiments collapse onto a single curve when scaled with centerline velocity deficit and δ_*, as illustrated in Figs. 3 and 4 for the data of Cannon[6] and Johansson[15,16], respectively. The other references show just as good a collapse.

- The turbulence intensity profiles presented by Carmody[1] and Cannon[6] do not collapse at all, even for fixed upstream conditions as shown in Fig. 5 for the data of Cannon[6] for the porous disk with $\sigma = 0.70$. Here, very large downstream distances, up to $x/\theta > 500$, are covered. By contrast, Fig. 6 shows profiles of u'_{max}/U_o for various downstream distances for the disk wake of Johansson[15,16]. Here, the turbulence intensity profiles seem to indeed collapse, but not before $x/\theta \approx 200$.

- Finally, curve fits to the screen wake data by

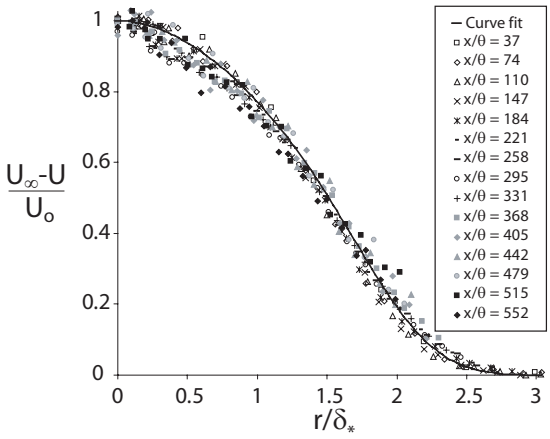

FIG. 4: Mean velocity profiles for disk, data from Johansson[15,16]. Solid line shows a curve fit according to Eq. (C7).

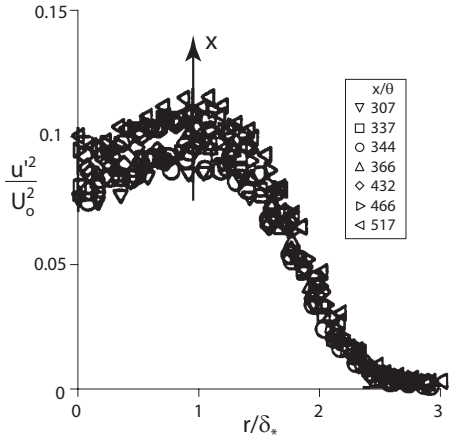

FIG. 5: Turbulence intensity profiles for the porous disk with $\sigma = 0.70$, data from Cannon[6].

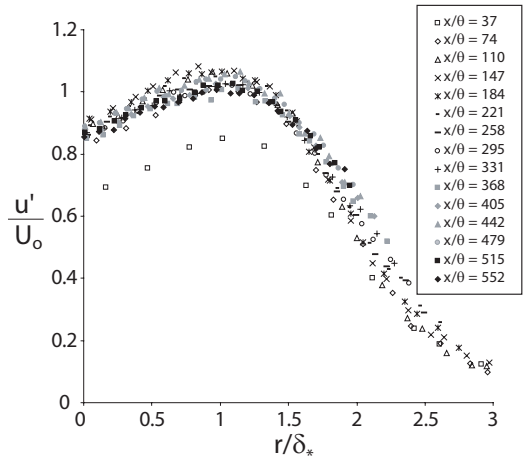

FIG. 6: Turbulence intensity profiles for disk, data from Johansson[15,16].

Cannon[6] indicate that square root and cube root downstream dependencies describe the wake growth equally well.

Clearly, there is much remaining to be explained. These issues cannot be reconciled simply by attributing them to measurement errors alone. Not all investigators could be incompetent, and in fact the internal consistency of the data suggests the opposite (e.g., momentum conservation, etc.) Nor are the problems presented by wake measurements more difficult than for grid turbulence for which hot-wire measurements have long been accepted.

The classical self-preservation approach to free shear flows was first questioned by George[19,20], who argued that it was based on assumptions that were not in general valid. He proposed a new methodology called *equilibrium similarity analysis*, and demonstrated with it that solutions were possible which depended *uniquely* on the upstream conditions. The new theory was in striking agreement with the nearly concurrent experiments of Wygnanski *et al.*[21] for two-dimensional wakes, which showed dramatic differences between spreading rates and eddy structure which depended on the wake generator.

George[19] also argued that the axisymmetric wake would behave similarly. He predicted that the mean velocity profiles from the different experiments would be the same, if scaled by the centerline deficit velocity and velocity deficit half-width, even if the wakes grew at different rates. This is consistent with the observations shown in Figs. 3 and 4. This result is very important, since previous researchers have often used the collapse of mean velocity profiles alone to argue that wakes are independent of upstream conditions. The whole point of George's analysis, however, is that *properly normalized mean velocity profiles always collapse*, and the *source-dependent differences only show up in the spreading rate and the higher turbulence moments*. This is clearly observed as noted above.

George[19] was unable to resolve whether the asymptotic axisymmetric wake would evolve as $\delta \sim x^{1/3}$ or as $\delta \sim x^{1/2}$. In fact, he showed from *ad hoc* assumptions about the dissipation that both solutions were consistent with the equations, depending on the Reynolds number. It did not appear to be possible, however, to decide which, if either, would be observed, or whether the flow would evolve from one to the other. Or even if such an evolution occurred, which would be observed first. As the careful experiment of Cannon[6] described earlier makes clear, these questions are still very much in doubt.

In this paper, the analysis of George[19] is re-visited, corrected, and extended. It will be shown *without ad hoc* assumptions that two different equilibrium similarity solutions for the axisymmetric wake are possible: one for very high *local* Reynolds numbers, and another for low. Most importantly, because the *local* Reynolds number *decreases* with distance downstream, the flow will indeed be shown to eventually evolve from the high Reynolds number state to the lower, no matter how high the initial Reynolds number of the flow. And if the initial Reynolds number of the flow is too low, the high Reynolds number solution will not be observed at all. The available experimental and numerical data is analyzed, especially addressing the particular points listed above. Not surprisingly (given the state of confusion), most of the laboratory experiments are shown to take place in the evolution region. The direct numerical simulation of Gourlay *et al.*[12] is the only case where both the high and low local Reynolds number solution are found, since it is the only investigation that covers far enough downstream distances with high enough initial Reynolds number.

III. EQUILIBRIUM SIMILARITY ANALYSIS

The necessary equations to study are: the momentum equation, conservation of momentum, continuity, and the individual transport equations for Reynolds stresses in cylindrical coordinates. These are summarized in Appendix A, since they are not easily available in standard texts. In the spirit of George[19,20], we seek solutions of the form (explicitly written here for the momentum equation and $\overline{u^2}$ equations only — the others are treated similarly):

$$U - U_\infty = U_s(x) f(\eta, *) \qquad -\overline{uv} = R_s(x) g(\eta, *) \tag{3a}$$

$$\frac{1}{2}\overline{u^2} = K_u(x) k_u(\eta, *) \qquad \frac{1}{2}\overline{u^2 v} = T_{u^2v} t_{u^2v}(\eta, *) \tag{3b}$$

$$\overline{\frac{p}{\rho}\frac{\partial u}{\partial x}} = P_u(x) p_u(\eta, *) \qquad \frac{1}{\rho}\overline{pu} = P_u^D(x) p_u^D(\eta, *) \tag{3c}$$

$$\varepsilon_u = D_u(x) d_u(\eta, *) \tag{3d}$$

where $\eta = r/\delta(x)$ and $*$ denotes a possible (unknown) dependence on initial conditions. Note that two different sets of solutions will be found below, so the symbols will have different meanings depending on which is being discussed. Since each regime is discussed separately there should be no confusion.

For the particular type of "equilibrium" similarity solutions suggested in George[20], *the terms in the governing equations must maintain the same relative balance as the flow evolves*. These "equilibrium" similarity solutions exist only if the terms within square brackets have the same x-dependence, and are independent of the similarity variable, η. (Thus, the bracketed terms must remain proportional to each other as the flow evolves.) This is denoted by the symbol $\sim$ which should be interpreted as "has the same x-dependence as". (Note that the symbol $\sim$ has nothing to do with "order of magnitude" in this paper.)

For the mean momentum equation, these equilibrium similarity constraints reduce to:

$$\left[\frac{\delta}{U_s}\frac{dU_s}{dx}\right] \sim \left[\frac{d\delta}{dx}\right] \sim \left[\frac{R_s}{U_\infty U_S}\right] \sim \left[\frac{\nu}{U_\infty \delta}\right] \tag{4}$$

There is nothing in the equations or the theory which suggests that the constants of proportionality are inde-

pendent of source conditions, nor in fact do they appear to be. This is contrary to the usual assumptions in self-preservation analysis (c. f., Townsend[22], Tennekes and Lumley[17]). It is trivial to show that the relation between the first and second terms of Eq. (4) is satisfied by the momentum integral result of Eq. (B2).

The proper scale for $-\overline{uv}$ is obtained by using the second and third terms, which yields:

$$R_s \sim U_\infty U_s \frac{d\delta}{dx} \tag{5}$$

It is immediately obvious how the equilibrium similarity approach yields a different and more general result than the classical approach, where it is *assumed* without justification that $R_s = U_s^2$ (c. f., Tennekes and Lumley[17]), with the coefficient determined by the conditions for a point source of drag.

The same equilibrium similarity hypothesis can be applied to the component Reynolds stress equations; namely that all of the bracketed terms should remain proportional (i.e., have the same x-dependence). For example, inserting Eq. (3) into Eq. (A4) yields after some elementary calculus that equilibrium similarity can be maintained only if:

$$\frac{\delta}{K_u}\frac{dK_u}{dx} \sim \frac{d\delta}{dx} \sim \frac{T_u\delta}{U_\infty K_u} \sim \frac{D_u\delta}{U_\infty K_u} \sim \frac{\nu}{U_\infty \delta} \tag{6}$$

Similar relations arise from the other component equations.

All of these relations *cannot* simultaneously be satisfied given the constraints already placed on U_s, δ, and R_s from the mean momentum equation. A solution is possible, however, *if the viscosity is identically zero*, since then all terms involving the viscosity fall out of the problem. And also *a solution for finite viscosity is possible* if it can be shown that the production term in the Reynolds shear stress equation, $\overline{v^2}\partial(U-U_\infty)/\partial r$, is negligible relative to the leading terms in the equation.

It will be demonstrated below that these are in fact limiting solutions for very large *local* Reynolds number, and for very low *local* Reynolds number. Note that the latter solution should *not* be confused with the laminar solution, but instead identified with turbulent flow for which the velocity spectra do not have a developed $k^{-5/3}$ range (see George[20]). And by contrast, the high Reynolds number limit applies to a flow which has an easily apparent inertial subrange in the spectra. Further it will be demonstrated that no matter how high the Reynolds number of the drag-producing device, say $R_\theta = U_\infty\theta/\nu$, the diminishing *local* Reynolds number downstream will cause the equations (and the solutions as well) to slowly evolve from one regime to the other.

IV. THE INFINITE REYNOLDS NUMBER SOLUTION

A solution having the same x-variation as the classical solution can be derived by setting the viscous terms in Eq. (B4) to (B8) exactly equal to zero, which corresponds to the limiting solutions at infinite Reynolds numbers. It is straightforward to show that all of the remaining constraints can be satisfied. Of particular interest are the following:

$$\frac{d\delta}{dx} \sim \frac{D_u\delta}{U_\infty K_u} \tag{7}$$

$$K_u \sim K_v \sim K_w \sim U_s^2 \tag{8}$$

$$D_u \sim D_v \sim D_w \sim U_s^3/\delta \tag{9}$$

Note that this is the solution obtained by George[19] by *assuming* the dissipation relation of equation 9. The scaling for the dissipation is just what one should expect for an infinite Reynolds number solution where the dissipation is completely controlled by the energetic turbulence (i. e., $\epsilon \propto u^3/l$ in the usual notation of texts).

It follows immediately after some manipulation that:

$$\frac{\delta_*}{\theta} = a\left[\frac{x-x_o}{\theta}\right]^{1/3} \tag{10}$$

$$\frac{U_s}{U_\infty} = b\left[\frac{x-x_o}{\theta}\right]^{-2/3} \tag{11}$$

where $a = a(*)$, $b = b(*)$, and $x_o = x_o(*)$ is a virtual origin. This is, of course, the classical solution with but a single difference — the dependence of the coefficients on upstream conditions, $*$. This possible dependence must be acknowledged, since there is *nothing in the equations themselves* to suggest independence of upstream conditions. The mean velocity profile, on the other hand, can be shown to be independent of upstream conditions. This is achieved by incorporating a factor of $[R_s/(U_\infty U_s)\, d\delta/dx]$ into the definition of g so that there are no parameters at all in Eq. (B4), as noted by George[19].

V. BOUNDS ON THE VALIDITY OF THE INFINITE REYNOLDS NUMBER SOLUTION

It was noted in the introduction that the cube root solutions simply do not account for most of the data, and especially the careful data of Cannon[6]. So where might the problem be? Firstly, even if the Reynolds number of the wake generator is high enough for the flow to be nearly inviscid, as required for the similarity theory to be valid, it clearly can only apply after the transients from the wake generator have died off. Coincident with this, the turbulence intensity ratio, u'/U_s, must also reach a constant value, as demanded by equation 8 above. Note that appropriate choices for the similarity parameters K_u and U_s are $U_s = U_o$ and $K_u = u'^2_{max}$, the centreline velocity deficit and maximum of the mean square streamwise fluctuating velocities respectively.

The ratio u'_{max}/U_o is plotted in Fig. 7 versus x/θ for the data of Johansson[15,16], Bevilaqua and Lykoudis[4], and Cannon[6]. There is a large uncertainty as to whether the

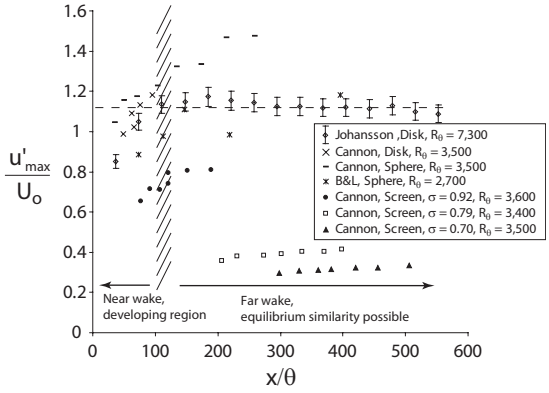

FIG. 7: Maximum turbulence intensities, data of Johansson[15,16], Cannon[6], and Bevilaqua and Lykoudis[4]. Shaded area shows lower limit for high Reynolds number solution.

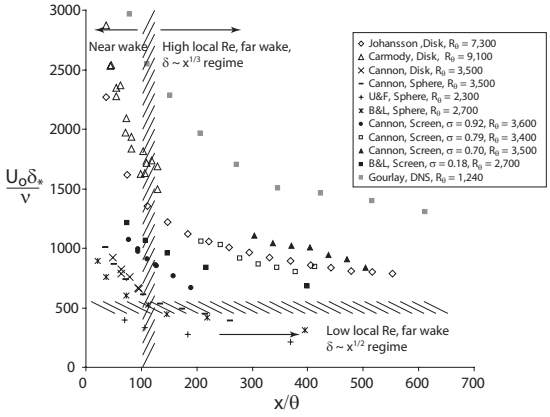

FIG. 8: Local Reynolds number. Shaded area shows lower limit for high Reynolds number solution.

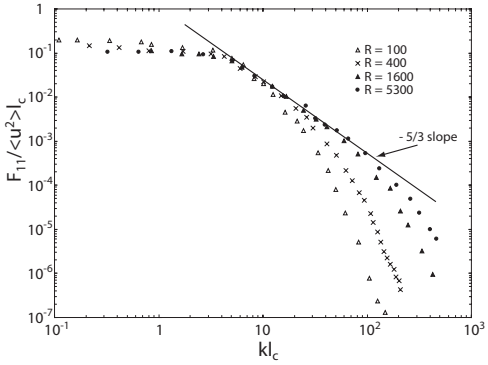

FIG. 9: Dependence of the spectra on *local* Reynolds number. Computed from data of Uberoi and Freymuth[3]. $R = U_o\delta_*/\nu$, $l_c = D^{2/3}(x - x_o)^{-2/3}$, $x_o = 12D$.

data of Bevilaqua and Lykoudis[4] and Cannon[6] reach a horizontal line. Note that the data of Cannon[6] for the screen with $\sigma = 0.70$ is based on Fig. 5 and the data of Johansson[15,16] are obtained from Fig. 6. The data from Johansson[15,16] tends to fall onto a line, at least after $x/\theta \approx 120$. The error bars indicate an uncertainty in the data of 4%. This error originates primarily in the difficulty of estimating the centreline mean velocity difference, since the mean velocity data is affected by drift in the anemometer calibration. This is discussed in detail in Johansson *et al.*[14]. There is no doubt, however, that the flow is still developing until at least $x/\theta = 120$ ($x/D \approx 30$), beyond which it appears to have settled in to an equilibrium similarity state.

This conclusion can be compared to the findings of the POD studies of Johansson and George[23] (see also George *et al.*[24]), who showed that the POD modal distribution was changing until $x/D \approx 50$ ($x/\theta \approx 184$). The energy distribution went from an azimuthal mode 1 dominance at $x/D = 10$ to an azimuthal mode 2 dominance by $x/D = 50$, with both modes being equally important at $x/D = 30$. Beyond $x/D = 50$, the decomposition hardly changed at all. Therefore, even though the turbulence intensity seems to have settled in by $x/\theta \approx 120$, the noticeable overshoot between $x/\theta \approx 120$ and 200 should not be left unnoticed. Other quantities, such as the growth rate must be taken into account before specifying the exact location of the start of the equilibrium range. Uberoi and Freymuth[3] concluded that their sphere wake became self-similar after $x/D = 50$ (corresponding to $x/\theta \approx 300$ in their case). Given the difference in initial conditions, there are no particular reasons that the these two flows should develop in exactly the same way, either initially or far downstream.

Secondly, it is easy to show that, unlike most other free shear flows, this infinite Reynolds number solution contains the seeds of its own destruction. The *local* Reynolds number, $R = U_s\delta_*/\nu$, controls the relative importance of the neglected viscous terms in the mean momentum and Reynolds shear stress equations. Substitution of Eqs. (10) and (11) into the definition of R yields:

$$R = \frac{U_s\delta_*}{\nu} = \frac{U_\infty\theta}{\nu}\left[\frac{x - x_o}{\theta}\right]^{-1/3} = R_\theta\left[\frac{x - x_o}{\theta}\right]^{-1/3} \tag{12}$$

Thus, no matter how large the initial Reynolds number, R_θ, eventually far enough downstream it is diminished until the viscous terms can no longer be neglected. And if the viscous terms are not negligible, the infinite Reynolds number similarity solution cannot be even approximately true. This is illustrated in Fig. 8, using the data of Johansson[15,16], Carmody[1], Cannon[6], Uberoi and Freymuth[3], Bevilaqua and Lykoudis[4], and Gourlay *et al.*[12]. Clearly the local Reynolds numbers in the experiments drops drastically as the flow evolves downstream, so eventually the viscous terms become important, even if initially negligible.

The effects of the changing *local* Reynolds number, R, can also be clearly seen in the one-dimensional velocity spectra of Uberoi and Freymuth[3] shown in Fig. 9. As noted by George[20], high Reynolds number solutions apply only if there is a clear inertial subrange in the power

spectrum. This insures that the energy and Reynolds stress scales of motion are effectively inviscid. For $R = 1600$, this is clearly the case, with about two decades of inertial subrange. By $R = 400$, the existence of an inertial subrange is questionable, and by $R = 100$ it is clearly gone.

The approximate lower limit for the high Reynolds number solution of $R \approx 500$ is indicated on Fig. 8 by the horizontal shaded line. None of the data below this line satisfy the conditions for the high Reynolds number solution. Also shown in Fig. 8 by the vertical shaded line is the approximate boundary of the transient (or near wake) region for the disk as described above. Clearly most of the experimental data do not satisfy the conditions for the high Reynolds number solution to apply. Before examining in detail those that do, the low Reynolds number solution will be developed below.

VI. THE LOW RE SOLUTION

As noted above (and by George[19]), there is another equilibrium similarity solution to the same set of equations. The difference is that this time all the terms involving viscosity are kept, in both the mean and Reynolds shear stress equations. This produces one additional constraint of the mean momentum equation (Eq. B4):

$$\frac{d\delta}{dx} \sim \frac{\nu}{U_\infty \delta} \tag{13}$$

It is extremely important to note that even though some of the relations are the same (e.g., $K_u/U_s^2 =$ constant), the constants of proportionality (or more properly, the parameters of proportionality since they all depend on $*$, the unknown details of the initial conditions) are most likely different from those governing the infinite Reynolds number solution.

There is one problem which at first glance appears to be quite serious. All of the constraints in the Reynolds shear stress equation cannot be met, in particular the one arising from the production term, $\overline{v^2}\partial(U - U_\infty)/\partial r$. This offending term dies off with distance downstream faster than the remaining terms in the equation, in fact as $x^{-7/2}$ compared to $x^{-5/2}$ for the rest. Therefore, it can also be neglected in the analysis since it does not survive asymptotically (exactly like the Reynolds stress convection terms in the outer boundary layer analysis of George and Castillo[25]). But since the difference in decay as $x^{-7/2}$ and $x^{-5/2}$ is very small, it clearly will take a considerable distance downstream to reach this new state of equilibrium. Moreover, it will be very difficult to recognize from δ_* and U_o alone.

It is straightforward to show that Eq. (13) can be integrated to obtain:

$$\frac{\delta_*}{\theta} = c\, R_\theta^{-1/2} \left[\frac{x - x_{oo}}{\theta}\right]^{1/2} \tag{14}$$

$$\frac{U_s}{U_\infty} = d\, R_\theta \left[\frac{x - x_{oo}}{\theta}\right]^{-1} \tag{15}$$

where as before $c = c(*)$, $d = d(*)$, and $x_{oo} = x_{oo}(*)$ is a virtual origin which most likely is different than the one obtained above. Unlike the infinite Reynolds number solutions, the mean velocity profile *cannot* be shown to be independent of upstream conditions because of the additional term in the momentum equation. Note that the mean profile is not the same as for the high *local* Reynolds number wake, at least in principle, because it is a solution to different equations involving viscosity.

It is easy to show that the local Reynolds number continues to fall with increasing distance downstream; therefore the approximations improve with distance downstream. Moreover, since the viscous stresses and Reynolds stresses both decay as $x^{-3/2}$, the flow will never relaminarize but will remain a low *local* Reynolds number wake forever.

An important clue as to if and when this low Reynolds number solution regime applies is the constancy of the ratio, K_u/U_s^2, or in the data the constancy of the ratio u'_{max}/U_o. This is exactly the same condition applied above to identify the high Reynolds number region, so if the constant is the same for both high and low Reynolds number solutions, it will be extraordinarily difficult to tell them apart since they differ by only $x^{1/2}/x^{1/3}$. Fortunately, the intensity ratios appear to differ significantly as will be seen below, so it is quite easy to decide where the infinite Reynolds number region ends and where the visous one begins, at least for the Gourlay *et al.*[12] data.

VII. IDENTIFICATION OF THE DIFFERENT REGIMES FROM DATA

A necessary condition for any data to be considered is that momentum is conserved. For the near wake this requires inclusion of the non-linear term in equation 1; but for all positions of interest here, momentum conservation reduces to:

$$U_o \delta_*^2 = U_\infty \theta^2. \tag{16}$$

All of the experimental data appear to satisfy this requirement, as does the DNS data of Gourlay for $x/\theta > 500$. Moreover, as noted above, for similarity to be valid the ratio u'_{max}/U_o has to be constant. The constant may be, in principle at least, different for the high and low Reynolds number regions. In fact, it is the constancy or lack of constancy of u'_{max}/U_o that most easily identifies the various similarity solution regimes.

As noted above, only a few of the many sets of experimental data actually satisfy the conditions for the

infinite Reynolds number solution to apply. Only the experimental data of Johansson[15,16] and the DNS data of Gourlay[12] will be considered further here. Of these, only the DNS data completes the evolution to the low Reynolds number solution.

A. A High Reynolds Number Experiment

The Johansson data were taken in the MTL tunnel of the Swedish Royal Institute (KTH), Stockholm using rakes of 15 hot-wires. The disk was 20 mm in diameter and the flow speed was 20.4 m/s, corresponding to $Re_\theta = 7,300$. The 7m long test section and very low turbulence background turbulence intensity permitted measurements downstream to $x/D = 150$, or $x/\theta = 552$. The experiment is described in detail in Johansson[15,16]. The mean velocity and turbulence intensity profiles have already been shown in figs. 4 and 6 respectively. Fig. 10 summarizes all the remaining important parameters mentioned above for the full picture of the high *local* Reynolds number similarity region for the disk wake.

The turbulence intensity normalized by the velocity deficit at the centerline is constant beyond $x/\theta \approx 120$. The *local* Reynolds number is above 500, even at the furthermost downstream position. The plot of $(\delta_*/\theta)^3$ versus x/θ is linear, as is the plot of $(U_c/U_o)^{-3/2}$, exactly as required by the high Reynolds number similarity results of equations 10 and 11 respectively. Linear regression yields values for the constants as: $a = 1.14$, $b = 0.77$, $x_o = -2.4\theta$.

B. Recent High Reynolds Number DNS

The DNS data of Gourlay *et al.*[12] covers very large downstream distances as mentioned in the introduction, and both high and low Reynolds number regimes can be observed. The original data was presented as a function of non-dimensionalized time, tU/L, where the reference velocity $U = 1$ and reference length $L = 1$. When converting to downstream distance, x/θ, it was first assumed that $tU = x$, and the velocity profiles were then integrated according to Eq. 1. All results presented here are plotted versus x/θ to facilitate comparison with the experimental data.

In Fig. 11, the turbulence intensities of Gourlay *et al.*[12] are shown. Two regions of constant normalized turbulence intensity can be observed: one for $1,000 < x/\theta < 8,000$ approximately (see insert), and the other for $200,000 < x/\theta < 600,000$ approximately.

This wake clearly reaches the first equilibrium similarity region much further downstream than the disk wake of Johansson[15,16] considered above. This might be related to the level of turbulence intensity which is much lower (almost a factor of two) than the disk wake results. (Note that the turbulence intensity is even lower for the porous screens of Cannon[6] shown in Fig. 7.) Because of the low turbulence intensity of these flows, it is possible it takes such large downstream distances for the flow to reach equilibrium because the time scale of the energy-containing eddies, δ_*/u' is correspondingly increased. Figure 12 summarizes the important parameter variation for the first region identified above.

The turbulence intensity normalized by the centerline velocity deficit begins to drop slowly after $x/\theta \approx 8,000$, which is about where the *local* Reynolds number has reached the previously suggested threshold of 500. Clearly, this region should be identified with the high Reynolds number solution. As for the disk data, both $(\delta_*/\theta)^3$ and $(U_o/U_\infty)^{-3/2}$ are both linear over the same range for which the intensity ratio is constant, and begin to deviate about when the intensity ratio begins to drop and the Reynolds number drops below the threshold value. Regression fits of equations 10 and 11 yields values for the constants of: $a = 0.84$, $b = 1.44$, and $x_o = 200\theta$. These are quite different from the values above for the disk wake above, making clear the effect of different initial conditions.

Fig. 13 shows the normalized mean velocity deficit profiles for this portion of the Gourlay data. Also shown on the plot is the best fit line to the mean velocity deficit data of Johansson shown in fig. 4. These should be exactly the same according to the similarity theory, since any differences should show up only in the growth rate and the magnitude of the Reynolds stress; and they are, but only at $x/\theta = 1030$. The differences may be due to the scatter in the DNS data because of the limited statistical sample. Alternatively, perhaps the mean velocity profile is affected somewhat earlier than the turbulence intensity ratio by the lower local Reynolds number of the DNS data. The low *local* Reynolds number similarity region can only identified in the DNS data of Gourlay *et al.*[12], the second region of constant intensity ratio identified above. The important parameters are shown in Fig. 14.

The local Reynolds number is well below the threshold for the high Reynolds number solution to be valid, so clearly the low Reynolds number solution is appropropriate. Thus is it is not surprising that the plots of $(\delta_*/\theta)^2$ and $(U_o/U_\infty)^{-1}$ are remarkably linear. Regressive fits of equations (14) and (15) yield values for the constants of $c = 1.90$, $d = 0.28$, $x_{oo} = -3.0 \times 10^5\theta$. Note that the high value for the virtual origin is consistent with the fact that this region does not begin until $\delta_*/\theta \approx 33$! In fact, instead of a virtual origin, it might be more appropriate to think of it as a starting value for δ_*/θ when the low Reynolds number equilbrium similarity region is begins.

Figure 15 shows the normalized mean velocity deficit profiles for $1.96 \times 10^5 \leq x/\theta \leq 8.41 \times 10^5$.

The collapse is remarkable. Also shown is the curve fit to the Johansson data. Clearly these are different, consistent with the fact that the mean momentum equation is different because of the presence of the viscous stress. Also shown is the exponential eddy viscosity profile de-

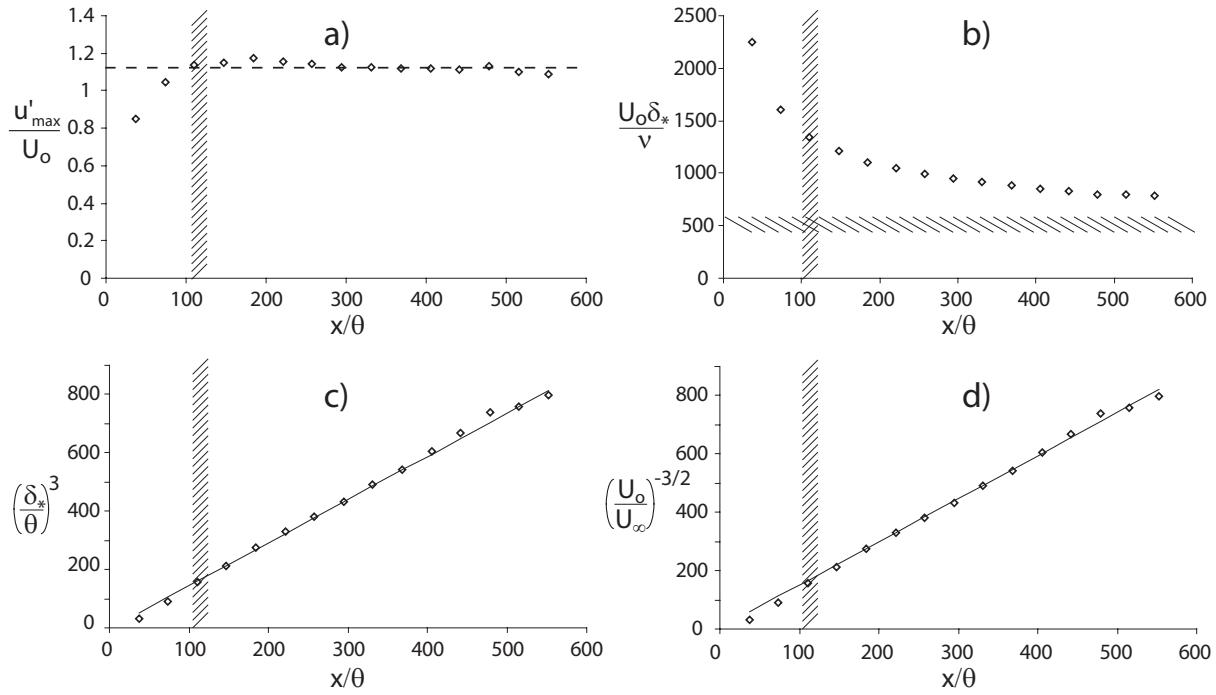

FIG. 10: a) Turbulence intensity, b) *local* Reynolds number, c) wake width, and d) velocity deficit. Data of Johansson[15,16]. Shaded area shows lower limit for high Reynolds number solution.

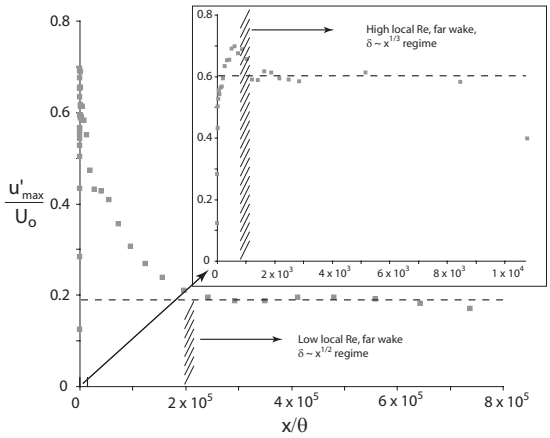

FIG. 11: Maximum turbulence intensities, data of Gourlay *et al.*[12]. Insert shows the region $0 \leq x/\theta \leq 10^4$. Shaded area shows lower limit for high Reynolds number solution.

veloped in Appendix C. Note that this is not the same as the laminar solution, first because the 'turbulent viscosity' is about 15 times the fluid viscosity. Also, the turbulence intensity ratio is non-zero and plays a significant role in the flow evolution.

Finally, fig. 16 shows a linear-linear plot of the Gourlay data for all values of x/θ. Also shown are the curve fits discussed above for the high and low Reynolds number regimes. The figure makes clear how truly far downstream these DNS data really go, and also what a small portion of the total is the truly high Reynolds number part of it. It is also clear why, in the absence of the theory developed herein, why previous experimenters have had such difficulty making sense of their data.

C. Summary of Data Analysis

Based on the results of the similarity theory stated above, the evolution of the axisymmetric wake flow can be described as following:

- In the vicinity of the wake generator, the "near wake" region, the flow does not obey the equations governing the equilibrium similarity state presented in Appendix A, since one or more assumptions in their derivation are violated. In other words, the flow is in non-equilibrium.

- Giving the flow time (or downstream distance) to adjust, the assumptions underlying the equilibrium similarity equations become justified. When the flow has reached the "far wake" region, characterized by the ratio $\sqrt{u^2}/U_o$ being constant, and provided that the initial *local* Reynolds number, $R = U_o\delta_*/\nu$, (that decrease downstream) is still is large enough, the flow will behave like it is in equilibrium with $\delta_* \sim x^{1/3}$, and $U_o \sim x^{-2/3}$. For the disk wake of Johansson[15,16], this was found to happen when $x/\theta \approx 120$. For the DNS simulation of Gourlay *et al.*[12] this was true after about

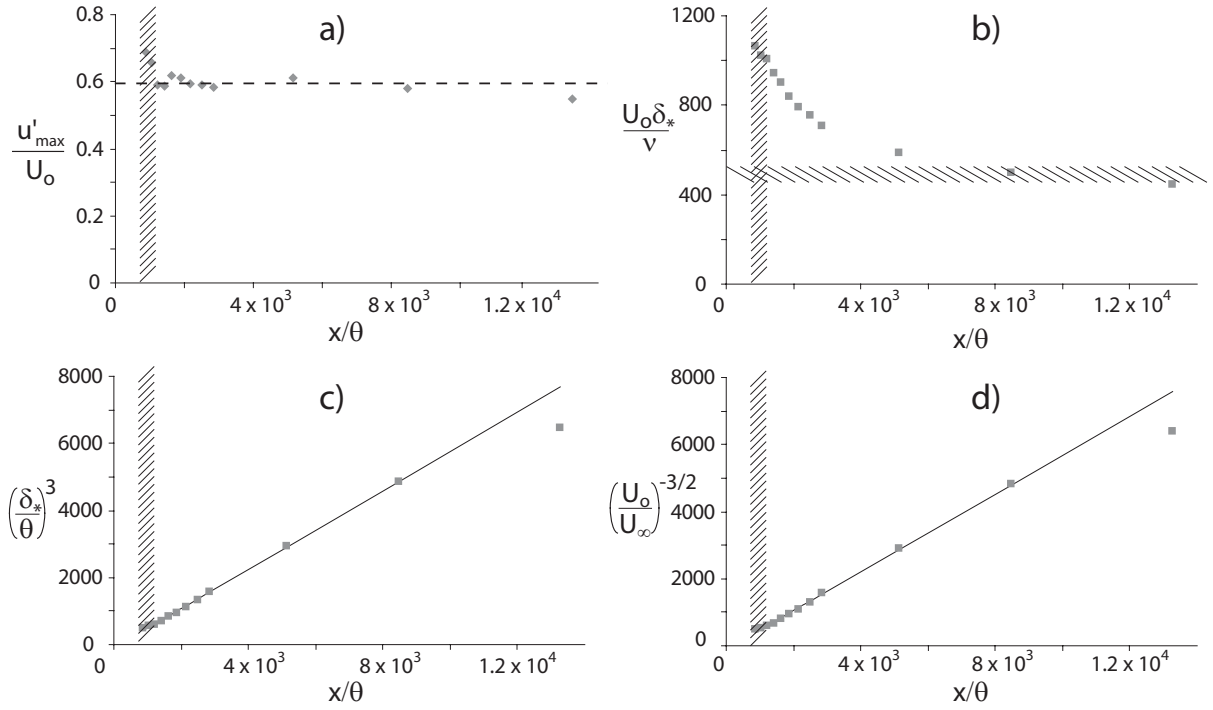

FIG. 12: a) Turbulence intensity, b) *local* Reynolds number, c) wake width, and d) velocity deficit. Data of Gourlay *et al.*[12]. Shaded area shows lower limit for high Reynolds number solution.

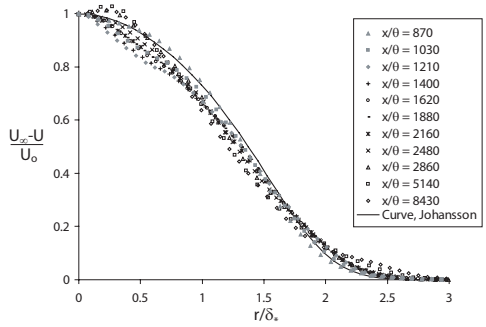

FIG. 13: Mean velocity profiles, near wake data of Gourlay *et al.*[12]. Solid line shows the fit according to Eq. (C7) to the data of Johansson[15,16] shown in Fig. 4.

$x/\theta \approx 1,000$.

- When the *local* Reynolds number, R, drops below a critical value, the flow is forced from its equilibrium similarity state by the leading order viscous term. Most notable is that the ratio $\sqrt{u^2}/U_o$ decreases. This adjustment continues for an extremely long distance downstream. The critical value of R for the beginning of this decline is seen to be about 500, consistent with the disappearance of the inertial range in the spectrum noted earlier.

- After sufficient time, the flow has readjusted into a different equilibrium state, with different governing equations including the leading order viscous term. Here, $\sqrt{u^2}/U_o$ is again constant, and now the flow now grows like $\delta_* \sim x^{1/2}$, and the velocity deficit decays like $U_o \sim x^{-1}$. This region was only found in the DNS simulation of Gourlay *et al.*[12] at about $x/\theta \approx 2 \times 10^5$.

- After $x/\theta \approx 5 \times 10^5$, the turbulence intensity drops again, and seems to decay exponentially. This is a behavior found in other simulations when the computational or experimental box-size is too small (e.g., by Moser *et al.*[26] and George and Wang[27]). Shortly thereafter, the momentum integral ceases to be constant.

VIII. CONCLUSIONS

Equilibrium similarity considerations can be applied to the axisymmetric turbulent wake, without the arbitrary assumptions of earlier theoretical studies. Two solutions for the turbulent flow are found: one for infinite *local* Reynolds number which grows spatially as $x^{1/3}$; and another for small *local* Reynolds number, which grows as $x^{1/2}$. Both solutions depend on the upstream conditions. For both solutions, the *local* Reynolds number of the flow diminishes with increasing downstream distance. As a consequence, even when the initial Reynolds number is large, the flow evolves downstream from one state to the other.

Most of the available experimental data were at too low an initial Reynolds number and/or were measured

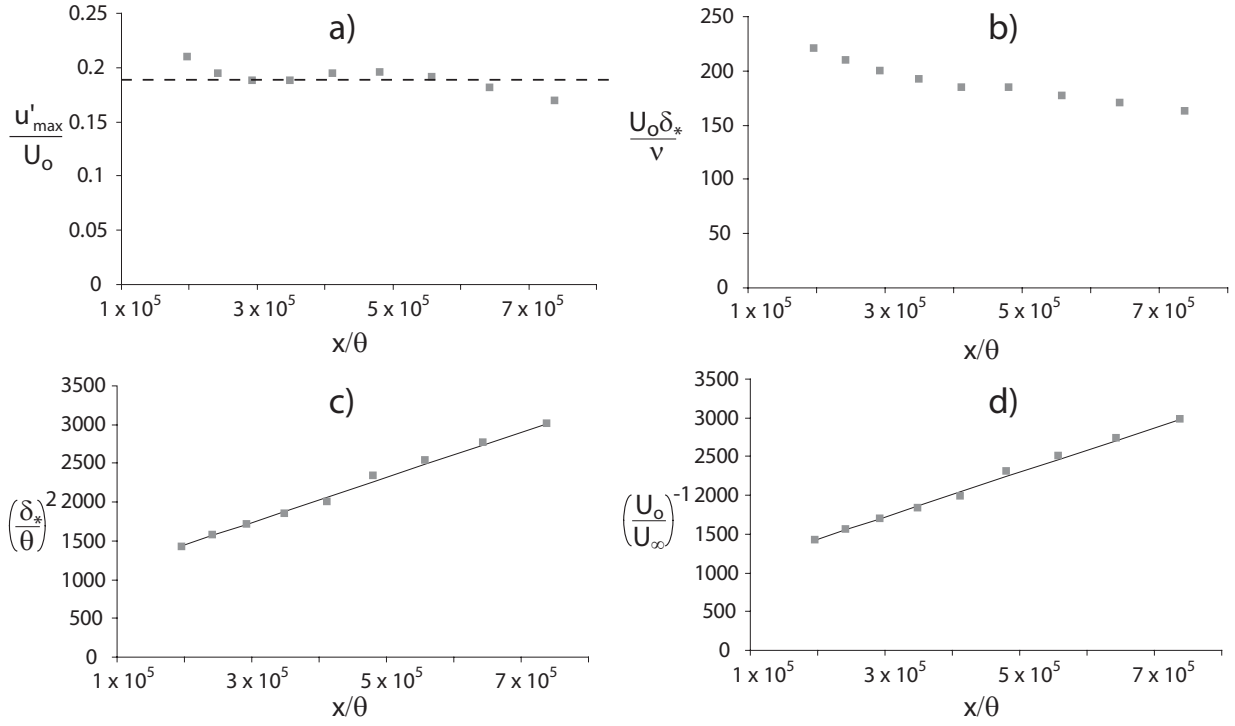

FIG. 14: a) Turbulence intensity, b) *local* Reynolds number, c) wake width, and d) velocity deficit. Data of Gourlay *et al.*[12].

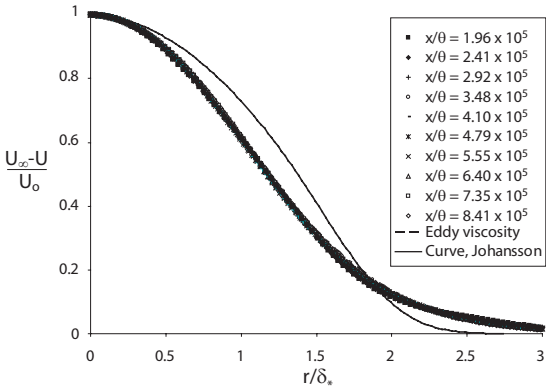

FIG. 15: Mean velocity profiles, far wake data of Gourlay *et al.*[12]. Dashed line shows the solution to the eddy viscosity model, Eq. (C4). Solid line shows the fit according to Eq. (C7) to the data of Johansson[15,16] shown in Fig. 4.

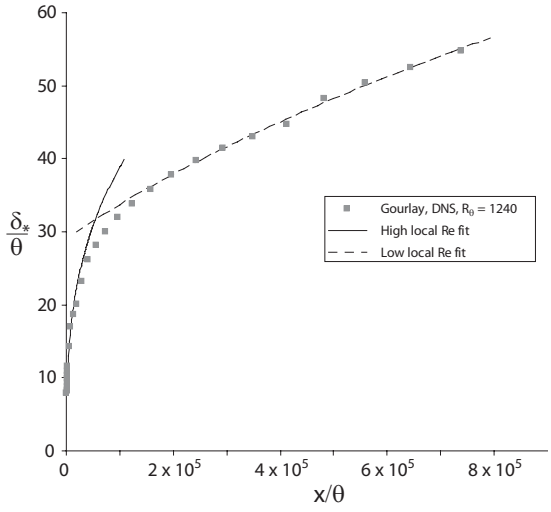

FIG. 16: Cross-stream length scale, δ_*/θ versus x/θ, data of Gourlay *et al.*[12].

too close to the wake generator to provide evidence for the $x^{1/3}$ solution. New results, however, from a laboratory experiment on a disk wake and DNS are in excellent agreement with this solution, once the flow has had large enough downstream distance to evolve. Beyond this, the ratio of turbulence intensity to centreline velocity deficit is constant until the flow unlocks itself from this behavior when the *local* Reynolds number goes below about 500. When this happens the turbulence intensity ratio falls slowly until the $x^{1/2}$ region is reached.

No experimental data is available far enough downstream to provide evidence for the $x^{1/2}$ solution. The prediction that the flow should evolve into such a state, however, is confirmed by recent direct numerical simulation (DNS) results which reach the $x^{1/2}$ at about 200,000 momentum thicknesses downstream, after which the turbulence intensity ratio is again constant until box-size affects the calculation.

The conclusions that can be drawn are that the initial conditions and local Reynolds number effects domi-

nate the axisymmetric wake. Thus previous speculations that near wake effects persist far downstream are correct. Moreover, contrary to popular belief, this effect is consistent with a proper similarity analysis. The effect of initial conditions does not show up in the normalized velocity profiles, but in growth rate and higher moments, exactly as the theory predicts.

IX. ACKNOWLEDGEMENTS

The authors would like to thank Professor Henrik Alfredsson of the Swedish Royal Institute (KTH) for the use of the their MTL windtunnel. This work was initially supported by Chalmers University of Technology. It continues with the support of the Swedish Research Council, grant number 2641.

[1] T. Carmody. Establishment of the wake behind a disk. *Journal of Basic Engineering*, 86:869–882, 1964.

[2] N. C. H. Hwang and L. V. Baldwin. Decay of turbulence in axisymmetric wakes. *Journal of Basic Engineering*, 88:261–268, 1966.

[3] M. S. Uberoi and P. Freymuth. Turbulent energy balance and spectra of the axisymmetric wake. *Phys. Fluids*, 13(9):2205–2210, 1970.

[4] P. M. Bevilaqua and P. S. Lykoudis. Turbulence memory in self-preserving wakes. *Journal of Fluid Mechanics*, 89(3):589–606, 1978.

[5] A. A. Townsend. *The Structure of Turbulent Shear Flow*. Cambridge University Press, Cambridge, UK, 1956.

[6] S. C. Cannon. *Large-scale structures and the spatial evolution of wakes behind axisymmetric bluff bodies*. PhD thesis, Dept. of Aerosp. and Mech. Engr., Univ. of Arizona, 1991.

[7] Ö. İlday, H. Acar, M. Kubilay Elbay, and V. Atli. Wakes of three axisymmetric bodies at zero angle of attack. *AIAA Journal*, 31:1152–1154, 1992.

[8] C. Ostowari and R. H. Page. Velocity defect of axisymmetric wakes. *Experiments in Fluids*, 7:284–285, 1989.

[9] J. L. F. Portiero and V. Perez-Villar. Wake development in turbulent subsonic axisymmetric flows. *Experiments in Fluids*, 21:145–150, 1996.

[10] A. I. Sirviente and V. C. Patel. Experiment in the turbulent near wake of an axisymmetric body. *AIAA Journal*, 37(12):1670–1673, 1999.

[11] A. J. Basu, R. Narasimha, and U. N. Sinha. Direct numerical simulation of the initial evolution of the axisymmetric wake. *Current Science*, 63(12):734–740, 1992.

[12] M. J. Gourlay, S. C. Arendt, D. C. Fritts, and J. Werne. Numerical modeling of initially turbulent wakes with net momentum. *Phys. Fluids*, 13:3783–3802, 2001.

[13] H. Schlichting. *Boundary-Layer Theory*. McGraw-Hill, New York, NY, 1968.

[14] P. B. V. Johansson, W. K. George, and S. H. Woodward. Proper orthogonal decomposition of an axisymmetric turbulent wake behind a disk. *Accepted for publication in Physics of Fluids*, June 2002.

[15] P. B. V. Johansson. *The axisymmetric wake*. PhD thesis, Chalmers University of Technology, Gothenburg, Sweden, 2002.

[16] P. B. V. Johansson and W. K. George. Investigation of the far downstream evolution of the high reynolds number axisymmetric wake behind a disk. *Submitted for publication*, 2002.

[17] H. Tennekes and J. L. Lumley. *A First Course in Turbulence*. MIT Press, Cambridge,MA, 1972.

[18] S. Cannon, F. Champagne, and A. Glezer. Observations of large-scale structures in wakes behind axisymmetric bodies. *Experiments in Fluids*, 14:447–450, 1993.

[19] W. K. George. The self-preservation of turbulent flows and its relation to initial conditions and coherent structures. In *Advances in Turbulence*, pages 39–73. Hemisphere Press, 1989.

[20] W. K. George. Some new ideas for similarity of turbulent shear flows. In *Proc. ICHMT Symposium on Turbulence, Heat and Mass Transfer, Lisbon, Portugal (1994)*, K. Hanjalic and J. C. F. Pereira, editors. Begell House, 1995.

[21] I. Wygnanski, F. Champagne, and B. Marasli. On the large-scale structures in two-dimensional, small-deficit, turbulent wakes. *Journal of Fluid Mechanics*, 168:31–71, 1986.

[22] A. A. Townsend. *The Structure of Turbulent Shear Flow*. Cambridge University Press, Cambridge, UK, second edition, 1976.

[23] P. B. V. Johansson and W. K. George. Further studies of the axisymmetric disk wake using the 'slice POD'. In *2002 ASME Fluid Engineering Division Summer Meeting*, Montreal, Canada, July 14-18, 2002.

[24] W. K. George, P. B. V. Johansson, and S. Gamard. How has the study of coherent structures contributed to our understanding of turbulent free shear flows? In *2002 ASME Fluid Engineering Division Summer Meeting*, Montreal, Canada, July 14-18, 2002.

[25] W. K. George and L. Castillo. Zero-pressure-gradient turbulent boundary layer. *Applied Mech. Rev.*, 50(12):689–729, 1997.

[26] R. D. Moser, M. M. Rogers, and D. W. Ewing. Self-similarity of time-evolving plane wakes. *Journal of Fluid Mechanics*, 367:255–289, 1998.

[27] W. K. George and H. Wang. The decay of confined turbulence. *Bulletin of the American Physical Society*, 46(10), 2001.

APPENDIX A: GOVERNING EQUATIONS

The Reynolds averaged x-momentum equation for the axisymmetric far wake without swirl reduces to second order to:

$$U_\infty \frac{\partial}{\partial x}\left(U - U_\infty\right) = -\frac{1}{r}\frac{\partial}{\partial r}\left(r\overline{uv}\right) + \nu\frac{1}{r}\frac{\partial}{\partial r}\left(r\frac{\partial}{\partial r}\left(U - U_\infty\right)\right) \tag{A1}$$

Here, upper case letters denote averaged quantities and lower case letters represent the fluctuating part. A bar over the quantity denotes an ensemble average. The viscous term is usually neglected, but retained here.

The momentum equation can be integrated over a cross-section to yield an integral constraint for the conservation of momentum:

$$U_\infty \int_0^\infty \left(U_\infty - U\right)\, r\, dr \cong \theta^2 U_\infty^2 \tag{A2}$$

where θ is the momentum thickness.

The equation of continuity for the mean and instantaneous velocities are:

$$\frac{\partial U}{\partial x} + \frac{1}{r}\frac{\partial}{\partial r}\left(rV\right) = 0, \qquad \frac{\partial u}{\partial x} + \frac{1}{r}\frac{\partial}{\partial r}\left(rv\right) + \frac{1}{r}\frac{\partial w}{\partial \theta} = 0 \tag{A3}$$

As noted by George[20], the momentum and continuity equations alone are not sufficient to determine the similarity constraints. Even the inclusion of the kinetic energy equation is not enough to close the system so that the x-dependence can be determined. Instead, the individual Reynolds stress equations have to be investigated. These, together with the constraint of continuity on the pressure-strain rate terms, provide the necessary conditions. The component Reynolds stress equations for the far wake are:

$\overline{u^2}$ balance

$$U_\infty \frac{\partial}{\partial x}\left(\frac{1}{2}\overline{u^2}\right) = -\overline{uv}\frac{\partial}{\partial r}\left(U - U_\infty\right) - \frac{1}{r}\frac{\partial}{\partial r}\left(r\frac{1}{2}\overline{u^2 v}\right) + \overline{\frac{p}{\rho}\frac{\partial u}{\partial x}} - \frac{1}{\rho}\frac{\partial}{\partial x}\overline{pu} + \nu\frac{1}{r}\frac{\partial}{\partial r}\left\{r\frac{\partial}{\partial r}\left(\frac{1}{2}\overline{u^2}\right)\right\} - \varepsilon_u \tag{A4}$$

$\overline{v^2}$ balance

$$U_\infty \frac{\partial}{\partial x}\left(\frac{1}{2}\overline{v^2}\right) = -\frac{1}{r}\frac{\partial}{\partial r}\left(r\frac{1}{2}\overline{v^3}\right) + \frac{\overline{vw^2}}{r} + \overline{\frac{p}{\rho}\frac{\partial v}{\partial r}} - \frac{1}{\rho}\frac{\partial}{\partial r}\overline{pv} + \nu\frac{\partial}{\partial r}\left\{\frac{1}{r}\frac{\partial}{\partial r}\left(r\frac{1}{2}\overline{v^2}\right)\right\} - \varepsilon_v \tag{A5}$$

$\overline{w^2}$ balance

$$U_\infty \frac{\partial}{\partial x}\left(\frac{1}{2}\overline{w^2}\right) = -\frac{1}{r}\frac{\partial}{\partial r}\left(r\frac{1}{2}\overline{uw^2}\right) - \frac{\overline{vw^2}}{r} + \nu\frac{\partial}{\partial r}\left\{\frac{1}{r}\frac{\partial}{\partial r}\left(r\frac{1}{2}\overline{w^2}\right)\right\} - \varepsilon_w \tag{A6}$$

$\overline{uv}$ balance

$$U_\infty \frac{\partial}{\partial x}\left(\overline{uv}\right) = -\overline{v^2}\frac{\partial}{\partial r}\left(U - U_\infty\right) - \frac{1}{r}\frac{\partial}{\partial r}\left(r\overline{uv^2}\right) + \frac{\overline{uw^2}}{r} + \overline{\frac{p}{\rho}\left(\frac{\partial u}{\partial r} + \frac{\partial v}{\partial x}\right)} - \frac{1}{\rho}\left(\frac{\partial}{\partial r}\overline{pu} + \frac{\partial}{\partial x}\overline{pv}\right) + \nu\frac{\partial}{\partial r}\left\{\frac{1}{r}\frac{\partial}{\partial r}\left(r\frac{1}{2}\overline{uv}\right)\right\} - \varepsilon_{uv} \tag{A7}$$

where ε_u, ε_v, ε_w, and ε_{uv} are the components of the homogenous dissipation.

APPENDIX B: TRANSFORMED EQUATIONS

1. The Momentum Integral

Substitution of Eq. (3) into Eq. (A2) yields:

$$U_s\delta^2 \int_0^\infty f\eta\, d\eta = U_\infty\theta^2 \tag{B1}$$

It follows immediately that if $\delta \equiv \delta_*$ and $U_s \equiv U_o$:

$$\frac{U_s}{U_\infty} = \left[\frac{\theta}{\delta_*}\right]^2 \tag{B2}$$

2. The Mean Momentum and Reynolds Stress Equation

Substituting Eq. (3) into the momentum equation, Eq. (A1), and rearranging the terms yields:

$$\left[\frac{\delta}{U_s}\frac{dU_s}{dx}\right] f - \left[\frac{d\delta}{dx}\right]\eta f' = \left[\frac{R_s}{U_\infty U_s}\right]\frac{(\eta g)'}{\eta} + \left[\frac{\nu}{U_\infty\delta}\right]\frac{(\eta f')'}{\eta} \tag{B3}$$

where $'$ denotes derivation with respect to η. To this point the mean momentum equations have simply been transformed by the separation of variables in Eq. (3) so that all of the explicit x-dependence is in the bracketed terms. Thus the results are completely general and no similarity assumptions have yet been made (although the form of the solutions has been restricted). Using Eq. (B1), Eq. (B3) can be rewritten as:

$$-\left[\frac{d\delta}{dx}\right](\eta^2 f)' = \left[\frac{R_s}{U_\infty U_s}\right]\frac{(\eta g)'}{\eta} + \left[\frac{\nu}{U_\infty\delta}\right]\frac{(\eta f')'}{\eta} \tag{B4}$$

Substituting Eq. (3) into the transport equations for Reynolds stresses yields:

$\overline{u^2}$-equation

$$\left[U_\infty\frac{dK_u}{dx}\right]k_u - \left[\frac{U_\infty K_u}{\delta}\frac{d\delta}{dx}\right]\eta k_u' = -\left[\frac{R_s U_s}{\delta}\right]f' - \left[\frac{T_{u^2v}}{\delta}\right]\frac{(\eta t_{u^2v})'}{\eta} + [P_u]\,p_u + \left[\frac{dP_u^D}{dx}\right]p_u^D - \left[\frac{P_u^D}{\delta}\frac{d\delta}{dx}\right]\eta(p_u^D)' + \left[\frac{\nu K_u}{\delta^2}\right]\frac{(\eta k_u')'}{\eta} - [D_u]\,d_u \tag{B5}$$

$\overline{v^2}$-equation

$$\left[U_\infty\frac{dK_v}{dx}\right]k_v - \left[\frac{U_\infty K_v}{\delta}\frac{d\delta}{dx}\right]\eta k_v' = - \left[\frac{T_{v^3}}{\delta}\right]\frac{(\eta t_{v^3})'}{\eta} + \left[\frac{T_{vw^2}}{\delta}\right]\frac{t_{vw^2}}{\eta} + [P_v]\,p_v + \left[\frac{P_v^D}{\delta}\right](p_v^D)' + \left[\frac{\nu K_v}{\delta^2}\right]\frac{(\eta k_v')'}{\eta} - [D_v]\,d_v \tag{B6}$$

$\overline{w^2}$-equation

$$\left[U_\infty \frac{dK_w}{dx}\right] k_w - \left[\frac{U_\infty K_w}{\delta}\frac{d\delta}{dx}\right]\eta k_w' = - \left[\frac{T_{uw^2}}{\delta}\right]\frac{(\eta t_{uw^2})'}{\eta} - \left[\frac{T_{vw^2}}{\delta}\right]\frac{t_{vw^2}}{\eta} + \left[\frac{\nu K_w}{\delta^2}\right]\frac{(\eta k_w')'}{\eta} - [D_w]\, d_w \quad \text{(B7)}$$

$\overline{uv}$-equation

$$- \left[U_\infty \frac{dR_s}{dx}\right] g - \left[\frac{U_\infty R_s}{\delta}\frac{d\delta}{dx}\right]\eta g' = \left[\frac{K_v U_s}{\delta}\right] f' k_v - \left[\frac{T_{uv^2}}{\delta}\right]\frac{(\eta t_{uv^2})'}{\eta} + \left[\frac{T_{uw^2}}{\delta}\right]\frac{t_{uw^2}}{\eta} + [P_{uv}]\, p_{uv} - \left[\frac{P_u^D}{\delta}\right](p_u^D)' - \left[\frac{dP_v^D}{dx}\right](p_v^D) - \left[\frac{P_v^D}{\delta}\frac{d\delta}{dx}\right]\eta (p_v^D)' - \left[\frac{\nu R_s}{\delta^2}\right]\left(\frac{(\eta g)'}{\eta}\right)' - [D_{uv}]\, d_{uv} \quad \text{(B8)}$$

As before, the equations have simply been transformed by the similarity transformations so that all the explicit x-dependence is in the bracketed terms.

APPENDIX C: A SOLUTION FOR A CONSTANT EDDY VISCOSITY MODEL

A solution of the momentum equation with the viscous term included (Eq. A1) can be obtained if an eddy viscosity assumption is made. Let

$$-\frac{1}{r}\frac{\partial}{\partial r}(r\overline{uv}) = \nu_T \frac{1}{r}\frac{\partial}{\partial r}\left(r\frac{\partial}{\partial r}(U - U_\infty)\right) \quad \text{(C1)}$$

Using Eq. (C1) and applying the similarity transformation, Eq (3), the governing equation in similarity form becomes:

$$-\left[\frac{d\delta}{dx}\right](\eta^2 f)' = \left[\frac{\widetilde{\nu}}{U_\infty \delta}\right]\frac{(\eta f')'}{\eta} \quad \text{(C2)}$$

where $\widetilde{\nu} = \nu + \nu_T$. Grouping the terms in square brackets, setting $k = (U_\infty \delta/\widetilde{\nu})\,\partial\delta/\partial x$, results in the following differential equation:

$$(k\eta^2 f + \eta f')' = 0 \quad \text{(C3)}$$

The boundary conditions are $f(0) = 1$, $f(\infty) = 0$, and $f'(0) = f'(\infty) = 0$. Assuming that $f(\eta)$ goes to zero faster than a polynomial, the solution is given by:

$$f(\eta) = e^{-k\eta^2/2} \quad \text{(C4)}$$

Defining $\delta = \delta_*$, Eq. (B1), gives:

$$\int_0^\infty f(\eta)\eta\, d\eta = 1 \quad \text{(C5)}$$

which is satisfied if $k = 1$. Then, the actual value of the eddy viscosity is given by:

$$\nu_T = U_\infty \delta_* \frac{d\delta_*}{dx} - \nu \quad \text{(C6)}$$

From the low local Reynolds number solution, Eq (14), we have $\delta_* d\delta_*/dx = c^2/2R_\theta$, which finally results in $\nu_T = U_\infty c^2/2R_\theta - \nu$. The value of ν_T can be estimated using the curve fit to the simulation of Gourlay *et al.*[12]. In this simulation, $c = 1.90$, $U_\infty = 1$ m/s, $R_\theta = 1240$, and $\nu = 10^{-4}$ m^2/s, so $\nu_T = 1.35 \times 10^{-3}$ m^2/s. Thus $\nu_T/\nu = 13.5$, and this value is maintained throughout the low local Reynolds number similarity regime.

As noted by Johansson[15,16], the simple exponential of the eddy viscosity solution is not a good fit to the high Reynolds number profile data, since it is too narrow near the centerline and falls off too slowly at large radius. Instead a curve was fitted to the data of the form:

$$f(\eta) = (1 + a\eta^2 + b\eta^4)e^{(-c\eta^2 - d\eta^4)} \quad \text{(C7)}$$

where $a = 0.049$, $b = 0.128$, $c = 0.345$, and $d = 0.134$. This curve is shown in Figs. 4, 13, and 15.

Paper 6

How has the study of coherent structures contributed to our understanding of turbulent free shear flows?

Invited Lecture
To appear in
Proceedings of the ASME Fluids Engineering Division Summer Meeting
FEDSM2002-31408
Montreal, Quebec, Canada, July 14-18, 2002

W. K. George
P. B. V. Johansson
S. Gamard

Proceedings of FEDSM'02
2002 ASME Fluid Engineering Division Summer Meeting
July 14-18, 2002, Montreal, Quebec, Canada

FEDSM2002-31408

HOW HAS THE STUDY OF COHERENT STRUCTURES CONTRIBUTED TO OUR UNDERSTANDING OF TURBULENT FREE SHEAR FLOWS?

William K. George
Turbulence Research Laboratory
Dept. of Thermo and Fluid Dynamics
Chalmers University of Technology
Gothenburg, SE-41 296, SWEDEN
E-mail: wkgeorge@tfd.chalmers.se

Peter B. V. Johansson
Turbulence Research Laboratory
Dept. of Thermo and Fluid Dynamics
Chalmers University of Technology
Gothenburg, SE-41 296, SWEDEN
E-mail: jope@tfd.chalmers.se

Stephan Gamard
Turbulence Research Laboratory
Dept. of Thermo and Fluid Dynamics
Chalmers University of Technology
Gothenburg, SE-41 296, SWEDEN
E-mail: gamard@tfd.chalmers.se

ABSTRACT

Recent applications of the 'slice POD' to the axisymmetric turbulent wake and jet are reviewed, and the results used to provide a critique of commonly held views about these flows. It is argued that the so-called 'coherent structures' are simply artifacts of the source conditions, and have little to do with the far downstream development of these flows. Also, experimental evidence is presented for the possible presence of Townsend's large eddies, eddies whose primary role is to warp the mean motion. Finally, classical linear stability analysis which 'predicted' that only azimuthal mode-1 could be unstable for these flows is shown to be deficient, with the result that at very least modes-0, 1 and 2 could be important, consistent with the experiments.

INTRODUCTION

It has been more than a half century since Townsend and his co-workers (v. Townsend, 1956) postulated the existence of large eddies. These were believed to be rather passive structures of very large scale containing 10 to 20% of the energy. The primary evidence for their existence were two-point velocity correlations at large separations.

Starting in the early 1970's and continuing for the next two decades, the turbulence community's attention was riveted on the search for coherent structures. In contrast with the large eddies of Townsend, these 'coherent structures' were believed to be responsible for most of the energetics of turbulence. Some even went so far as to claim that the study of turbulence, and especially using averages, made no sense without explicitly accounting for coherent structures. There are numerous reviews of the coherent structure literature, all of which together summarize the important observations, and none of which show how this knowledge can be incorporated into a turbulence model. This absence of a mathematical theory has left the concept of 'coherent structures' in limbo — everyone more or less believes they exist, no one knows what to do about them.

Originally posed as a means to objectively identify Townsend's large eddies, the Proper Orthogonal Decomposition (POD) was introduced by Lumley (1967). Early applications were limited by the lack of sufficient correlation data, but the POD became viable with the advent of computers in the laboratory and DNS. Leib *et al.* (1984) showed the first reconstructions of time signals in a cross-section of a jet mixing layer, and illustrated dramatically the dynamic possibilities presented by the POD. Subsequent applications using rakes of hot-wires (Glauser and George, 1987) and DNS (Moin and Moser, 1989) made it clear that the POD was indeed a useful way to capture the dynamics of shear flow turbulence.

But the POD is not limited to merely reducing data. Unlike the subjective approaches generally employed in coherent structures research, it also could be used for carrying out dynamic calculations using reduced versions of the Navier-Stokes equations. The contribution of Aubry *et al.* (1988) using a Galerkin projection of the measured POD eigenfunctions onto the Navier-Stokes equations for the near-wall region of channel flow was the beginning of a flood of applications to the POD using dynamic

systems theory (v. Holmes *et al.*, 1996).

There have been a number of recent papers reporting the application of POD techniques to turbulent free shear flows including the plane mixing layer (Delville *et al.*, 1999, Ukeiley *et al.*, 2001), the plane jet (Gordeyev and Thomas, 2000), the axisymmetric jet mixing layer (Citriniti and George, 2000, Jung *et al.*, 2002), the far jet (Gamard *et al.*, 2002), and the axisymmetric wake (Johansson *et al.*, 2002). This paper begins by summarizing some of our recent results from two axisymmetric shear flows — the turbulent jet and the wake behind a disk.

AN OVERVIEW OF THE POD

At the core of the theoretical and experimental application of the POD is the replacement by deterministic functions of the instantaneous random flow which have maximal projection on it. These deterministic functions (or eigenfunctions) are obtained either analytically or empirically from the resulting integral equation, the kernel of which is the two-point correlation of the velocity itself. The original field can be recovered by summing together (or integrating over) the contributions of each eigenfunction and its random coefficient, the latter determined by projecting each eigenfunction onto the instantaneous field (exactly like the determination of coefficients in ordinary Fourier analysis). This sequence of operations is often collectively referred to as the POD, but this is a misnomer as will be shown below, since strictly speaking only the inhomogeneous problem leads to a "proper" (in the sense of ordered) decomposition.

The two flows considered below (the turbulent axisymmetric wake and jet) are both stationary in time and homogeneous, periodic in the azimuthal direction. The POD integral equations can be immediately solved in these directions to yield Fourier modes, continuous in temporal frequency, f, and discrete in azimuthal mode number, m, (George, 1988). The streamwise direction is problematical, since it is neither homogenous nor of finite total energy. Hence in the absence of other considerations, the eigenfunctions will be determined by how the domain is truncated. Fortunately, the similarity of the two-point Reynolds stress equations resolves the problem for the flows considered here, and the streamwise eigenfunctions can be shown to be harmonic functions of the variable $\ln x$. This was first noted by Ewing and George (1995), and has been discussed in some detail by George (1988, 1999).

In general it is easier to proceed if the field is first decomposed using the known eigenfunctions, then the POD applied to this transformed field in the remaining inhomogeneous variables. Experimentally it is almost impossible (at the moment) to measure an entire field simultaneously, so the applications below utilize the 'slice-POD' — the POD applied to a single cross-section, x. Thus the problem becomes to seek empirical eigenfunctions which optimally project a deterministic function, $\phi_i(m,f,x;r)$, onto the transformed random velocity field, $\hat{u}_i(m,f,x;r)$. The variables m, f, and x are essentially parameters. In general there are an infinite number of eigenfunctions, $\phi_i^{(n)}$, which are solutions to the integral equation:

$$\int_0^\infty \Phi_{ij}(m,f,x;r,r')\phi_j^{(n)}(m,f,x;r')\,r'\,dr' \tag{1}$$

$$= \lambda^{(n)}(m,f,x)\phi_i^{(n)}(m,f,x;r) \tag{2}$$

where Φ_{ij} is the cross-spectral tensor.

The decomposition is optimal in the sense that the lowest order eigenfunction contains the maximum possible amount of energy. Moreover the total "energy spectrum" at a cross-section is the sum of the eigenvalues; i.e.,

$$\tilde{E}(m,f,x) = \sum_{n=1}^{\infty} \lambda^{(n)}(m,f,x) \tag{3}$$

These can in turn be summed over all frequencies and azimuthal modes numbers to recover the total energy in a cross-section as shown below. In practice the number of eigenfunctions is limited by the finite number of resolved points of the kernel.

THE RECENT OBSERVATIONS

Johansson *et al.* (2002) report applications of the 'slice' POD using rakes of hot-wires at various downstream cross-sections of the axisymmetric wake behind a disk at a Reynolds number based on diameter and free stream velocity of $28,000$. Jung *et al.* (2002) and Gamard *et al.* (2002) report similar application of the slice POD using 138 hot-wires in the axisymmetric jet with nearly top-hat source conditions at source Reynolds numbers ranging from $40,000$ to $157,000$. In both experiments the first radial POD mode contains approximately 60% of the resolved streamwise energy (about 40 % of the total streamwise energy), and only it will be of interest herein. Of primary interest will be the eigenspectrum of this first POD mode which shows how the energy of the cross-section is distributed with azimuthal mode number, m, and temporal frequency, f; i.e., $\lambda^{(1)}(m,f)$. Note that the variable f is considered to be continuous, while m is integer and positive only for the eigenspectra considered.

The eigenspectra can be integrated over frequency, f, to obtain the distribution of energy with only the azimuthal mode number, m. If this is normalized by the total energy at the cross-section the result is:

$$\xi^{(1)}(m) = \frac{\int_0^\infty \lambda^{(1)}(m,f)\,df}{\sum_{m=0}^{M}\int_0^\infty \lambda^{(1)}(m,f)\,df} \tag{4}$$

where M is the highest resolved azimuthal mode. Figure 1 is compiled from Jung *et al.* (2002) and Gamard *et al.* (2002), and

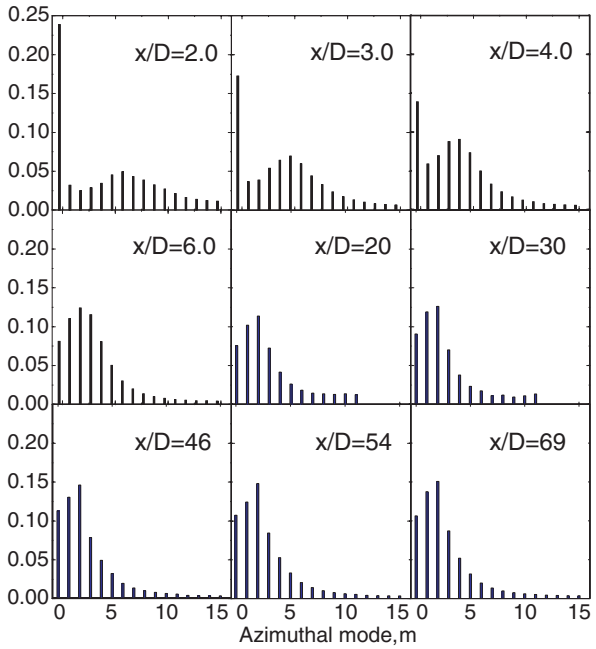

Figure 1. ENERGY DISTRIBUTION FOR THE LOWEST ORDER POD MODE. AXISYMMETRIC TURBULENT JET.

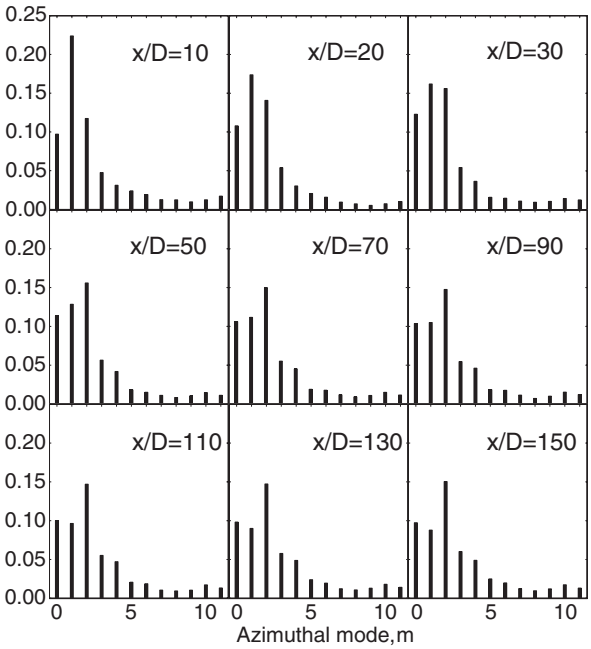

Figure 2. ENERGY DISTRIBUTION FOR THE LOWEST ORDER POD MODE. AXISYMMETRIC TURBULENT WAKE.

shows the downstream evolution of this first azimuthal eigenspectrum, $\xi^{(1)}(m)$ for the jet.

The azimuthal mode distribution in Fig. 1 at $x/D = 2$ shows a dominant peak at mode-0, and a distribution of energy centered about mode-6. As the distance from the exit plane is increased, mode-0 diminishes and the center of the distribution moves to lower values, from mode-5 at $x/D = 3$ (as noted by Glauser and George, 1987 and more recently Citriniti and George, 2000) to only a distribution around mode-2 by $x/D = 6$. After $x/D \approx 6$, the distribution shows no further evolution, coincident with the fact that the mean centerline velocity has approximately reached near similarity behaviour (about $x/D \approx 10$). Also the ratio of centerline rms velocity to the mean centerline velocity is constant shortly after this evolution is complete, and the mean velocity profiles and turbulence intensity profiles begin to collapse as well. Obviously the diminishing value of mode-0 and the emergence of the mode-2 peak both reflect (or are responsible for) the process by which a top-hat profile evolves into a self-preserving jet.

Figure 2 from Johansson and George (2002 b) (and Johansson *et al.*, 2002) shows a similar azimuthal mode evolution for the axisymmetric wake behind a disk. For the near wake, at $x/D = 10$, mode-1 dominates, exactly as reported by others (Fuchs *et al.*, 1979, Berger *et al.*, 1990). But by $x/D = 30$, the energy in mode-2 is nearly equal to that in mode-1. By $x/D = 50$, mode-2 dominates, as it does for all positions downstream.

Like the jet, the emergence of this mode-2 dominance corresponds also to the emergence of the similarity state, particularly evident in the normalized turbulence intensity which does not approach a constant until about $x/D = 50 - 70$. The implications of this for attempts to study axisymmetric wakes are profound, since most attempts seldom measure much beyond this point (e.g., Cannon, 1991, Uberoi and Freymuth, 1970) due to the extremely low turbulence intensities and limited wind tunnel lengths.

THE EIGENSPECTRA AS FUNCTIONS OF m AND f.

It is important to first discuss what the variable f means, or more precisely, what it does *not* mean. Experimentally it is the frequency (or temporal variation) observed by the measuring apparatus. Unfortunately its interpretation as space or time is complicated by the fact the turbulence is being convected by the probes while it is also evolving in time. The so-called "Taylor's frozen field hypothesis" assumes that convection dominates evolution, so temporal variations can be interpreted as spatial variations. For the wake where $u'/U < 10\%$, Taylor's hypothesis is certainly valid, at least for all but the very lowest frequencies. For the far jet though, $u'/U > 25\%$ always, so Taylor's hypothesis can be applied only for the small scales, and it is not possible to interpret unambiguously the large scales.

Figure 3 shows three-dimensional plots of the first eigen-

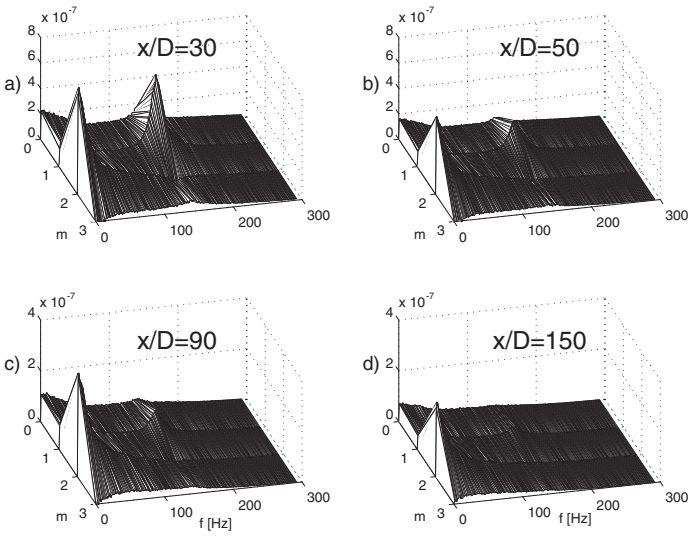

Figure 3. FIRST EIGENSPECTRUM, $\lambda^{(1)}(m, f, x)$, FOR THE DISK WAKE AT VARIOUS x/D. a) 30, b) 50, c) 90, AND d) 150.

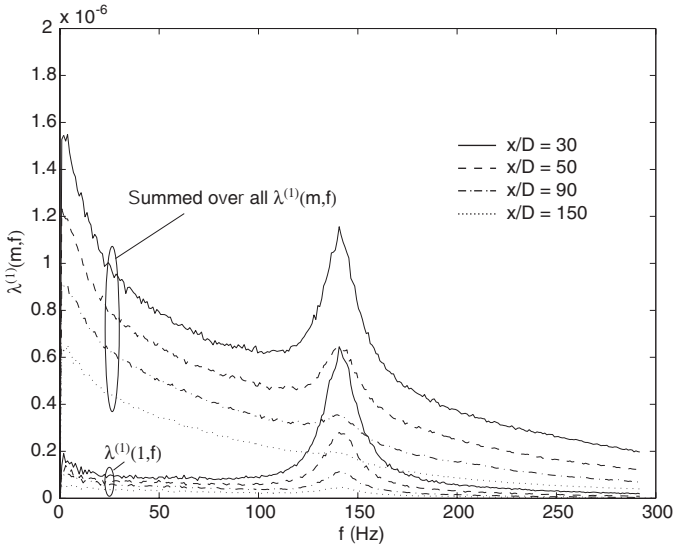

Figure 4. THE TOTAL ENERGY AND MODE-1 ALONE AS A FUNCTION OF FREQUENCY AT $x/D = 30, 50, 90$ AND 150.

spectrum, $\lambda^{(1)}(m, f, x)$, for the disk wake at $x/D = 30$, 50, 90 and 150. The most striking feature is the clear separation of the frequency content of the various modes. Only mode-1 has a peak at a non-zero frequency. The other eigenspectra (of which mode-2 is predominant) all resemble the usual broadband one-dimensional spectra of turbulence which peak at zero frequency (usually due to aliasing from the unresolved directions). The eigenspectra have not been normalized, so their heights decay downstream as the wake itself decays. But even from just these four plots it is obvious that mode-1 dies more quickly than the other modes, and especially mode-2. In fact, the reason for the behaviour of the normalized azimuthal mode number plots above (Fig. 2) is clearly not that mode-2 is increasing its contribution, but that mode-1 is fading more rapidly.

Figure 4 shows plots of the total energy and mode-1 alone as a function of frequency for the same downstream positions. Most striking is that the peak frequency of the band which contains most of the energy for mode-1 does not evolve downstream, but is fixed. Moreover its contribution to the total energy is clearly diminishing downstream, as noted above. Thus the primary contribution of mode-1 clearly does not scale in local shear layer variables, but is instead determined only by the Strouhal number of the near wake. It seems apparent that the primary contribution to mode-1 has been convected in from the near wake, and is virtually independent of the local shear layer of the wake.

By contrast, the behaviour of mode-2 is quite different. Figure 5 shows mode-2 normalized by the energy remaining *after* the energy from mode-1 is removed. These data have been plotted as wavenumber spectra using Taylor's frozen field hypothesis. Note first of all the remarkable 'notch' in mode-2 (all the

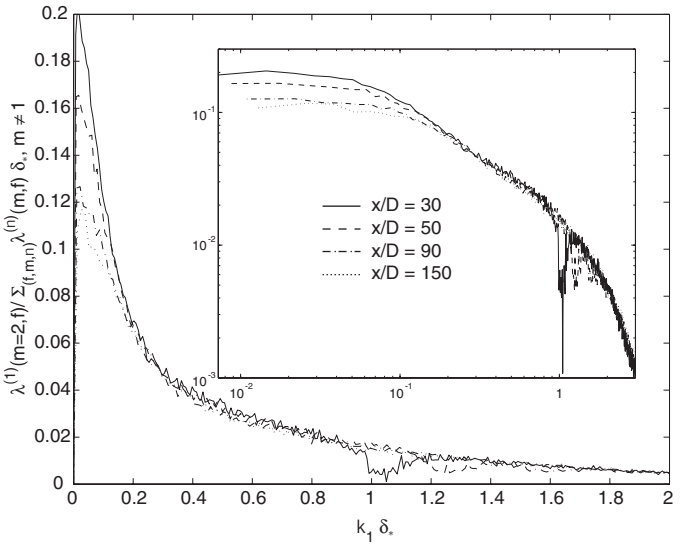

Figure 5. MODE-2 AT x/D = $30, 50, 90$ AND 150, NORMALIZED BY THE ENERGY REMAINING *AFTER* THE ENERGY FROM MODE-1 IS REMOVED. THESE DATA HAVE BEEN PLOTTED AS WAVENUMBER SPECTRA USING TAYLOR'S HYPOTHESIS.

way to zero!) for the position closest to the disk at exactly the frequency where mode-1 is dominant. Clearly mode-1 is suppressing the development of mode-2 at the dominant frequency. As the wake develops downstream, this notch fills in, and except for the very lowest wavenumbers (for which Taylor's hypothesis

is of doubtful validity), these data collapse wonderfully in shear layer variables. Thus, once the contribution of mode-1 has been removed, the rest of the turbulence behaves exactly as might be expected from an equilibrium similarity wake. This is certainly not the case if mode-1 is not removed, which explains the frustrations of many authors in trying to explain their measurements for this flow.

One additional observation can be made. There is a very interesting problem presented by the lack of collapse of the spectra for mode-2 at very low wavenumbers (or perhaps just low frequencies). These very large scales clearly satisfy Townsend's idea of the large eddies. They contain about 5 - 10 % of the energy and do not appear to interact with the main motion. Interestingly, if these data are NOT normalized as wavenumbers, but simply by the energy present at all mode numbers with mode-1 removed, they collapse without any scaling of the frequency axis at all. So what is their role, if any? This is not at all clear as of this writing. One possibility is that they simply slowly twist the mean flow. If so this could account for the remarkably high *local* turbulence intensity for this flow for which at the centerline $u'/(U_\infty - U) \approx 110\%$! In effect, the mean profile is simply being moved around by this very large and slow modulation. There is some evidence for this in the azimuthally averaged instantaneous DNS profiles of Gourlay (2001).

Finally, it is worth commenting on what the usual conditional sampling approaches to coherent structures would have (and have) focused on for this flow. The most coherent energetic motion is the transient mode-1, and this is indeed what such studies have yielded. But this *is the least important part of the problem* for the far wake. Similar considerations apply to the jet as well where the most apparent coherent feature of the flow has seemingly nothing to do with the far jet's evolution, but is simply dying off.

USING THE POD WITH THE NAVIER-STOKES EQUATIONS

One of the advantages the orthogonality of the functions is that they can be easily used to decompose the continuity and Navier-Stokes equations themselves. There are two possible routes:

1. The eigenfunctions, ϕ_i, can be assumed known (usually from experiment like those outlined above) and a hierarchy of dynamical equations can be developed for the time dependent interactions of the coefficients which turn them on and off. An example of this for free shear flows is the recent paper by Ukeiley *et al.* (2001). These approaches need to find some way to dissipate the energy which is transferred to small scales not included in the model.
2. Alternately, the orthogonality of the coefficients can be used to develop equations for the eigenfunctions themselves. If the non-linear terms are included, this approach suffers from the same closure problem of the Reynolds averaged equations. As first noticed by Lumley (1967), there is no closure problem if the equations are linearized. But, of course, linearization precludes mode interaction.

Obviously it would be nice if the second approach could be used to establish the eigenfunctions, and the first to analyze how they interact. There is some reason to hope that this might be possible. For example, both Ukeiley *et al.* (2001) and Rempfer and Fasel (1994) note the close relation between the eigenfunctions derived from linear stability considerations and those in a plane mixing layer and boundary layers respectively.

The linear approach offers a particular advantage in that there is more than one hundred years of rather sophisticated mathematics and experience to help us understand what the results mean. This is especially true for free shear flows where much can be learned by analysis, without the difficulties of interpreting numerical results when many parameters are varying. At the same time, it is important to re-examine each result in turn, to be certain that the assumptions and conclusions previously derived for the instability of laminar flows are applicable to their turbulent counterparts. One such analysis will be examined below, and it will be shown that at least some features of the flows above can be explained when the differences in base flow between laminar and turbulent are accounted for.

WHAT CAN LINEAR THEORY TELL US?

There have been suggestions for many years that linear analysis based on the mean profile might account for features of both turbulence wakes and jets (c.f. Michalke, 1965, 1984). From the perspective of the POD, this is no surprise since the linearized POD equations and the stability equations are the same. Therefore the results should be equally applicable — if the correct problem has been analyzed!

For the statistically axisymmetric flows considered here, the linearized POD equations are exactly those originally considered by Batchelor and Gill (1962). These authors considered only temporally growing disturbances, and it fell to Michalke (1964) to extend the analysis to spatially growing disturbances. All authors appear to agree that while azimuthal mode-0 may dominate during the early top-hat portion of the jet or wake, it is azimuthal mode-1 that dominates the far wake or jet. In fact, it is widely believed that Batchelor and Gill "proved" that ONLY mode-1 could be unstable. Moreover, experimental studies of 'coherent structures' of axisymmetric free shear flows have routinely confirmed the dominance of mode-1. There is little evidence that this view has been challenged until now. Obviously in view of the results reported above, either linear stability analysis is irrelevant, or the 'mode-1 only' belief must be proved wrong. It will be demonstrated in the following paragraphs that the 'mode-1 only' belief

is in fact false.

In brief, Batchelor and Gill assumed a base flow which is an axisymmetric parallel shear flow. Unlike parallel two-dimensional shear flows, there is no counterpart to Squires theorem, so fully three-dimensional disturbances must be considered. Moreover, in the absence of walls, these flows are inviscidly unstable, so the effects of viscosity can be neglected, certainly at the Reynolds numbers of interest here. Linearization, and Fourier decomposition in time and azimuthal coordinate led them to the following equation (equation 2.16 in Batchelor and Gill, 1962) for the radial dependence of the velocity disturbance amplitude:

$$(U-c)\frac{d}{dr}\left\{\frac{r}{m^2+\alpha^2r^2}\frac{d(rG)}{dr}\right\} - (U-c)G - rG\frac{d}{dr}\left(\frac{rU'}{m^2+\alpha^2r^2}\right)=0 \tag{5}$$

where α is a wavenumber in the streamwise direction (since the flow is assumed parallel in x), c is the speed of the disturbance, and as above m is the azimuthal mode number. Note that taking c to be complex means that the disturbance will grow exponentially in time if its imaginary part is negative. The critical layer occurs when $U = c_r$, and neutral disturbances will correspond to $c_i = 0$. The counterpart to equation 5 for parallel shear flows is the famous Rayleigh equation for inviscid parallel shear flows which can be found in most fluids texts. (Note that spatially growing disturbances require a real phase speed and a complex wavenumber, but the mathematics are not as simple or elegant as for the temporal case from which our point can be more easily made.)

Now Batchelor and Gill were presumably interested only in the instability of laminar jets. We are interested in turbulence — in particular turbulence which is statistically axisymmetric and for the moment, homogeneous in x. Thus we will consider the mean velocity profile $U(r)$ to be the base flow, and analyze its stability to small disturbances around it. For our purposes G is exactly $\phi_2^{(n)}(m,\alpha)$ where each POD radial mode satisfies the same equation — assuming the decomposed equations have been linearized. Obviously non-parallel effects and non-linear effects may be of interest, but perhaps less so if the primary energy transfer from mean flow to turbulence is captured by the parallel linear analysis.

In parallel with the derivation of the famous inflection point criteria of Rayleigh and Fjørtoft, Batchelor and Gill divide equation 5 by $U-c$, multiply by the complex conjugate of rG, subtract the complex conjugate of the entire equation, then integrate from $r = 0$ to infinity to obtain the quite simple result:

$$c_i\int_0^\infty |g^2|Q'dr = 0 \tag{6}$$

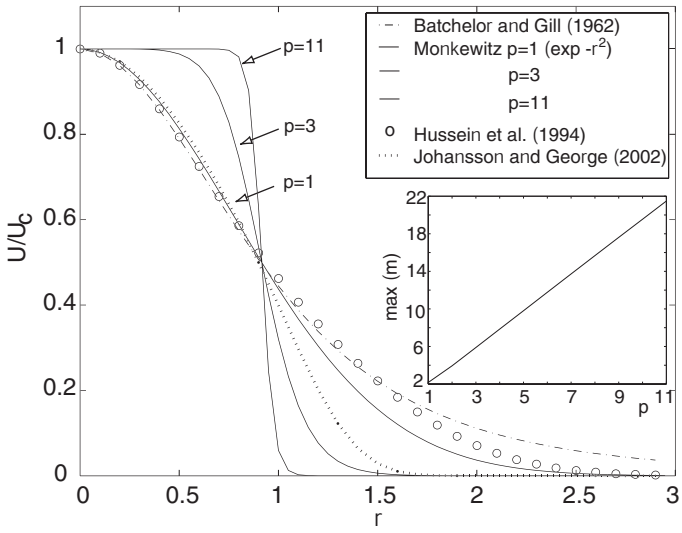

Figure 6. DIFFERENT ANALYTICAL VELOCITY PROFILES. INSERT SHOWS THE MAXIMUM OF m AS A FUNCTION OF p, FROM EQUATION 15

where $g(r) \equiv rG(r)/(U-c)$ and

$$Q(r) \equiv \frac{rU'}{m^2+\alpha^2r^2} \tag{7}$$

Obviously either g must be identically zero (no disturbance at all), or Q' must change sign for some finite and non-zero value of r. This is the axisymmetric counterpart of the famous Rayleigh inflection point criterion.

Azimuthal mode-0

Now Batchelor and Gill argue that mode zero disturbances cannot grow in the 'far jet'. Figure 6 shows several profiles which are commonly used to describe jets and wake deficits. Batchelor and Gill used what they referred to as the 'far-downstream jet profile' *by which they mean*:

$$U/U_c = [1/1+r^2]^2 \tag{8}$$

It is easy to show by differentiation and substitution into the definition of Q that $Q = constant$ for $m = 0$. Thus no mode-0 disturbance can grow, hence their conclusion (*but only valid for this profile!*).

Another profile commonly used for wakes (in fact the exact viscous and eddy viscosity solution) is the simple exponential given by:

$$U/U_c = \exp[-cr^2] \tag{9}$$

It is easy to show that the same is true for this profile as well: the $m = 0$ mode is stable.

By contrast, Batchelor and Gill do argue that a top-hat profile, like that found near the entrance of a jet, does satisfy the conditions for mode-0 to grow. But they state without qualification that profiles which are slowly varying with r do not.

Now the profile given by equation 8 is indeed the 'far-downstream jet' solution to the boundary layer equations for a *laminar* jet. And it is also the eddy-viscosity similarity solution of the Reynolds averaged equations for a turbulent jet. But as shown by Hussein *et al.* (1994), it places too much weight at large values of r so that when the constants are chosen to satisfy the momentum integral, the entrainment is badly over-estimated. From careful fits to their LDA and flying hot-wire profiles, Hussein *et al.* recommended a profile for the far jet of the following form:

$$U/U_c = (1 + ar^2 + br^4)\exp[-cr^2] \tag{10}$$

It is easy to show, again by substitution and differentiation, that this profile does indeed have an interior inflexion point, even for $m = 0$, because of the additional terms before the exponential. The same is true for the similarity wake profile suggested by Johansson and George (2002 a) which is given by:

$$U/U_c = (1 + ar^2 + br^4)\exp[-cr^2 - dr^4] \tag{11}$$

Therefore, it follows immediately that the mean velocity profiles for these two turbulent flows *do* satisfy the necessary condition for mode-0 disturbances, even far downstream. This is certainly contrary to popular belief which has focussed attention almost entirely on mode-1, the so-called *helical mode*. But it is, of course, consistent with all the observations above, where mode-0 is present for all values of x/D, exactly as one should expect from the measured mean velocity profiles.

The upper limit on which modes can grow

A necessary condition for unstable disturbances is that Q have an inflection point; i.e., $Q'' = 0$. It is straightforward to show that this is possible only if there is a non-zero and finite value of r, say $r = r_c$, satisfying:

$$(m^2 - \alpha^2 r_c^2)/(m^2 + \alpha^2 r_c^2) = -rU''/U' \tag{12}$$

If so, then $r = r_c$ is the location of the critical layer.

Because of the Batchelor and Gill deductions, it has been commonly believed that modes higher than mode-1 cannot be unstable. What does not seem to be realized is that *this result is entirely based on the assumed 'far-jet downstream profile (equation 8)'*.

To see this, consider Batchelor and Gill's equation 5.14 which is given for $m \neq 0$ by:

$$r\frac{d}{dr}\left\{\frac{r}{1+\beta^2 r^2}\frac{d(rG)}{dr}\right\} = [m^2 - N^2(r,\beta)]rG \tag{13}$$

where $\beta \equiv \alpha/m$ and N^2 is the positive-valued function defined by:

$$N^2(r,\beta) = \frac{r}{U(r_c) - U(r)}\frac{d}{dr}\left[\frac{rU'}{1+\beta^2 r^2}\right] \tag{14}$$

Now Batchelor and Gill argue from equation 14 that neutral disturbances with $c = U(r_c)$ can not exist unless the azimuthal mode number, m, satisfies:

$$m^2 < max_{r,\beta} N^2(r,\beta) \tag{15}$$

In other words, the highest azimuthal mode number must be *less* than the square root of the highest possible value of N^2.

From its definition in equation 14, it is clear that it is reasonable to expect the maximum value of N^2 to depend on the velocity profile. For the 'far downstream jet profile' of Batchelor and Gill, equation 8, the maximum value of N^2 is 2.73. Therefore the largest value of the azimuthal mode number satisfying the inequality of equation 14 is $m = 1$, hence the Batchelor and Gill deduction that $m = 1$ is the only unstable disturbance (*but only for their assumed profile*).

Other profiles produce different values of N^2. The simple exponential of equation 9 produces $N^2 = 4.70$, so $m = 2$ is a clearly a possibility for unstable solutions. In fact, mode-2 solutions can be unstable by this criterion for all of the turbulent jet and wake profiles considered above. Of particular interest is the profile of Monkewitz (1988) shown in Fig. 6 for various values of p. This family of profiles evolves from the top-hat for $p >> 1$ to the exponential for $p = 1$. The figure insert shows the maximum of m according to equation 15 as a function of the shape parameter, p. The rapid rise with increasing p suggests that all values of m are possible in the limit, exactly as observed in the near jet measurements.

SUMMARY AND CONCLUSIONS

This paper began by summarizing our recent results from two axisymmetric shear flows — the turbulent jet and disk wake. Both showed a surprising evolution downstream to an energy

distribution which peaked at azimuthal mode-2. The completion of the evolution to azimuthal mode-2 predominance corresponded almost exactly to the evolution from a state dominated by the initial conditions to the final similarity state. The findings are surprising because it has long been believed that azimuthal mode-1 would dominate the dynamics, both because of previous experiments and the believed relevance of linear stability theory. These findings for the jet are consistent, however, with the experiments of Ukeiley *et al.* (1999), the recent noise measurements of Kopiev (2000), and *et al.* (1999), and the subsequent DNS/POD results of Freund and Colonius (2002). Further confirmation of these results will be discussed in Johansson and George (2002 b) and Gamard and George (2002).

Obviously such startling results demand explanation, especially since they contradict previous 'coherent structure' experimental results, and appear to contradict the well-established results of linear stability theory as well. We have attempted to deal with both. First we have argued that the mode-1 events believed to dominate the wake are simply decaying transients convected downstream from the source. As such they play little to no role in the far downstream evolution, however coherent they may appear to be. Second, we have demonstrated that theory which argued for such mode-1 disturbances, while applicable to laminar jet flows, was too restrictive for turbulent flows. By considering the effect of more general mean profiles on stability, both mode-2 and mode-0 as well as mode-1 could be shown to contribute to the downstream energetics.

Most importantly we have attempted to provide a reconciliation of all the ideas mentioned in the introduction — passive large eddies with little energy, dynamic coherent structures (passed downstream from the source), the POD, and the relevance of linear stability theory.

The title of this paper asks a question: "How has coherent structure research contributed to our understanding of turbulence?" Clearly it has generated a lot of excitement over the past two decades, and it has certainly enhanced our recognition of the beauty and complexities of turbulence. But aside from this, the message of this paper is that it has not contributed much, at least from the perspective of understanding the dynamics of the flow. In fact, given that such research (at least for these axisymmetric flows) has mostly confirmed theoretical ideas which were wrong (e.g., the dominance of mode-1), it might be argued that the contribution of such studies was negative. Such is probably the ultimate fate of all experimental techniques which are not at the outset based on ideas that are derived from or lead to the Navier-Stokes equations. By contrast, in spite of their complexity, the POD and properly applied stability theory have increased our understanding.

Perhaps the lesson is that the turbulence problem is not easy. So why should we expect the solution to be? The great solid mechanician James Bell once said: "Experimentalists sort theories" (personal communication to WKG). A corollary might be: "An experimentalist is lost when there are no theories to sort." Unfortunately this means experimentalists need to know at least enough about theories to sort them. Hopefully this paper provides an incentive to both theoreticians and experimentalists alike.

REFERENCES

N. Aubry, P. Holmes, J. L. Lumley, and E. stone. The dynamics of coherent structures in the wall region of a turbulent boundary layer. *Journal of Fluid Mechanics*, 192:115–173, 1988.

G. K. Batchelor and E. A. Gill. Analysis of the instability of axisymmetic jets. *Journal of Fluid Mechanics*, 14:529–551, 1962.

E. Berger, D. Scholz, and M. Schumm. Coherent vortex structures in the wake of a sphere and a circular disk at rest and under forced vibrations. *Journal of Fluids and Structures*, 4:231–257, 1990.

S. C. Cannon. *Large-scale structures and the spatial evolution of wakes behind axisymmetric bluff bodies*. PhD thesis, Dept. of Aerosp. and Mech. Engr., Univ. of Arizona, 1991.

J. H. Citriniti and W. K. George. Reconstruction of the global velocity field in the axisymmetric mixing layer utilizing the proper orthogonal decomposition. *Journal of Fluid Mechanics*, 418:137–166, 2000.

J. Delville, L. Ukeiley, L. Cordier, J. P. Bonnet, and M. Glauser. Examination of large–scale structures in a turbulent plane mixing layer. Part 1. Proper orthogonal decomposition. *Journal of Fluid Mechanics*, 391:91–122, 1999.

D. Ewing and W. K. George. Implication of a similarity hypothesis on the application of the proper orthogonal decomposition. In Hanjalic and Pereira, editors, *Proc. ICHMT Symposium on Turbulence, Heat and Mass Transfer, Lisbon, Portugal (1994)*. Elsevier, Amsterdam, 1995.

J. B. Freund and T. Colonius. POD analysis of sound generation by a turbulent jet. *AIAA Paper*, 2002-0072, 2002.

H. V. Fuchs, E. Mercker, and U. Michel. Large scale coherent structures in the wake of axisymmetric bodies. *Journal of Fluid Mechanics*, 93:189–211, 1979.

S. Gamard and W. K. George. Application of the pod to the similarity region of an axisymmetric turbulent jet. In *Proceedings of the ASME Fluids Engineering Division Summer Meeting*, Montreal, Quebec, Canada, July 2002.

S. Gamard, W. K. George, D. Jung, and S. Woodward. Application of a "slice" proper orthogonal decomposition to the far field of an axisymmetric turbulent jet. *Physics of Fluids*, 14(6), 2002.

W. K. George. Insight into the dynamics of coherent structures from a proper orthogonal decomposition. In S. Kline, editor, *The Structure of near Wall Turbulence, Proc. of Symp. on Near Wall Turbulence*, pages 168–180, Dubrovnik, Yugoslavia, 1988. Hemisphere, NY.

W. K. George. Some thoughts on similarity, the POD, and finite boundaries. In A. Gyr and A. Tsinober, editors, *Trends in Mathematics, Proc. of the Second Monte Verita Colloquium*. Birkhauser, Sw., 1999.

M. Glauser and W. K. George. An orthogonal decomposition of the axisymmetric jet mixing layer utilizing cross-wire measurements. In *Proceedings of the Sixth Symposium on Turbulent Shear Flow*, pages 10.1.1–10.1.6, Toulouse, France, 1987.

M. N. Glauser and W. K. George. Orthogonal decomposition of the axisymmetric jet mixing layer including azimuthal dependence. In G. Comte-Bellot and J. Mathieu, editors, *Advances in Turbulence*, pages 357–366. Spring-Verlag, 1987.

S. Gordeyev and F. O. Thomas. Coherent structure in the turbulent planar jet. Part 1. Extraction of proper orthogonal decomposition eigenmodes and their similarity. *Journal of Fluid Mechanics*, 414:145–194, 2000.

M. J. Gourlay, S. C. Arendt, D. C. Fritts, and J. Werne. Numerical modeling of initially turbulent wakes with net momentum. *Phys. Fluids*, 13:3783–3802, 2001.

P. Holmes, J. L. Lumley, and G. Berkooz. *Turbulence, Coherent Structures, Dynamical Systems and Symmetry*. Cambridge, 1996.

H. J. Hussein, S. P. Capp, and W. K. George. Velocity measurements in a high-reynolds-number, momentum-conserving, axisymmetric, turbulent jet. *Journal of Fluid Mechanics*, 258:31–75, 1994.

P. B. V. Johansson and W. K. George. Equilibrium similarity, effects of initial conditions and local reynolds number on the axisymmetric wake. *Submitted to Physics of Fluids*, 2002 (a).

P. B. V. Johansson and W. K. George. POD studies in the axisymmetric wake. In *Proceedings of the ASME Fluids Engineering Division Summer Meeting*, Montreal, Quebec, Canada, July 2002 (b).

P. B. V. Johansson, W. K. George, and S. H. Woodward. Proper Orthogonal Decomposition of an axisymmetric turbulent wake behind a disk. *Physics of Fluids*, 14(6), 2002.

D. Jung, S. Gamard, W. K. George, and S. H. Woodward. Downstream evolution of the most energetic POD modes in the mixing layer of a high reynolds number axisymmetric jet. In A. Pollard and S. Candel, editors, *Turbulent Mixing and Combustion, Proceedings of the IUTAM Symposium, Kingston June 3-6 2001*, pages 23–32. Kluwer Academic Publisher, Dortrecht, 2002.

V. F. Kopiev. Aeroacoustics of vortex ring. *Applied Mechanics Review*, 53(7):195–205, 2000.

V. F. Kopiev, M. Yu Zaitsev, S. A. Chernyshev, and A. N. Kotova. The role of large-scale vortex in a turbulent jet noise. *AIAA Paper*, 99-1839, 1999.

S.J. Leib, M.N. Glauser, and W.K. George. An application of lumley's orthogonal decomposition to the axisymmetric turbulent jet mixing layer. In *Proceedings of the 9th Rolla Symp. on Turbulence in Fluids*, Univ. of Missouri-Rolla, Rolla, Missouri., 1984.

J. L. Lumley. The structure of inhomogeneous turbulent flows. In A. M. Yaglom and V. I. Tatarsky, editors, *Atmospheric Turbulence and Radio Wave Propagation*, Moscow, USSR, 1967. Nauka.

A. Michalke. On the inviscid instability of the hyperbolic-tangent velocity profile. *Journal of Fluid Mechanics*, 19:543–556, 1964.

A. Michalke. On spatially growing disturbances in an inviscid shear layer. *Journal of Fluid Mechanics*, 23:521–544, 1965.

A. Michalke. Survey on jet instability theory. *Prog. Aerospace Sci.*, 21:159–199, 1984.

P. Moin and R. D. Moser. Characteristic-eddy decomposition of turbulence in a channel. *Journal of Fluid Mechanics*, 200:471–509, 1989.

P. A. Monkewitz. A note on vortex shedding from axisymmetric bluff bodies. *Journal of Fluid Mechanics*, 192:561–575, 1988.

D. Rempfer and H. F. Fasel. Evolution of three-dimensional coherent structures in a flat-plate boundary layer. *Journal of Fluid Mechanics*, 260:351–375, 1994.

A. A. Townsend. *The Structure of Turbulent Shear Flow*. Cambridge University Press, Cambridge, UK, 1956.

M. S. Uberoi and P. Freymuth. Turbulent energy balance and spectra of the axisymmetric wake. *Phys. Fluids*, 13(9):2205–2210, 1970.

L. Ukeiley, L. Cordier, R. Manceau, J. Delville, M. Glauser, and J. P. Bonnet. Examination of large–scale structures in a turbulent plane mixing layer. Part 2. Dynamical systems model. *Journal of Fluid Mechanics*, 441:67–108, 2001.

L. S. Ukeiley, J. M. Seiner, and M. K. Ponton. Azimuthal structure of an axisymmetric jet mixing layer. In *ASME FEDSM99-7252*, 1999.

Paper 7

Another look at the Batchelor and Gill temporal stability analysis of parallel axisymmetric flows

Submitted to
The Journal of Fluid Mechanics

S. Gamard
P. B. V. Johansson
W. K. George

Another look at the Batchelor and Gill temporal stability analysis of parallel axisymmetric flows

By S. GAMARD, P. B. V. JOHANSSON AND W. K. GEORGE

Turbulence Research Laboratory, Department of Thermo and Fluid Dynamics
Chalmers University of Technology, Gothenburg, SE-41296, Sweden

(Received 7 May 2002)

The classical temporally evolving linear stability analysis of Batchelor & Gill (1962) is reexamined using different mean velocity profiles more representative of the actual behavior of axisymmetric turbulent free shear flows. It is found that the widely accepted belief that azimuthal mode-1 is the only unstable mode in the far region is not true in general. In fact, azimuthal modes 0 and 2 also satisfy the necessary condition for instability, consistent with recent Proper Orthogonal Decomposition experimental data.

1. Introduction

Recent turbulence experiments (Jung, Gamard, George & Woodward 2002*b*; Gamard, George, Jung & Woodward 2002; Johansson, George & Woodward 2002) and DNS simulations (Freund & Colonius 2002) using Proper Orthogonal Decomposition (POD) techniques in axisymmetric free shear flows show a dominance of azimuthal mode-2 at the end of the initial transient. These results challenge the long history of results from the different linear stability theories developed over the last 50 years, which suggest that only azimuthal mode-1 can be unstable downstream. Either such linear theories are not relevant to turbulence, or this particular prediction is wrong.

This paper re-visits the linear analysis of Batchelor & Gill (1962) and shows that the mean velocity profile they considered was not appropriate for turbulence. When more realistic profiles are substituted into their criteria for neutral disturbances, the results are consistent with the recent POD results, suggesting that linear stability theory may be indeed appropriate in understanding how turbulence gets energy from the mean flow.

2. The Batchelor and Gill necessary conditions for instability

In brief, Batchelor & Gill (1962) looked at the temporally growing instabilities to infinitesimal disturbances of an axisymmetric parallel shear flow. Unlike parallel two-dimensional shear flows, there is no counterpart to Squires theorem, so fully three-dimensional disturbances had to be considered. Moreover, since these flows are inviscidly unstable, in the absence of walls, the effects of viscosity were neglected. Linearization, and Fourier decomposition in time and azimuthal coordinate led them to the following equation (Equation (2.16) in Batchelor & Gill 1962) for the radial dependence of the

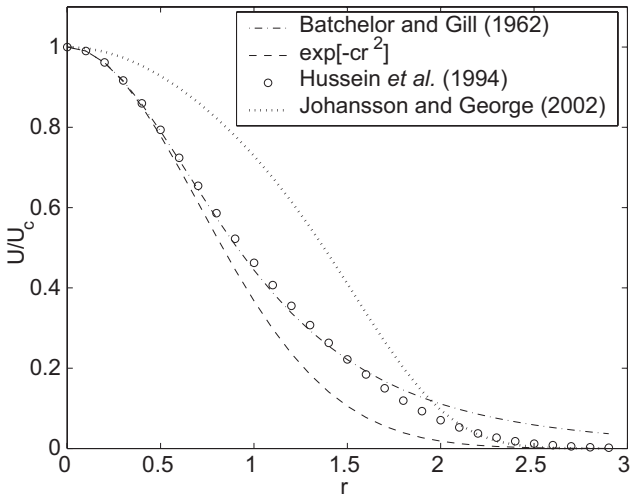

FIGURE 1. Different analytical velocity profiles.

velocity disturbance amplitude $rG(r)$:

$$(U-c)\frac{d}{dr}\left\{\frac{r}{m^2+\alpha^2r^2}\frac{d(rG)}{dr}\right\}-(U-c)G-rG\frac{d}{dr}\left(\frac{rU'}{m^2+\alpha^2r^2}\right)=0 \tag{2.1}$$

where α is a wavenumber in the streamwise direction (since the flow is assumed parallel in x), c is the speed of the disturbance, and m is the azimuthal mode number. Note that taking c to be complex means that the disturbance will grow exponentially in time if its imaginary part is negative. The critical layer occurs when $U = c_r$, and neutral disturbances will correspond to $c_i = 0$. The counterpart to equation (2.1) for parallel shear flows is the Rayleigh equation for inviscid parallel shear flows. Note that Batchelor and Gill did not consider spatially growing disturbances, nor will they be considered herein (although similar considerations may apply to them as well).

In parallel with the derivation of the inflection point criteria of Rayleigh and Fjørtoft, Batchelor & Gill (1962) divided equation (2.1) by $U - c$, multiplied it by the complex conjugate of rG, subtracted the complex conjugate of the entire equation, then integrated from $r = 0$ to infinity to obtain the quite simple result:

$$c_i\int_0^\infty |g^2|Q'dr=0, \tag{2.2}$$

where $g(r) \equiv rG(r)/(U-c)$ and

$$Q(r)\equiv\frac{rU'}{m^2+\alpha^2r^2}. \tag{2.3}$$

Obviously either g must be identically zero (no disturbance at all), or Q' must change sign for some finite and non-zero value of r for a non-zero disturbance amplitude to be possible. This is the axisymmetric counterpart of the Rayleigh inflection point criterion. Similar considerations also led them to a Fjørtoft-type condition, but that is not of interest here.

3. Azimuthal mode-0

Now Batchelor and Gill argue that mode-0 disturbances cannot grow in the 'far jet'. Figure 1 shows several profiles which are commonly used to describe jets and wake deficits. Batchelor and Gill used what they referred to as the 'far-downstream jet profile' *by which they mean*:

$$U/U_c = [1/1 + r^2]^2 \tag{3.1}$$

It is easy to show by differentiation and substitution into the definition of Q that $Q =$ *constant* for $m = 0$. Thus no mode-0 disturbance can grow, at least for this profile.

Another profile commonly used for wakes (in fact the exact viscous and eddy viscosity solution) is the simple exponential given by:

$$U/U_c = \exp[-r^2] \tag{3.2}$$

It is easy to show that the same is true for this profile as well: the $m = 0$ mode is stable.

By contrast, Batchelor and Gill argue that a top-hat profile, like that found near the entrance of a jet, does satisfy the conditions for mode-0 to grow. But they state without further justification that profiles which are slowly varying with r are stable .

Now the profile given by equation (3.1) is indeed the 'far-downstream jet' solution to the boundary layer equations for a *laminar* jet. And it is also the eddy-viscosity similarity solution of the Reynolds averaged equations for a turbulent jet. But as shown by Hussein, Capp & George (1994), it places too much weight at large values of r so that when the constants are chosen to satisfy the momentum integral, the entrainment is badly over-estimated. From careful fits to their LDA and flying hot-wire profiles, Hussein *et al.* (1994) recommended a profile for the far turbulent jet of the following form:

$$U/U_c = (1 + ar^2 + br^4)\exp[-cr^2], \tag{3.3}$$

where $a = 0.1212$, $b = 0.2815$, and $c = 1.11$.

It is easy to show, again by substitution and differentiation, that this profile does indeed have an interior inflexion point, even for $m = 0$, because of the additional terms before the exponential. The same is true for the similarity turbulent wake profile suggested by Johansson & George (2002) which is given by:

$$U/U_c = (1 + ar^2 + br^4)\exp[-cr^2 - dr^4], \tag{3.4}$$

where $a = 0.04907$, $b = 0.1276$, $c = 0.3448$, and $d = 0.1339$.

Therefore, it follows immediately that the mean velocity profiles for these two turbulent flows *do* satisfy the necessary condition for mode-0 disturbances to be unstable, even far downstream. This is certainly contrary to popular belief, but is consistent with the recent POD observations mentioned above (Jung *et al.* 2002*b*; Gamard *et al.* 2002; Johansson *et al.* 2002; Freund & Colonius 2002), where mode-0 is present for all values of x/D, exactly as one might expect from the measured mean velocity profiles.

4. Azimuthal modes ≥ 1

As for the upper limit on which azimuthal modes can grow, Batchelor & Gill (1962) showed that a necessary condition for unstable disturbances is that Q have an inflection point; i.e., $Q'' = 0$. It is straightforward to show that this is possible only if there is a non-zero and finite value of r, say $r = r_c$, satisfying:

$$(m^2 - \alpha^2 r_c^2)/(m^2 + \alpha^2 r_c^2) = -rU''/U' \tag{4.1}$$

If so, then $r = r_c$ is the location of the critical layer.

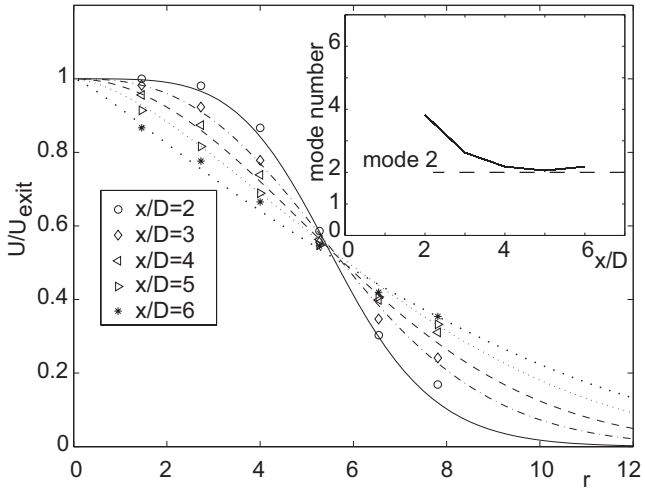

FIGURE 2. Mean velocity profile at 5 positions downstream of an axisymmetric jet. Open symbols are the measured velocity of Jung, Gamard, George & Woodward (2002*b*), while the lines are the corresponding matching velocity profile from equation (4.5). The upper insert shows the maximum value of N following equation (4.3).

Batchelor and Gill then deduced that modes higher than mode-1 cannot be unstable for the 'far jet'. What does not seem to be widely understood is that *this result is entirely based on the assumed 'far-jet downstream profile [equation (3.1)]'*. Moreover, their conclusions are not valid for profiles of turbulent jets and wakes.

To see this, consider Batchelor and Gill's equation (5.14) which is given for $m \neq 0$ by:

$$r\frac{d}{dr}\left\{\frac{r}{1+\beta^2 r^2}\frac{d(rG)}{dr}\right\} = [m^2 - N^2(r,\beta)]rG \tag{4.2}$$

where $\beta \equiv \alpha/m$ and N^2 is the positive-valued function defined by:

$$N^2(r,\beta) = \frac{r}{U(r_c)-U(r)}\frac{d}{dr}\left[\frac{rU'}{1+\beta^2 r^2}\right] \tag{4.3}$$

Now Batchelor and Gill argue from equation (4.3) that neutral disturbances with $c = U(r_c)$ can not exist unless the azimuthal mode number, m, satisfies:

$$m^2 < max_{r,\beta} N^2(r,\beta) \tag{4.4}$$

In other words, the highest azimuthal mode number must be *less* than the square root of the highest possible value of N^2.

From its definition in equation (4.3), it is clear that it is reasonable to expect the maximum value of N^2 to depend on the velocity profile. For the 'far downstream jet profile' of Batchelor and Gill, equation (3.1), the maximum value of N^2 is 2.73. Therefore the largest value of the azimuthal mode number satisfying the inequality of equation (4.3) is $m = 1$.

But, other profiles produce different values of N^2. The simple exponential of equation (3.2) produces $N^2 = 4.70$, so $m = 2$ is a clearly a possibility for unstable solutions. Profiles from equation (3.3) for the jet, and equation (3.4) for the wake, produce values of $N^2 = 5.97$ and 19.60, allowing a maximum mode number of 2 and 4 respectively. Thus, mode-2 solutions can be unstable by the criterion of equation (4.4) alone for both

the turbulent jet and wake profiles considered above. Again this is consistent with recent POD observations of the 'far jet' and 'far wakes' where the peak in the azimuthal energy is at mode-2.

Figure 2 shows the mean velocity results in the axisymmetric jet mixing layer recently reported by Jung *et al.* (2002*b*,*a*) as a function of x/D, the distance from the jet exit. The Reynolds number was 78,400 (based on jet exit velocity and diameter) and the mean profile at the exit was a top-hat, except for the thin boundary layer. Also shown fitted to these data are the profiles adapted from Monkewitz (1988) as:

$$\frac{U(r)}{U_{\text{exit}}} = \frac{1}{1 + (\exp(cr^2) - 1)^p}. \tag{4.5}$$

The parameter p determines the shape of the profile, which evolves from the 'top-hat' for $p \to \infty$ to a decaying exponential for $p = 1$. The figure insert shows the maximum values of N according to equation (4.4) as a function of the shape parameter, p, and the corresponding value of x/D. Clearly the range of azimuthal modes which satisfy the necessary condition for instability increases as the jet exit is approached. Also, azimuthal mode-2 is the limiting value at the end of the potential core. These observations are consistent with the POD results (Jung *et al.* 2002*b*,*a*) that the energy distribution in the mixing layer is bimodal, with a strong peak in mode-0 near the jet exit which diminishes, and a second peak at mode-6 at $x/D = 2$ which evolves to a peak at mode-2 by $x/D = 6$.

5. Summary

We have proved that the widespread belief that linear temporal stability theory only predicts a dominance of azimuthal mode-1 after the transient region is not correct, since this result is highly dependent on the mean velocity profile chosen. The results are in general agreement with the recent experimental (Jung *et al.* 2002*b*; Gamard *et al.* 2002; Johansson *et al.* 2002) and DNS (Freund & Colonius 2002) POD results showing a dominance in the far region of azimuthal mode-2.

Only the temporal analysis of Batchelor & Gill (1962) have been revisited. Much has been learned about stability since then. It would seem that a case can be made for reexamining other analyses as well, especially those involving spatially growing disturbances and non-parallel mean flows. It may well be that they can provide a more realistic description of fully turbulent flow than currently believed possible.

The authors are grateful to Professor J. Bergh of Chalmers mathematics department for his input regarding the analytical aspects of this work.

REFERENCES

Batchelor, G. K. & Gill, E. A. 1962 Analysis of the instability of axisymmetic jets. *Journal of Fluid Mechanics* **14**, 529–551.

Chan, Y. Y. 1974 Spatial waves in turbulent jets. *Physics of Fluids* **17** (1), 46–53.

Chan, Y. Y. 1977 Wavelike eddies in a turbulent jet. *AIAA Journal* **15** (7), 992–1001.

Crow, S. C. & Champagne, F. H. 1971 Orderly structure in jet turbulence. *Journal of Fluid Mechanics* **48**, 547–591.

Dimotakis, P. E., Miake-Lye, R. C. & Papantoniou, D. A. 1983 Structure and dynamics of round turbulent jets. *Physics of Fluids* **26** (11), 3185–3192.

Freund, J. B. & Colonius, T. 2002 POD analysis of sound generation by a turbulent jet. *AIAA Paper* **2002-0072**.

Gamard, S., George, W. K., Jung, D. & Woodward, S. 2002 Application of a "slice"

proper orthogonal decomposition to the far field of an axisymmetric turbulent jet. *Physics of Fluids* **14** (6).

Huerre, P. & Monkewitz, P. A. 1990 Local and global instabilities in spatially developing flows. *Annual Review of Fluid Mechanics* **22**, 473–537.

Hussein, H. J., Capp, S. P. & George, W. K. 1994 Velocity measurements in a high-reynolds-number, momentum-conserving, axisymmetric, turbulent jet. *Journal of Fluid Mechanics* **258**, 31–75.

Johansson, P. B. V. & George, W. K. 2002 Equilibrium similarity, effects of initial conditions and local reynolds number on the axisymmetric wake. *Submitted to Physics of Fluids* .

Johansson, P. B. V., George, W. K. & Woodward, S. H. 2002 Proper Orthogonal Decomposition of an axisymmetric turbulent wake behind a disk. *Physics of Fluids* **14** (6).

Jung, D., Gamard, S. & George, W. K. 2002*a* Downstream evolution of the most energetic modes in a turbulent axisymmetric jet at high reynolds number. part 1. the near field region. *Submitted to the Journal of Fluid Mechanics* .

Jung, D., Gamard, S., George, W. K. & Woodward, S. H. 2002*b* Downstream evolution of the most energetic POD modes in the mixing layer of a high reynolds number axisymmetric jet. In *Turbulent Mixing and Combustion, Proceedings of the IUTAM Symposium, Kingston June 3-6 2001* (ed. A. Pollard & S. Candel), pp. 23–32. Kluwer Academic Publisher, Dortrecht.

Michalke, A. 1964 On the inviscid instability of the hyperbolic-tangent velocity profile. *Journal of Fluid Mechanics* **19**, 543–556.

Michalke, A. 1984 Survey on jet instability theory. *Prog. Aerospace Sci.* **21**, 159–199.

Monkewitz, P. A. 1988 A note on vortex shedding from axisymmetric bluff bodies. *Journal of Fluid Mechanics* **192**, 561–575.

Plaschko, P. 1979 Helical instabilities of slowly divergent jets. *Journal of Fluid Mechanics* **92**, 209–216.

Tso, J. & Hussain, F. 1989 Organized motions in a fully developed turbulent axisymmetric jet. *Journal of Fluid Mechanics* **203**, 425–448.

Yoda, M., Hesselink, L. & Mungal, M. G. 1992 The evolution and nature of large-scale structures in the turbulent jet. *Physics of Fluids A* **4** (4), 803–811.

Yoda, M., Hesselink, L. & Mungal, M. G. 1994 Instantaneous three-dimensional concentration measurements in the self-similar region of a round high-schmidt-number jet. *Journal of Fluid Mechanics* **279**, 313–350.

Paper 8

The far downstream evolution of the high Reynolds number axisymmetric wake behind a disk. Part 1. Single point statistics

Prepared for submission to the
Journal of Fluid Mechanics

P. B. V. Johansson
W. K. George

The far downstream evolution of the high Reynolds number axisymmetric wake behind a disk. Part 1. Single point statistics

By PETER B. V. JOHANSSON
AND WILLIAM K. GEORGE

Turbulence Research Laboratory, Department of Thermo and Fluid Dynamics, Chalmers University of Technology, Gothenburg, SE-412 96, SWEDEN

(Received May 6)

The high Reynolds number axisymmetric wake behind a disk has been studied from $10 \leqslant x/D \leqslant 150$ ($36 \leqslant x/\theta \leqslant 552$) using a rake of 15 hot-wires. The disk had a diameter of 20 mm, and the Reynolds number based on the free-stream velocity was 26,400. Mean velocity profiles, root mean square profiles, and power spectra are presented. By using regression techniques to fit the velocity profiles it was possible to obtain accurate velocity centreline deficit and transverse length scale to even the furthermost downstream position. Beyond the initial region which extends to $x/D = 30$, the data are in excellent agreement with the high Reynolds number equilibrium similarity solution.

1. Introduction

The axisymmetric far wake is a very challenging flow to investigate experimentally, since the velocity differences of interest are very small. A sketch of the axisymmetric wake together with the coordinate system used in this study is shown in figure 1. The mean velocity deficit at the centreline is here defined as $U_o = U_\infty - U_{CL}$. The Reynolds decomposition is applied, and averaged values are denoted with upper case letters, and fluctuating quantities with lower case letters. It has been found experimentally that U_o falls rapidly downstream from about 10% of the free stream velocity at $x/D = 10$ to about 1% of the free stream velocity at the farthest downstream position ($x/D = 150$) in this experiment. The root mean square of the fluctuations, u', is of the same order as the velocity deficit, i.e., $u'/U_o \approx 1$. These low levels place extreme demands on the wind tunnel itself, both in terms of its length and flow quality. Moreover, this rules out the use of most laser based techniques, like laser Doppler anemometry (LDA), or particle image velocimetry (PIV) which simply do not have enough resolution. The only measurement technique that is capable of resolving such weak fluctuations is hot-wire anemometry, but this technique also has accuracy limitations. These are recognized here, and a method to account for them is provided.

2. Basic equations

The Reynolds averaged x-momentum equation for the axisymmetric far wake without swirl reduces to first order to a balance between the advection of the deficit and the radial gradient of the Reynolds stress:

$$U_\infty \frac{\partial}{\partial x}\left(U - U_\infty\right) = -\frac{1}{r}\frac{\partial}{\partial r}\left(r\overline{uv}\right). \tag{2.1}$$

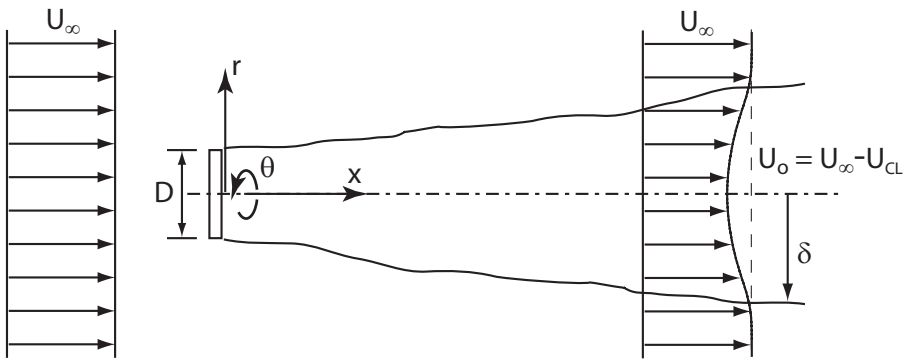

FIGURE 1. Axisymmetric wake coordinates.

The viscous term has been neglected, since only high Reynolds number flows are of interest here. (Note that Johansson, George & Gourlay (2002*a*) consider also viscous solutions to this equation.)

The momentum equation can be integrated over a cross-section to yield an integral constraint for the conservation of momentum:

$$U_\infty \int_0^\infty (U_\infty - U)\; r\, dr \cong \theta^2 U_\infty^2. \tag{2.2}$$

where θ is the momentum thickness. This equation is satisfied to within a few percent beyond $x/D = 10$.

A convenient choice for the transverse length scale is

$$\delta_*^2 = \lim_{r\to\infty} \frac{1}{U_o} \int_0^r (U_\infty - U)\, r\, dr. \tag{2.3}$$

The advantage of this choice is that it satisfies equation (2.1) exactly: i. e.,

$$U_o \delta_*^2 = U_\infty \theta^2. \tag{2.4}$$

3. Historical review

Using hot-wire anemometry, Carmody (1964) presented the findings of an experiment on a circular disk oriented perpendicular to the flow at a Reynolds number based on the disk diameter and free stream velocity (Re) of 70,000. He presented mean velocity, root mean square fluctuations, and Reynolds stress profiles, as well streamwise as wake growth. Shortly thereafter, Hwang & Baldwin (1966) presented measured turbulence intensities and wake growth for a large span of downstream locations, $x/D = 5$ to $x/D \approx 900$ behind various circular disks. Curiously, they did not present the centreline mean velocity decay. The reliability of the hot-wire technique was discussed thoroughly in their paper, but the accuracy in terms of a percentage was not given. Both sets of data show significant scatter, most likely closely linked to the capability of the hot-wire anemometers used at that time. Hwang & Baldwin (1966) even reported difficulties in reproducing their own results on a day-to-day basis.

Gibson, Chen & Lin (1968) presented mean velocity and turbulence intensity profiles for a sphere wake at a Reynolds number of 65,000 using hot-wires and Pitot tubes. The investigation covered only downstream distances to $x/D = 60$, but they stated that the root mean square fluctuations of the velocity was of the same order as the mean velocity

deficit to within the accuracy of the experiment. They credited this finding to Cooper & Lutzky (1955) who made an experiment on a disk wake.

Uberoi & Freymuth (1970) measured the sphere wake at a Reynolds number of 8,600. Their investigation covered a downstream distance up to $x/D = 150$, but their presented results of the mean velocity deficit only go to $x/D = 100$. They did, however, claim that their data behaved according to the classical cube root solution, if the virtual origin was chosen appropriately. But they showed no downstream variation of either the centreline deficit or wake width, and showed only two collapsed profiles at $x/D = 50$ and 100.

In none of these experiments (Carmody (1964); Hwang & Baldwin (1966); Gibson *et al.* (1968)), was the conservation of momentum addressed. This was, however, thoroughly investigated by Cannon (1991). He examined both the integral and differential mean momentum equations, and showed that his mean velocity and Reynolds stress data satisfied both for five different wake generators (disk, sphere and three porous disks with different porosity). The common denominator of these flows was that they had the same drag, which is why conservation of momentum was important. The Reynolds number based on diameter varied between 13,000 for the solid disk, 14,000—17,000 for the screens, and 21,500 for the sphere. The measurements extended over a range of x/D of about 10 to 125. Unfortunately, however, it was not clear that any of the wakes achieved a region downstream where u'/U_o appeared constant.

Johansson, George & Woodward (2002*b*) studied the axisymmetric disk wake using a rake of 13 hot-wires in order to obtain two-point cross-spectra in cross-sections of the flow from $x/D = 10$ to $x/D = 50$. These two-point cross-spectra were then used in the kernel of a proper orthogonal decomposition to extract the energetic features of the flow in a manner similar to Part 2 of this paper. They noted that their mean velocity profiles were affected by thermal drift of the anemometers. The centreline mean velocity deficit, U_o, was about 3% of the free stream velocity at the farthest downstream location.

The present investigation extends this study to a greatly increased distance downstream (to $x/D = 150$) using a different facility. Here the influence of the thermal drift in the anemometers is even more pronounced, because of the smaller centreline deficit and accompanying low turbulence intensity. A thorough investigation of the accuracy of the measured data and a method of handling such small velocity difference flows is presented here. By using regression techniques to fit the profiles and using momentum conservation as a requisite condition, it is shown to be possible to obtain reliable results much further downstream than previously possible.

The data described here have been used by Johansson *et al.* (2002*a*), together with the extensive DNS data of Gourlay *et al.* (2001), as a part of a general reanalysis of axisymmetric wakes. Their equilibrium similarity considerations showed the existence of two similarity regimes, both possibly retaining an asymptotic dependence on upstream conditions. Criteria were established there for when the initial transients die off, when the high Reynolds number solution might be expected, and when the low Reynolds number solution might emerge. Almost none of the earlier experiments described above satisfy these criteria. Both the data described here and the DNS data, however, show evidence for the high Reynolds number solution. Only the DNS data, though, evolves far enough downstream for the low Reynolds number solution to emerge.

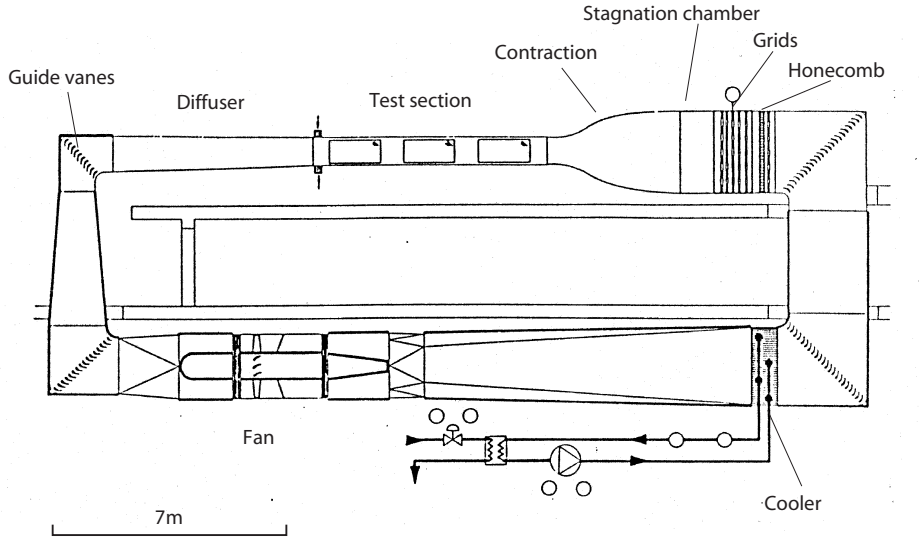

FIGURE 2. Wind Tunnel MTL at KTH, from Johansson (1992)

D (mm)	θ (mm)	U_∞ (m. s^{-1})	T (°C)	ν (m^2. s^{-1})	ρ (kg. m^{-3})
20	5.43	20.1	20.4	15.2×10^{-6}	1.189

TABLE 1. Summary of experiment variables.

4. Experimental Setup

4.1. *Facility*

The experiment presented in this paper was performed in the MTL wind tunnel located at the Royal Institute of Technology (KTH) in Stockholm, Sweden. The MTL tunnel shown schematically in figure 2, is of closed loop type and is very suitable for measuring low turbulence intensity flows like the axisymmetric wake because of its relatively long test section and high flow quality. The streamwise free-stream turbulence intensity is lower than 0.03%, and the cross-stream turbulence intensities are less than 0.06%. The tunnel has a temperature uniformity in the test section of ± 0.2°C. The test section has an area of 1.2×0.8 m^2 and the downstream length is 7 m. Further characteristics of the tunnel can be found in Johansson (1992). The tunnel walls can be adjusted in order to set the desired pressure gradient, but for this experiment they were in the same configuration described by Österlund (1999) for which the pressure gradient was very close to zero.

The wind tunnel velocity was monitored using a Pitot tube connected to a Furness FCO510 electronic manometer. The manometer was equipped with an absolute pressure sensor and a temperature sensor to provide the value of the velocity via the RS232 port directly to the computer. The velocity was monitored throughout the experiment and kept constant at 20.1 m/s ± 0.05 m/s, resulting in a Reynolds number based on the free stream velocity and disk diameter of 26,400. The measurement was automated using the integrated traverse and wind-tunnel speed control of the MTL.

4.2. *Probe configuration*

The sensing device was composed of two rakes consisting of 15 hot-wires in total. The primary reason for using rakes of probes was to be able to compute the numerous two-point

cross-spectral quantities as described in Part 2 of this paper. Fortunately, the simultaneous measurement at many points made it possible to overcome the intrinsic limitation of the instrumentation. The rakes and probes, shown in figure 3a, were constructed in-house at the Turbulence Research Laboratory of Chalmers. The rakes were made of steel wing profiles with a maximum thickness of 10 mm and a chord of 25 mm. The lower rake is fixed, while the upper can be rotated around the axis of the centre probe. The rotation allows an angular separation of the rakes between 15° and 335° with an accuracy of ±1°. The probe holders were fixed to the wings and were made of brass telescopic tubing with an outer diameter of 4 mm. At the end of the probe holder, the probe body was attached. The probe body consisted of a brass tube with an outer diameter of 3.2 mm, containing a ceramic tubing with an outer diameter of 2.4 mm for prong insulation. Inside the ceramic tube, 0.4 mm steel piano wires were used as prongs, protruding 8 mm from the ceramic tube. The ends of the prongs were sharpened in order to reduce the effects of the prongs on the sensing wire. The total distance between the movable steel wing and the sensing wire was 195 mm. The sensing wire was made of tungsten with diameter 5 μm (Sigmund-Cohn, Mt. Vernon, NY) and length 3 mm.

4.3. *Anemometers and data aquisition*

The anemometers consisted of a five channel AA Lab Systems AN1003 constant temperature anemometer that was available at KTH. For the remaining channels, nine DANTEC Miniature-CTA 54T30 were used. The differing thermal drifts of these anemometers considerably complicated their use, as will be discussed in detail later.

The data was digitized using an IO Tech Wavebook 516 16 bit 1 MHz sample and hold A/D converter, with an expansion module to enable 16 channels simultaneous sample and hold, connected to the computer via a fast parallel port PCI board. For the power spectra measured at downstream locations $x/D = 30$, 50, 70, 90, 110 , 130, and 150, the signals were sampled at 4 kHz, consistent with the wire length cut-off, U_∞/l_w. This cut off the spectra well into the inertial subrange which was intentional since the primary purpose of the experiment was to apply the POD to determine the evolution of the energy containing scales. Measurements were made simultaneously for all 15 probes. Each data block had 4096 samples, and a total of 360 blocks of data was taken per probe for each angular probe rake location. This large amount of data yields a variability of the power spectra at each radial position of 1.08%.

For the single point statistics, mean velocity and rms velocity, separate scans of the flow were made for the downstream locations $x/D = 10$, 20,..., 150 using fewer blocks. For these runs, no spectral quantities were evaluated, so the sampling frequency was reduced to 1 kHz and only 60 blocks of 1000 samples were taken. This gives a statistical uncertainty of the mean velocity of at most 0.1% (for the nearest downstream position where $u'/U \approx 10\%$). For the root mean square of the fluctuations, the statistical uncertainty is around 0.6%.

4.4. *Disk suspension*

The disk had a diameter of 20 mm, a thickness of 2 mm with sharp edges, and was made of acrylic. It was suspended with three pairs of steel wires, each with the diameter 0.2 mm. The disk was placed one meter into the measuring section to allow for probe calibration upstream of the disk, and to avoid the continuing acceleration of the flow near the contraction. The mounted disk in the test section is depicted in figure 3, which also shows the rake of probes downstream of it. The disk was centered by adjusting the tension of the supporting wires. By using pairs of support wires, the planar orientation of the disk could also be adjusted, since the tension of each support wire could be set individually. The final

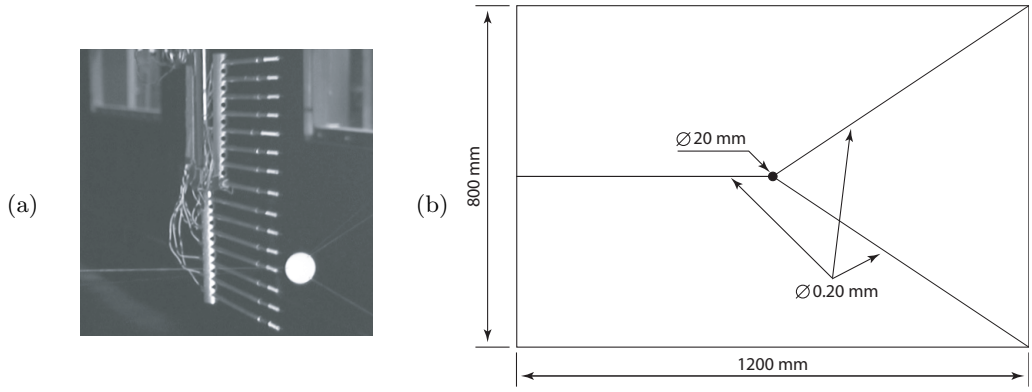

FIGURE 3. (a) Probe rake and disk, and (b) disk suspension in the cross-section in the MTL wind tunnel at KTH

tuning of the disk centering was achieved by several preliminary test measurements, where the velocity field was measured for all available angular positions of the movable rake. The disk was moved based on the input from these velocity measurements and the procedure was repeated until a satisfying result was achieved. For reasons that will be discussed in detail later, the centering was not performed using mean velocity distributions only, but instead the centering was based on obtaining reasonably similar profiles of u' and power spectra for locations on either side of the plane $\Delta\theta = 180°$ (i.e., it was moved until the u' values and the power spectra compared favorably for the angular separations of $\Delta\theta = 120°$ and $\Delta\theta = 240°$). (See figure 4 for the definition of the separation angle.) At the same time, it was ensured that the flow was indeed axisymmetric within experimental accuracy.

The effects of the disk support wires were of considerable interest in ensuring that the energy distribution of the POD modes were not affected by them. In Johansson *et al.* (2002*b*), four pairs of support wires were used. With such a configuration of support wires, the disk centering is easier, but it also creates a problem. Four pairs of support wires precludes some angular positions for the movable probe rake to be used without the velocity measurements being affected by the wakes of the supporting wires. The symmetry of the flow cannot be used to overcome this problem. The effect on the POD modes of the disk suspension method is further discussed in Part 2 of this paper. In the three-support wire configuration used throughout this investigation, the wakes of the support wires did not affect the velocity measurements at any angular position of the movable probe rake, since the asymmetrical positioning of the support wires allowed replacement of the $\Delta\theta = 90°$ measuring position by the one at $\Delta\theta = 270°$.

4.5. *Spatial resolution*

The arrays were used in the same manner as Glauser & George (1987) and Johansson *et al.* (2002*b*) to obtain the single point statistics and two-point velocity cross-spectra for all combinations of locations shown in figure 4, $7 \times 7 \times 12 \times 15 = 8,820$ in total at $1,260$ different positions. The measurement grid was originally chosen so that the angular resolution was acceptable for obtaining azimuthal Fourier transforms of the cross-spectra. This aspect is further discussed in Part 2. The movable array of probes was traversed from a 15° separation up to 180° with 15° increments in $\Delta\theta$. The 15° separation was chosen since it is approximately half the azimuthal integral scale, a methodology recently confirmed to be adequate by Gamard *et al.* (2002) in a jet, using both rakes of probes like these here, and also a 139-hot-wire array of very long wires especially designed to reduce

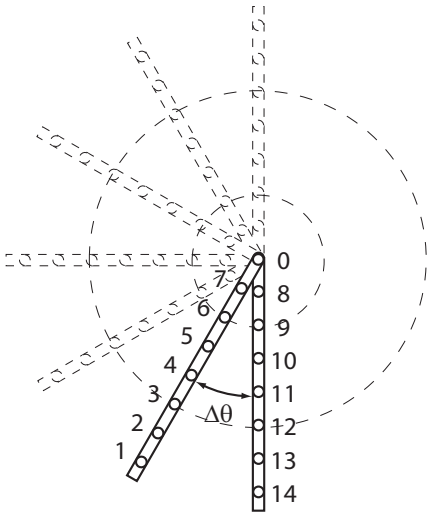

FIGURE 4. Map of traverse scheme, shown in increments of $\Delta\theta = 30^\circ$.

spatial aliasing. The numbering of the probes is shown in figure 4, with each hot-wire probe marked by a circle. The radial spacing of the probes beginning at the center probe numbered 0 at $r = 0$ was 93, 80, 67, 54, 41, 28, 14, (mm) for probes numbered 1 to 7 on the movable rake, and -14, -28, -41, -54, -67, -80, -93, (mm) for the probes numbered 8 to 15 on the fixed rake. Negative values of r are used for separating the probes on the fixed rake from those of the movable. Probes 0, 1, 3, 5, and 6 were connected to the AN1003 anemometer channels, while the others were connected to the DANTEC 54T30 anemometers.

The mean velocity and rms profiles were obtained with the rakes kept at the angular separation of $\Delta\theta = 180^\circ$. To add more points in the velocity profiles, the rake was traversed in the direction of positive r an amount of 5 and 10 mm for these data sets.

5. Single point statistics

5.1. *The mean velocity*

Obtaining the mean velocity profiles was by far the most difficult part of this entire experiment. The accuracy of the results of an experiment using hot-wires is very sensitive to the reliability of the calibration, but this is not the major source of error in this investigation. Here, fourth-order polynomials were used to map the voltage output of the anemometer into velocity, as discussed by Shabbir & George (1994). (Because of the low turbulence intensity, u'/U_∞, any lower order polynomial would probably have worked just as well, as long as the range of velocities encountered was not outside the range of calibration.) The relative error of the calibration was less than ± 0.02 % over the range of velocities in the actual measurement.

The primary source of difficulty in the experiment was the thermal drift of the anemometers, especially from the offset amplifiers. This problem is easily overlooked when measuring flows with large velocity differences, e. g., a boundary layer or a jet, but is immediately obvious in a 'weak' turbulent flow like the axisymmetric wake. This was previously noted by Johansson *et al.* (2002*b*), who stated that this mainly affected the mean velocity, leaving the root mean square of the velocity unaffected. This problem is more pronounced here than in the earlier study because the distance downstream is greater (150 disk di-

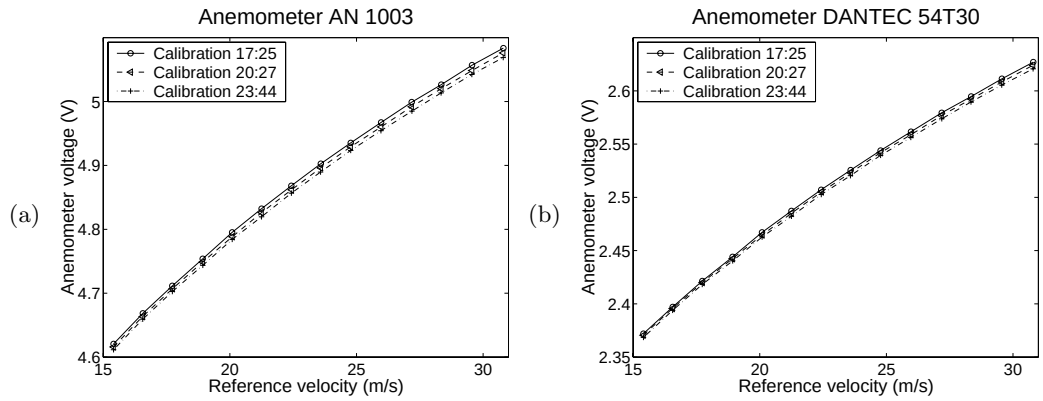

FIGURE 5. Calibration curves for (a) AN1003 and (b) DANTEC 54T30. Calibrations before, in the middle, and after for two downstream positions of measurement.

ameters vs. 50) and the mean velocity deficit along with the turbulence intensity is much lower. (1% in the present vs. 3% in the previous study.) Part of the problem was solved by setting the troublesome anemometer offsets to zero, but the anemometers still drifted.

Figure 5 shows two typical calibrations for both types of anemometers (AN1003 and 54T30) used. The different times correspond to calibrations before, in between, and after the experiments at two downstream positions. Although the differences in calibration before and after are slight, this difference is significant compared to the mean velocity deficit. This most certainly is the reason for the scatter of profiles in previous investigations (or perhaps even their complete absence from many). One significant advantage, however, is that equation (2.4) must be satisfied at and beyond $x/D \approx 10$ (i. e., momentum is conserved).

The method applied here to overcome these difficulties is presented in detail in Appendix A. The method considers data sets from all measured positions at a given downstream location simultaneously. It assumes only that the anemometers drift together (which was certainly true for the mini-Dantecs), so that the measured profile shifts uniformly in time. The method can be summarized as:

(a) A hypothesis of a general velocity profile is made. This profile has only a single length scale, δ_*, and velocity scale, $U_o = U_\infty - U_{CL}$, both assumed unknown for each profile.

(b) This profile is regressively fitted to each velocity profile at every downstream location for both rakes, requiring only conservation of momentum.

Since the rake does not unambiguously cover the whole wake for the furthest downstream positions, the mean velocity deficit must be treated as an unknown quantity, but is linked to the transverse length scale through the conservation of momentum, equation (2.4). The method also provides as a bonus the necessary scaling parameters: the velocity deficit scale, U_o, and the wake width, δ_*. The evolution of these quantities is summarized in table 2.

The resulting corrected mean velocity profiles, normalized with the free stream velocity for the downstream positions $x/D = 10$, 20, 30, 40, and 50 are shown in figure 6. Also shown next to the plots of the mean velocity deficit are the corresponding normalized turbulence intensities which will be discussed in the next section. The mean velocity deficit decreases rapidly initially, from about 9.5 % at $x/D = 10$, to 2.2 % at $x/D = 50$. The points in the velocity profiles associated with negative r were obtained from the fixed rake. Here, all the probes were connected to the same brand of anemometers (DANTEC).

x/D	U_{CL}	U_o	u'_{max}	u'_{max}/U_o	δ_*	$U_o\delta_*/\nu$
10	18.15	1.95	1.67	0.86	17.46	2234
20	19.11	0.99	1.02	1.03	24.45	1595
30	19.41	0.69	0.77	1.11	29.25	1334
40	19.54	0.56	0.63	1.12	32.48	1201
50	19.63	0.47	0.54	1.13	35.41	1102
60	19.68	0.42	0.47	1.12	37.48	1041
70	19.72	0.38	0.43	1.11	39.37	991
80	19.75	0.35	0.39	1.10	41.12	949
90	19.78	0.32	0.36	1.10	42.82	911
100	19.80	0.30	0.33	1.10	44.31	880
110	19.82	0.28	0.31	1.10	45.97	849
120	19.84	0.26	0.29	1.11	47.47	822
130	19.85	0.25	0.28	1.12	49.13	794
140	19.86	0.24	0.26	1.08	49.53	788
150	19.87	0.23	0.25	1.06	50.37	774

TABLE 2. Downstream variation of measured quantities. Velocities in m/s and δ_* in mm.

The probe labelled 1 in figure 4 shows least agreement to the curve fit. This probe was connected to one of the AN1003 channels, which is the main reason for it behaving differently, because of the different characteristics of the anemometer. Note that the velocity differences are extremely small. The difference in velocity measured by probes 1 and 2 is 0.4% of the free stream velocity. The same trend is seen for probes 1, 3, 5 and 6, which are also connected to AN1003 anemometers. But clearly, it is probe 1 that deviates the most. The solid lines in the figure shows the curve fit explained in Appendix A. All profiles show very good agreement to this fit. The centering of the rake is seen to have been performed in a satisfactory manner. Note that the right side of the measured positions, positive r, extends to larger radius than the curve for negative r, since the entire probe rake was traversed to two positions in the positive r direction (5 and 10 mm) to fill out the profiles as mentioned in section 4.5.

The further evolution of the mean velocity profiles for $x/D = 60$ to 150 is shown in figures 7 and 8. For these positions, the mean velocity deficit continues to fall, from 2% at $x/D = 60$ to about 1.1% at $x/D = 150$. The curve fits continue to be in very good agreement with the measured points, especially for negative r. As noted above, probe 1 continues to be off the curve. The probe rake centering is still found to be accurate, ensuring that the flow direction in the wind tunnel test section is uniform within the accuracy of the experiment, so no re-centering of the probe rakes was found necessary. For the later positions, it is clear from the curve fits that the outermost point is not located in the free stream. Hence, the curve fit is essential in the estimation of the mean velocity deficit.

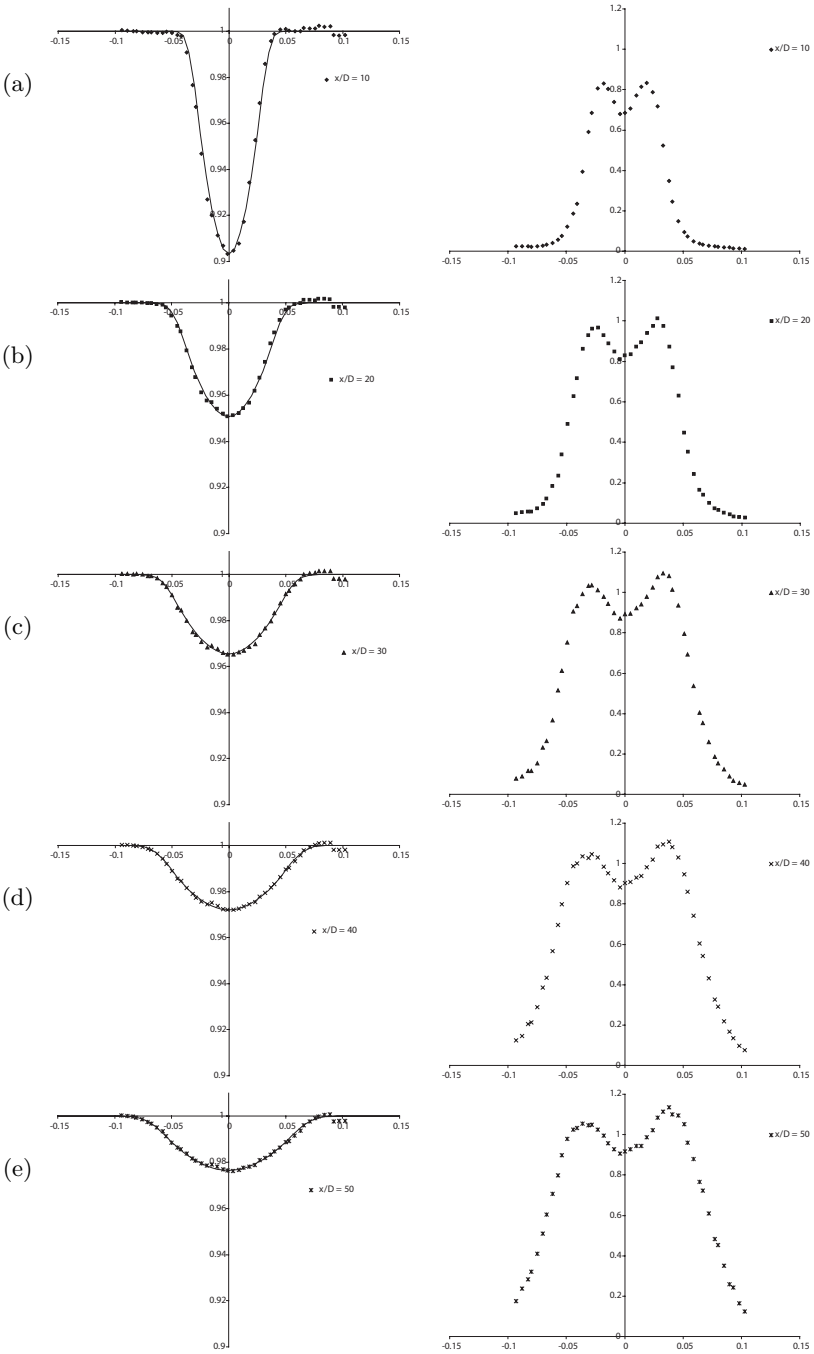

FIGURE 6. Mean velocity profiles and root mean square of the velocity vs. r. (a), $x/D = 10$, (b) 20, (c) 30, (d) 40, (e) 50.

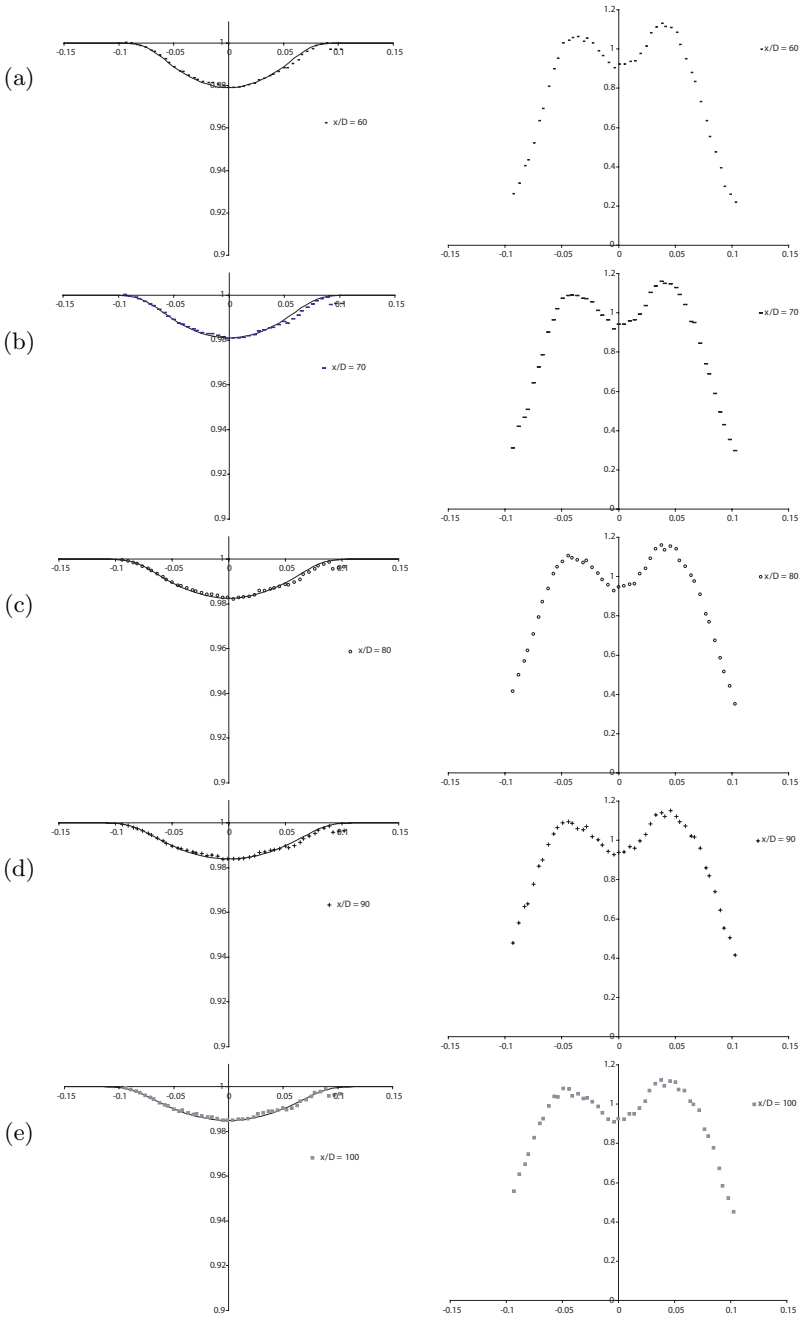

FIGURE 7. Mean velocity profiles and root mean square of the velocity vs. r. (a), $x/D = 60$, (b) 70, (c) 80, (d) 90, (e) 100.

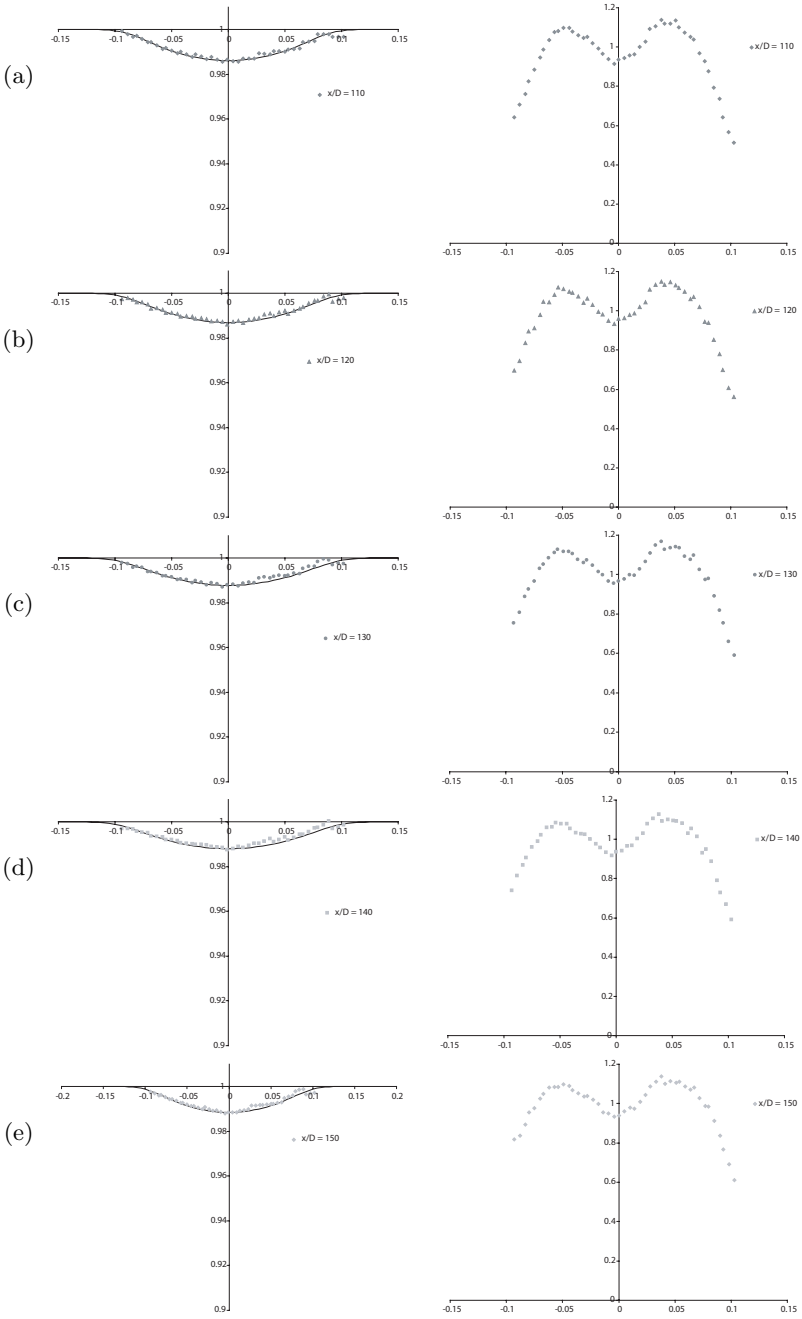

FIGURE 8. Mean velocity profiles and root mean square of the velocity vs. r. (a), $x/D = 110$, (b) 120, (c) 130, (d) 140, (e) 150.

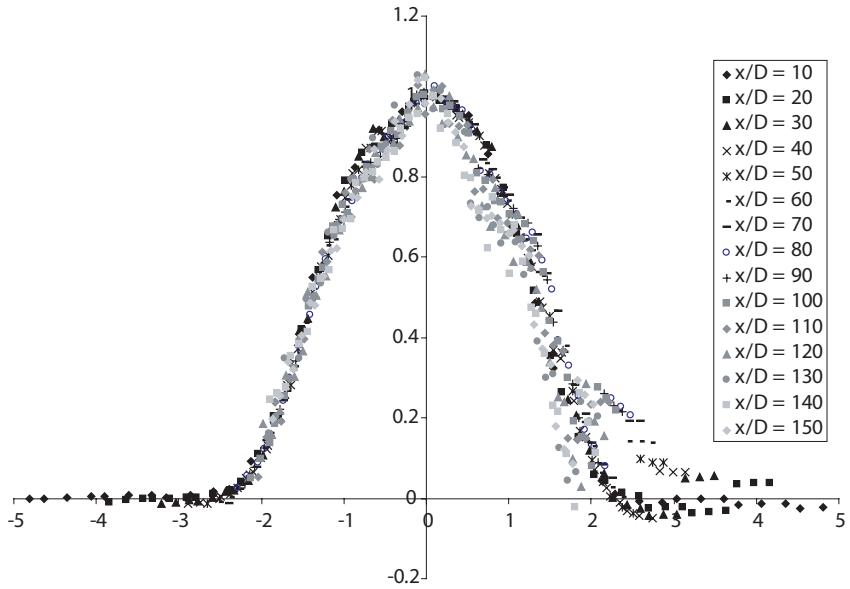

FIGURE 9. Normalized mean velocity profiles, $(U_\infty - U(r))/U_o$ vs r/δ_*.

The normalized mean velocity deficit profiles, $(U_\infty - U(r))/U_o$ are plotted versus r/δ_* in figure 9. In this figure, all profiles obtained with the probes on the fixed rake (negative r) show a remarkable collapse. The previously identified problematic probe 1 in the outer part of the movable rake shows least agreement to the profile. In fact, the points measured by this probe seem to fall on a curve of its own, slightly elevated from the curve that ties all the others together. It would be very tempting to just shift these points to fall on top of the curve fit (or omit this data entirely). Also, the increased scatter for positive r is due to probes 1, 3, 5, and 6 that are connected to AN1003 anemometers, which have a different thermal drift characteristic than those of 54T40.

Figure 9 also gives an indication of why previous experiments show large scatter in the mean velocity profiles (if they show profiles at all), since the largest deviation in figure 9 is only 0.4% of the mean velocity. If a probe rake had not been used, the accuracy would have been even more seriously affected by the anemometer drift, since the profile would have been obtained by traversing a single probe through the wake. If the traversing were made at random positions spanning the wake, the thermal drift of the anemometers would have shown up as increased scatter in the profiles. Or if the traversing were sequential, the profiles would have been significantly skewed. The measurements of very small mean velocity differences in the wake are indeed very difficult to make correctly, but made possible in this experiment by simultaneously measuring with a number of probes and many nearly identical anemometers.

6. Streamwise variation of scaling parameters

The scaling parameters obtained through the regressive fit described in Appendix A, the centerline mean velocity deficit, U_o, and the lateral wake width, δ_*, clearly provide the collapse of the mean velocity profiles as shown in figure 9. The streamwise variation of the mean velocity deficit is shown in figure 10. It is clear that U_o decreases monotonically and in a smooth manner. The solid line shows the high Reynolds number equilibrium similarity solution discussed below in equation (8.2).

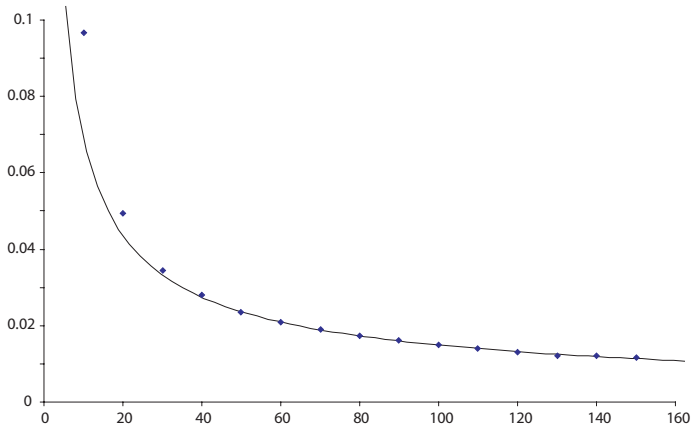

FIGURE 10. Downstream evolution of the centerline velocity deficit, U_o/U_∞, vs. x/D.

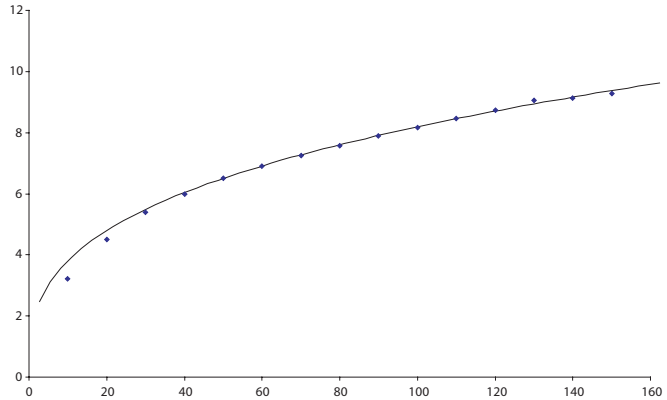

FIGURE 11. Downstream evolution of the lateral wake length scale, δ_*/θ, vs. x/D.

In figure 11, the streamwise evolution of the lateral length scale, δ_*, defined by equation (2.3) is shown. It is seen from this figure that δ_* grows monotonically from about 3θ (17 mm), or slightly less than the disk diameter at $x/D = 10$, to about 9θ (50 mm) or 2.5 times the disk diameter at $x/D = 150$. The solid line shows the high Reynolds number equilibrium similarity solution discussed below in equation (8.1).

These two scaling parameters, U_o and δ_*, can be used to obtain the *local* Reynolds number of the flow, $R = U_o\delta_*/\nu$. The downstream variation of the local Reynolds number is shown in figure 12. Clearly it decreases with downstream distance, which distinguishes this flow from most other free shear flows where the local Reynolds number either increases or remains constant. In fact, it is this decreasing local Reynolds number which is the reason for the existence of two different equilibrium similarity solutions for the axisymmetric wake, one for high and one for low Reynolds number, v. George (1989) and Johansson *et al.* (2002*a*). The dashed line in the figure marks the value of the local Reynolds number where the high Reynolds number equilibrium similarity solution ceases to be valid, and viscous effects drive the flow to its other turbulent state as discussed in detail by Johansson *et al.* (2002*a*). In this experiment, the local Reynolds number falls from 2234 at $x/D = 10$, to 774 at $x/D = 150$, which is well above the suggested threshold of 500 below which the high Reynolds number solution does not apply.

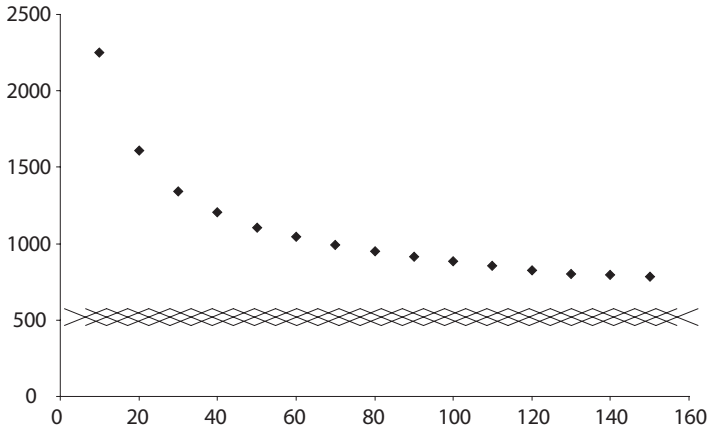

FIGURE 12. Downstream evolution of the local Reynolds number, $U_o\delta_*/\nu$, vs. x/D.

7. Turbulence intensity profiles

The reason for the RMS velocity not being so sensitive to the thermal drift of the anemometers can also be seen in figure 5. Although the curve has shifted from one time to another, the slopes are nearly unchanged. For such weak fluctuations, the fluctuating velocity is proportional to the fluctuating voltage times the derivative of the function that relates voltage and velocity (see Perry (1982) for a more detailed discussion). Thus the fluctuating part of the velocity is hardly affected at all, while the mean is seriously compromised. But there remains a problem for the turbulence intensities, since the rms values must be divided by the centerline mean velocity deficit, which is the least accurately determined quantity. It is the constancy (or lack thereof) of u'/U_o that is the surest indicator of a similarity scaling regime, so even the establishment of flow regime is prisoner to the drift problem.

The root mean square of the fluctuations, u', is shown for the downstream positions of $x/D = 10$, 20, 30, 40, and 50 in figure 6. Here, u' is normalized by the centerline mean velocity deficit determined above. As with the mean velocity profiles, the radial direction is left unscaled to show the profile width in physical dimensions. As is clear in figure 6, the hot-wire array almost covers the whole wake, since the tails of u'/U_∞ goes to a value just below 0.1%. The tunnel free stream turbulence intensity with an empty test section is reported by Johansson (2002) to be less than 0.03%. Figure 6 further supports the indications provided by the study of the mean velocity profiles in the previous section that the rakes were properly centered. The slightly higher peak value on the right hand side is really due to one probe. The probes that prevent the profiles from being really smooth are actually the ones numbered 0, 1, 3, 5, and 6, all connected to AN1003 anemometers. But the effects of the different anemometers are not at all as pronounced as for the mean velocity profiles. There is also another possible cause of the higher turbulence intensity on the upper side, and that is if the disk was not absolutely aligned with the wind tunnel cross-section.

Figures 7 and 8 show the downstream evolution of the turbulence intensities between $60 \leqslant x/D \leqslant 150$. Here, the peak values (as well as the centerline values) of u'/U_o have reached a constant level, and remain constant for all the remaining measured downstream positions. The profiles eventually start to show more scatter, but it must be noted that the ratio of u'/U_∞ has dropped to below 1.3% at $x/D = 150$.

The normalized turbulence intensity profiles for all downstream locations are shown

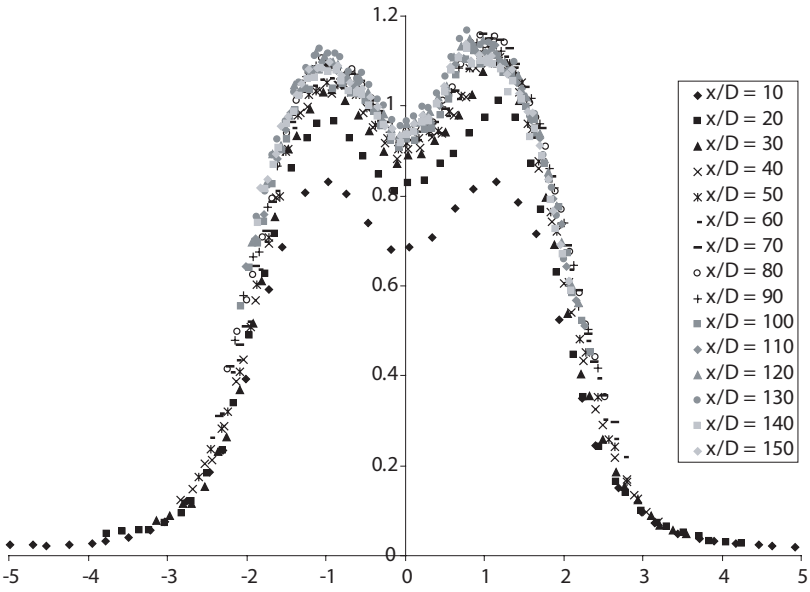

FIGURE 13. Normalized turbulence intensity profiles, u'/U_o vs. r/δ_*.

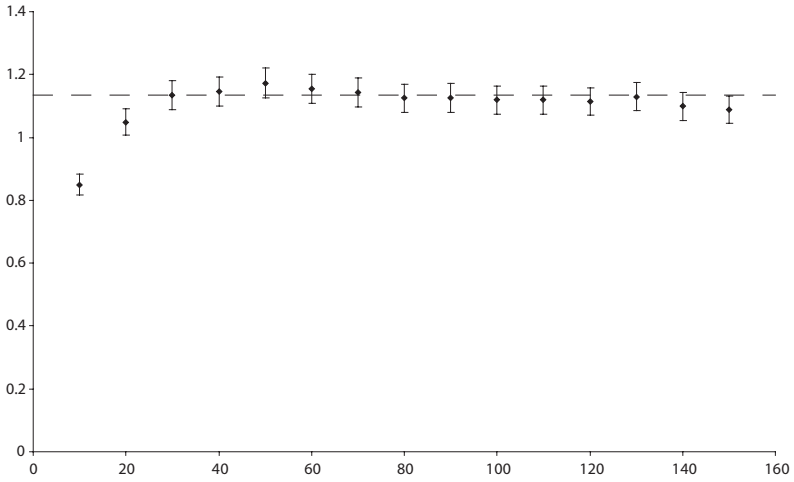

FIGURE 14. Downstream evolution of the normalized turbulence intensity, u'/U_o, vs. x/D.

in figure 13; i.e., u'/U_o vs. r/δ_*. These profiles collapse quite well for all downstream positions greater than about $x/D = 30$. This is remarkable, considering the difficulties in obtaining correct mean velocity profiles using the different anemometer systems described above. Clearly, thermal drift of the anemometers has very little direct influence on fluctuating quantities. This is especially important for Part 2 of this investigation which uses the cross-spectra in conjunction with the proper orthogonal decomposition.

The downstream evolution of the maximum of the normalized turbulence intensities is shown in figure 14. Here, it is further highlighted that the ratio u'/U_o approaches a constant value which is reached approximately at $x/D = 30$. This ratio remains constant throughout the downstream positions covered in this experiment. This is of considerable importance in establishing the existence of the high Reynolds number equilibrium simi-

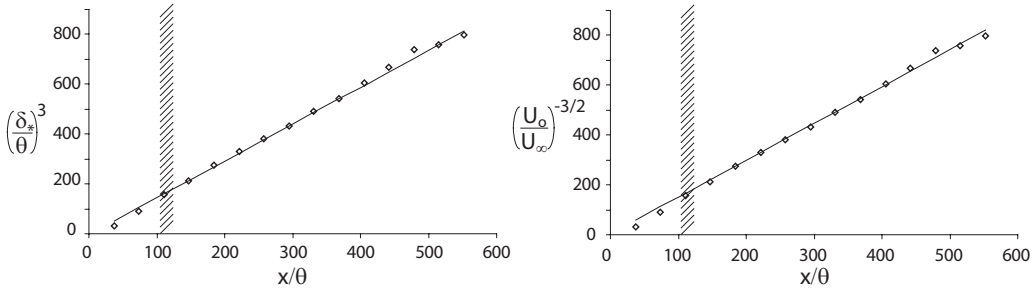

FIGURE 15. $(\delta_*/\theta)^3$ and $(U_o/U_\infty)^{-3/2}$, vs. x/θ.

larity regime as noted below. The presented points are the average of the peak values from either side of the centerline shown in figure 13. The error bars indicate an uncertainty of $\pm 2\%$, which cover both peak values.

8. High Reynolds number similarity solution

The high Reynolds number similarity theory of George (1989) and Johansson *et al.* (2002*a*) predicts that the evolution of the scaling parameters U_o and δ_* should behave as:

$$\frac{\delta_*}{\theta} = a\left[\tfrac{x-x_o}{\theta}\right]^{1/3} \tag{8.1}$$

$$\frac{U_s}{U_\infty} = b\left[\tfrac{x-x_o}{\theta}\right]^{-2/3} \tag{8.2}$$

The latter suggest this theory should apply *only* after the initial transient has decayed and *only* as long as the *local* Reynolds number is greater than 500 (i.e., $R = U_o\delta_*/\nu > 500$). They further suggest that the best measure of when the initial transients have died off is when $u'/U_o = constant$, as required by application of the equilibrium similarity theory to the kinetic energy equation. From figure 14, it clear that this condition is satisfied for $x/D > 30$ for this experiment. Moreover, from figure 12, $R > 500$ for all downstream positions. Therefore, if any data should be in agreement with the high Reynolds number solution, this data should.

It is. The solid lines on figures 9 and 11 show fits of equations (8.1) and (8.2) to the experimental data. Clearly the agreement is excellent. Linear regression yields values for the constants as: $a = 1.14$, $b = 0.77$, and $x_o = -2.4\theta$ where the virtual origin must be the same for both data sets to satisfy the momentum constraint $a^2b = 1$. Even a stronger indication of the agreement between theory and data is provided by the plots of $(\delta_*/\theta)^3$ versus x/θ and $(U_c/U_o)^{-3/2}$ in figure 15. These plots do not depend on a virtual origin, but clearly are linear for $x/D > 30$.

The collapse of the mean velocity and intensity profiles in figures 9 and 13 is further confirmation of the equilibrium similarity theory. Note, the curve fits used for the regressive fits to the velocity profiles did *not* assume similarity, but optimized the choice of parameters for each position downstream. But the equilibrium similarity theory also predicts that the individual curves described in Appendix A should collapse, and to an excellent approximation they do.

9. Power spectral densities

Power spectral densities were obtained for downstream positions of $x/D = 50$, 70, 90, 110, 130, and 150. As mentioned in section 4.3, these data were obtained from a much more extensive data set. The downstream evolution of the power spectra for each radial position in the wake covered by the fixed hot-wire rake is shown in figure 16. The power spectra for each radius shown in figure 16 are the averaged values of the probes located on the same radius of the fixed and movable rake. It is clear from these figures that the peak at the Strouhal number 0.13 is visible at all off-center spectra for all downstream positions. Thus, this structure remains in the flow for a substantial distance downstream. It is noticeable also, that the frequency is not changing at all with downstream distance, confirming the findings of Cannon *et al.* (1993) that this is truly a convected structure. A peak at this frequency does not at all appear in the spectra at the centerline (a certain confirmation of a properly centered disk).

Using the obtained scaling parameter δ_* and applying Taylor's frozen field hypothesis, with the convection velocity taken as the free stream velocity, the spectra at the centerline was normalized. This is shown in figure 17. Here, it is very clear that this collapses the spectra for high wave numbers. Taylor's hypothesis is not in general valid for low wave numbers, as pointed out by Lumley (1967), but it is remarkable how different the spectra are for low wave numbers. It is not at all clear from this single point statistical investigation what causes this behavior. This is investigated further in Part 2 of this paper using multi-point statistics and POD.

Finally, a very clear inertial subrange is visible, especially in figure 17. This is exactly as predicted by Johansson *et al.* (2002*a*), who argued that the existence of such an inertial subrange in the spectrum was a necessary condition for the applicability of the high Reynolds number solution. Because of the wire roll-off and sampling rate, it is not clear how far this inertial subrange extends. This experiment was originally designed to capture the large scale, energy containing scales, which is the reason for the spectra being cut at relatively low wave numbers. If the high wave number dissipative range were to be investigated, much shorter hot-wires must be used to increase the resolution.

10. Summary

In this paper, the high Reynolds number wake behind a disk has been investigated using rakes of hot-wire probes. The initial Reynolds number was 26,400. The measurement downstream range was $10 \leqslant x/D \leqslant 150$ ($36 \leqslant x/\theta \leqslant 552$). It was found that in spite of the limitations imposed by anemometer drift, the accuracy of mean velocity profiles can be substantially improved by using regression techniques to fit the simultaneous data from rakes of hot-wires to a predicted profile shape.

A number of open questions from earlier investigations have been resolved. It has also been shown that the turbulence intensity ratio u'/U_o truly does reach a constant value. This happens once the initial transients have settled, which can take a substantial distance downstream ($x/D > 30$ in this investigation). Moreover, it has been shown that this flow satisfied all necessary conditions for the high Reynolds number equilibrium similarity analysis of Johansson *et al.* (2002*a*) to apply, most notably that the local Reynolds number be greater than 500 throughout the entire experiment, that the spectra exhibit an inertial subrange, and that u'/U_o has reached a constant value. Indeed the data and theory are in excellent agreement.

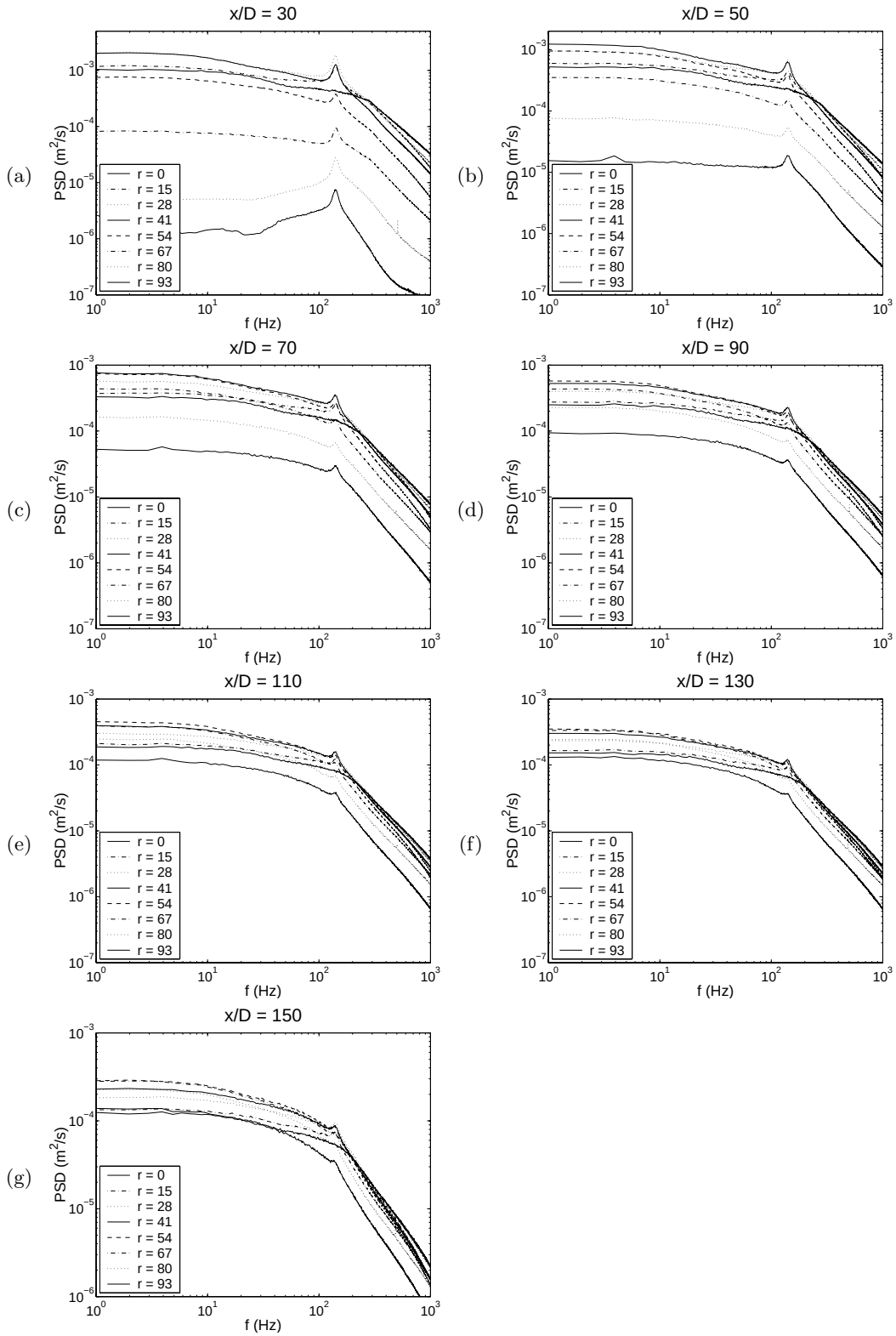

FIGURE 16. Power spectral densities at each radius of the wake at different positions: (a) $x/D = 30$, (b) 50, (c) 70, (d) 90, (e) 110, (f) 130, and (g) 150.

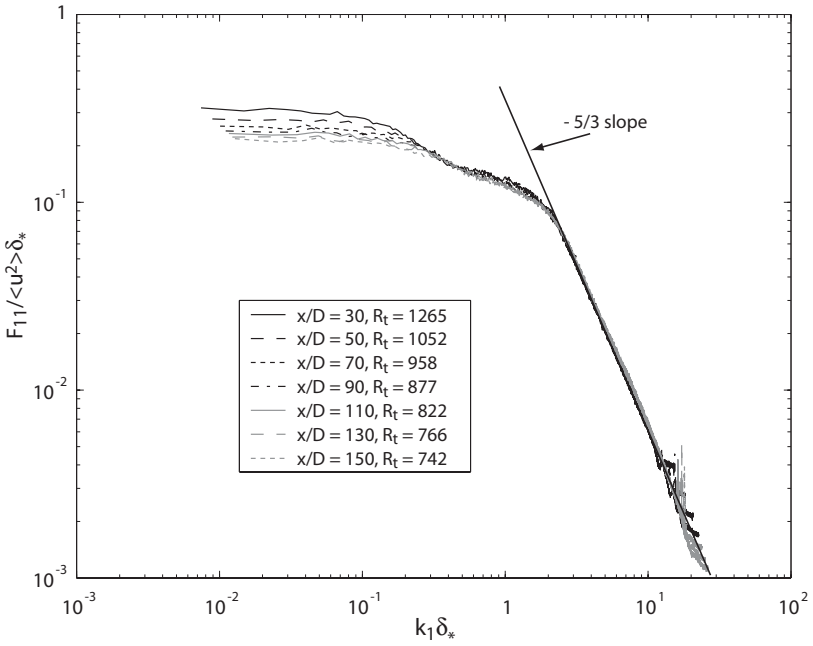

FIGURE 17. Normalized wave number spectra at the centreline.

11. Acknowledgements

The authors would like to thank Professor Henrik Alfredsson of the Swedish Royal Institute of Technology (KTH) for the use of the MTL windtunnel. The first author would also especially like to thank Mr. Davide Medici for sharing the tunnel time and for the company during the experiment. This work was initially supported by Chalmers University of Technology. It continues with the support of the Swedish Research Council, grant number 2641.

Appendix A. Correction for anemometer drift

The correction method for taking the thermal drift of the anemometers into account applied in to the data presented in this paper were performed in the following steps:

(*a*) A general curve is fitted to the velocity profile at each downstream position using a regressive scheme. The theory of laminar wakes (c.f. Schlichting (1968)) states that the laminar wake velocity profile is of the form $\exp(-r^2)$. This profile was found to undershoot the data points near the center and fall off too slowly for large r. Instead, a more general curve that could better account for the actual behavior of the data was needed. The jet velocity profile was previously fitted by Hussein *et al.* (1994), but their jet profile was found to also undershoot the data in the near-center region. Instead, the following curve form was adapted:

$$U_{fs} - U(r) = (U_{fs} - U_{CL})\left(1 + C_2 r^2 + ... + C_n r^n\right)\exp(-D_2 r^2 - D_4 r^4). \qquad \text{(A 1)}$$

Here, n is an integer multiple of 2. Only multiples of 2 were of interest in this application since the velocity profile is symmetric. The sufficient order of the polynomial was found to be $n = 4$. U_{fs} denotes the apparent free stream velocity that will deviate from the correct free stream velocity, U_∞, because of the thermal drift of the anemometers. Thus, the free parameters of the curve fit are U_{fs}, C_2, C_4, D_2, and D_4, while U_{CL} and $U(r)$ are

the values obtained from the experiment. Note that U_{fs} simply shifts the whole velocity profile up and down.

(b) The curve fit for each position (that covered the wake enough to permit an estimate of the momentum from a direct integration of data) was integrated to check whether the flow conserved momentum. This was found to be the case already from the first measured downstream position, $x/D = 10$.

(c) Since the flow was found to conserve momentum, the link between the velocity deficit scale and the lateral length scale was known. This relation, $U_o\delta_*^2 = U_\infty\theta^2$, had to be satisfied at all downstream locations. Hence, the curve fit was modified to be valid for all downstream positions simultaneously, by rewriting equation (A 1) as:

$$U_{fs}-U(r) = (U_{fs} - U_{CL})\left(1 + A(r/\delta_*)^2 + B(r/\delta_*)^4\right)\exp(-C(r/\delta_*)^2 - D(r/\delta_*)^4). \quad \text{(A 2)}$$

Here, A, B, C, D are now constants common for all the velocity profiles. A regressive scheme was used to fit also equation (A 2) to the measured profiles, with the added constraint of momentum conservation. This resulted in values of δ_* for all the downstream locations, from which the velocity scale, U_o, could be computed. The values for the general profile constants were found to be: $A = 0.049$, $B = 0.128$, $C = 0.345$, and $D = 0.134$.

REFERENCES

Cannon, S., Champagne, F. & Glezer, A. 1993 Observations of large-scale structures in wakes behind axisymmetric bodies. *Experiments in Fluids* **14**, 447–450.

Cannon, S. C. 1991 Large-scale structures and the spatial evolution of wakes behind axisymmetric bluff bodies. PhD thesis, Dept. of Aerosp. and Mech. Engr., Univ. of Arizona.

Carmody, T. 1964 Establishment of the wake behind a disk. *Journal of Basic Engineering* **86**, 869–882.

Cooper, R. D. & Lutzky, M. 1955 Exploratory investigation of the turbulent wakes behind bluff bodies. *DTMB report* **963**.

Gamard, S., Jung, D., Woodward, S. & George, W. K. 2002 Application of a 'slice' POD to the far field of an axisymmetric turbulent jet. *Accepted for publication in Physics of Fluids* **14** (6).

George, W. K. 1989 The self-preservation of turbulent flows and its relation to initial conditions and coherent structures. In *Advances in Turbulence*, pp. 39–73. Hemisphere Press.

Gibson, C. H., Chen, C. C. & Lin, S. C. 1968 Measurements of turbulent velocity and temperature fluctuations in the wake of a sphere. *AIAA Journal* **6**, 642–649.

Glauser, M. & George, W. 1987 Orthogonal decomposition of the axisymmetric jet mixing layer including azimuthal dependence. In *Advances in Turbulence* (ed. G. Comte-Bellot & J. Mathieu), pp. 357–366. Spring-Verlag.

Gourlay, M. J., Arendt, S. C., Fritts, D. C. & Werne, J. 2001 Numerical modeling of initially turbulent wakes with net momentum. *Phys. Fluids* **13**, 3783–3802.

Hussein, H. J., Capp, S. P., & George, W. K. 1994 Velocity measurements in a high-reynolds-number, momentum-conserving, axisymmetric, turbulent jet. *Journal of Fluid Mechanics* **258**, 31–75.

Hwang, N. C. H. & Baldwin, L. V. 1966 Decay of turbulence in axisymmetric wakes. *Journal of Basic Engineering* **88**, 261–268.

Johansson, A. V. 1992 A low speed wind-tunnel with extreme flow quality - design and tests. In *Prog. ICAS congress 1992*, pp. 1603–1611. ICAS-92-3.8.1.

Johansson, P. B. V. 2002 The axisymmetric turbulent wake. PhD thesis, Chalmers University of Technology, Gothenburg, Sweden.

Johansson, P. B. V., George, W. K. & Gourlay, M. J. 2002*a* Investigation of the far downstream evolution of the high reynolds number axisymmetric wake behind a disk. *Submitted to Physics of Fluids* .

Johansson, P. B. V., George, W. K. & Woodward, S. H. 2002*b* Proper orthogonal decomposition of an axisymmetric turbulent wake behind a disk. *Physics of Fluids* **14** (6).

Lumley, J. L. 1967 The inertial subrange in nonequilibrium turbulence. In *Atmospheric Turbulence and Radio Wave Propagation* (ed. A. M. Yaglom & V. I. Tatarsky), pp. 157–164. Moscow, USSR: Nauka.

Österlund, J. M. 1999 Experimental studies of zero pressure-gradient turbulent boundary layer flow. PhD thesis, Royal Institute of Technology, Sweden.

Perry, A. 1982 *Hot Wire anemometry*. Oxford: Clardedon Press.

Schlichting, H. 1968 *Boundary-Layer Theory*. McGraw-Hill, New York, NY.

Shabbir, A. & George, W. K. 1994 Experiments on a round turbulent buoyant plume. *Journal of Fluid Mechanics* **275**, 1–32.

Uberoi, M. S. & Freymuth, P. 1970 Turbulent energy balance and spectra of the axisymmetric wake. *Phys. Fluids* **13** (9), 2205–2210.

Paper 9

The far downstream evolution of the high Reynolds number axisymmetric wake behind a disk. Part 2. Slice proper orthogonal decomposition

Prepared for submission to the
Journal of Fluid Mechanics

P. B. V. Johansson
W. K. George

The far downstream evolution of the high Reynolds number axisymmetric wake behind a disk. Part 2. Slice proper orthogonal decomposition

By PETER B. V. JOHANSSON
AND WILLIAM K. GEORGE

Turbulence Research Laboratory, Department of Thermo and Fluid Dynamics, Chalmers University of Technology, Gothenburg, SE-412 96, SWEDEN

(Received May 6)

The high Reynolds number axisymmetric wake behind a disk has been studied from $x/D = 30$ to $x/D = 150$ using the proper orthogonal decomposition (POD). It was found that the energetic structure of the axisymmetric wake can very efficiently be described in terms of POD modes. The first radial (or lowest order) POD mode has 56 % of the energy. Two major features dominate the eigenspectra, which manifest themselves as two major peaks. The first peak is an azimuthal mode 1 peak at a frequency corresponding to the Strouhal number of the near wake. The second is an azimuthal mode-2 peak at near-zero frequency. The mode-1 peak dies off faster than the mode-2 peak, so that the far wake is dominated by the latter.

This evolution from azimuthal mode-1 dominance in the near wake to mode-2 dominance in the far wake corresponds closely to the approach to equilibrium similarity. Once azimuthal mode-2 becomes equally important as azimuthal mode-1 (after $x/D = 30$ or $x/\theta = 110$), the ratio of turbulence intensity to centerline velocity deficit is constant, the mean deficit and turbulence intensity collapse in similarity variables, and the wake grows as $x^{1/3}$.

1. Introduction

The structure of the three-dimensional wake was perhaps first studied by Marshall & Stanton (1931). They presented photographs of wakes behind circular disks in water. The dye trace revealed un unsteady pattern when the Reynolds number based on the free stream velocity and disk diameter, Re, exceeded about 200. They also concluded that there was a periodic discharge of a series of rings of vortices. The sphere wake was also studied by flow visualization in a water tank by Möller (1938), who found a spiral vortex in the wake in a certain range of Reynolds numbers.

Flow visualization experiments were performed on low Reynolds number wakes by Magarvey & Bishop (1961) who studied falling drops up to $Re = 2500$. They used dye visualization techniques to study the vortex structure of the wake attempting to describe the mechanisms of transition and to provide limits to when the flow undergoes transition from laminar to turbulent flow. This study was followed by Magarvey & MacLatchy (1965), who studied falling spheres for $Re < 500$, attempting to describe the manner in which vortices are released to the free stream.

The vortex structure for a sphere wake at a higher Re was studied by Pao & Kao

(1977). They investigated wakes with Re up to 2×10^4. The main findings were that without stratification, vorticity was shed three-dimensionally, and that stable stratification resulted in the wake collapsing. Based on their observations, they made a model of the vortex configuration in the wake.

The sphere wake was later studied by Taneda (1978), who used the surface oil-flow method, smoke visualization and a tuft-grid to visualize the flow for Re up to 10^6. He showed evidence of the wake performing a wave motion up to $Re = 3.8 \times 10^5$, and that it forms a pair of streamwise vortices at higher values of Re.

For a general axisymmetric parallel shear flow, Batchelor & Gill (1962) studied temporally growing instabilities and arrived at a criteria for which azimuthal modes that can possibly be unstable. They applied their criteria to a 'far' jet profile and concluded that their specific choice of velocity profile only permitted azimuthal mode 1 to be unstable.

An experimental and analytical investigation of the stability of the axisymmetric wake was made by Sato & Okada (1966), who studied a slender axisymmetric body of revolution. Analytically, Sato & Okada (1966) applied the criteria of Batchelor & Gill (1962) to their laminar wake velocity profile, and concluded that according to this criteria, azimuthal modes 1 and 2 could possibly be unstable. They were not able to numerically find a solution for mode 2, and their experimental data was found to be in agreement with mode 1 being the only unstable mode.

The stability of the axisymmetric wake was also investigated theoretically by Monkewitz (1988), who expanded previous studies by investigating a family of wake velocity profiles. He confirmed previous conclusions that azimuthal mode 1 was the most unstable, and in fact the only one that can trigger absolute instability of this flow.

Numerically, the transition was studied by Kim & Pearlstein (1990), who used a spectral technique to create a base flow that was disturbed by axisymmetric and non-axisymmetric disturbances and studied the linear stability. Their main finding was that azimuthal mode 1 was the most unstable. This was followed up by Natarajan & Acrivos (1993), who used finite-element methods to numerically study the transitional stages of spheres and disks. They did not agree with Kim & Pearlstein (1990) on the manner which the wake passes through the initial stages of transition, but they confirmed the conclusion that mode-1 was the most unstable. This was also found by Tomboulides & Orszag (2000) as well as by Ghidersa & Dušek (2000).

Johnson & Patel (1999) investigated the flow behind a sphere at low Reynolds number numerically and experimentally. They proposed a symmetry breaking mechanism to advance the basic understanding of the steady, non axisymmetric regime between $Re = 210$ and 270. At $Re = 300$, a highly organized periodic flow was found that was dominated by vortex shedding.

The large scale, 'coherent' features of this flow have not only been studied using flow visualization, but also by means of phase averaging and conditional sampling techniques, (Lee & Bearman 1992; Miau *et al.* 1997; Perry & Lim 1978; Perry & Watmuff 1981). Most interestingly in context of this paper, Roberts (1973), and later Fuchs, Mercker & Michel (1979) used two hot-wires to measure cross-spectra at a single radius of the near wake. Fuchs *et al.* (1979) varied the angular separation of the probes and were able to decompose the cross-spectra into Fourier modes. The azimuthal modal content was then studied at the frequencies that were found to be eventful. At $x/D = 9$, they found a strong azimuthal mode-1 peak at a frequency corresponding to the vortex shedding frequency, but also a peak for mode-2 at very low frequencies. The mode-1 peak was clearly dominant. Berger, Scholz & Schumm (1990) also conducted a similar investigation, and reported a dominant mode-1 peak. They did not at all mention mode-2, even though it is clearly present in their results.

Subsequently, Cannon, Champagne & Glezer (1993) investigated the axisymmetric wake, in part by means of flow visualization. They showed that the wakes from five different wake generators (sphere, disk, and three screens of different porosity) behaved very differently. They also performed an azimuthal decomposition of the velocity field at a fixed radius of the wake at $x/\theta = 105$ for the disk and one of the screens, and concluded that azimuthal mode-1 was the dominating feature. They further suggested this might be connected to the vortical structures seen in the flow visualization photographs. They also noted that these vortical structures were still present at considerable downstream distances.

The proper orthogonal decomposition (POD) is in essence a structured way of organizing the azimuthally transformed cross-spectra. Originally introduced to the field of turbulence by Lumley (1967), the POD has been applied to many flows. One recent example is the plane mixing layer by Bonnet *et al.* (1998), where different techniques of eddy structure identification methods were compared. This role of the POD was further discussed in detail by Delville *et al.* (1999). The 'slice' version of the proper orthogonal decomposition (POD) technique was first applied to the jet mixing layer by Glauser (1987); Glauser & George (1987); Citriniti & George (2000) and to the far jet by Gamard *et al.* (2002*b*).

Johansson, George & Woodward (2002) recently investigated the near wake of a disk (to $x/D = 50$) using the 'slice' POD technique. It was found that azimuthal mode-1 dominated the eigenspectra until $x/D = 10$. This was not surprising in view in view of the many earlier investigations, After this position, however, the magnitude of both modes decreased, but azimuthal mode-1 fell much more rapidly than azimuthal mode-2. They were equally important at $x/D = 30$, after which the dominance was overtaken by mode-2. The emergence of and eventual dominance of mode-2 was not expected. No theories had predicted this, nor had azimuthal mode-2 ever been observed to be of importance experimentally. Similar behavior was observed, however, almost simultaneously in the high Reynolds number axisymmetric jet by Gamard *et al.* (2002*b*) and subsequently in the low Reynolds number DNS simulation of the same flow.

The temporal linear parallel stability theory of Batchelor & Gill (1962) has recently been re-visited by Gamard, Johansson & George (2002*a*), who found that the conclusion of Batchelor & Gill (1962) that azimuthal mode 1 is the only possible unstable mode is directly related to the particular choice of the mean velocity profile. Indeed, the profile selected by Batchelor & Gill (1962) only allows mode 1 to be unstable, but the very same analysis applied on a more realistic profile for the far jet or wake reveals that azimuthal modes 0, 1, and 2 can be unstable.

Our previous experiments were carried out in the Chalmers wind tunnel. In view of the surprising nature of the results and their theoretical implications, it was deemed highly desirable to repeat the experiments in a longer facility of superior flow quality. The results reported here extend downstream a factor of three past the earlier study. Also several additional studies were made to evaluate the effects of array coverage, number of probes, and even the manner in which the disk is suspended in the flow. These are included in the Appendix.

2. Experimental Setup

The experiment was performed in the MTL wind tunnel at KTH. The experimental setup and single point flow characterization are described in Part 1 of this paper. Detailed characteristics of the tunnel can be found in Johansson (1992). Here, only the issues directly related to the POD are discussed.

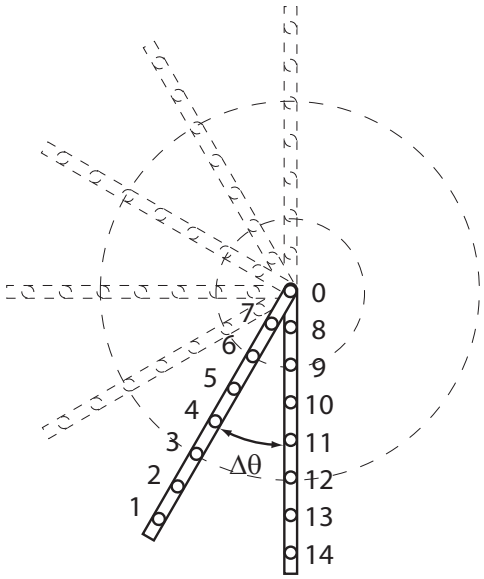

FIGURE 1. Map of traverse scheme, shown in increments of $\Delta\theta = 30^\circ$ for simplicity.

2.1. *Disk suspension*

The disk used had a diameter of 20 mm, was made of acrylic and was suspended with three pairs of wires, each with the diameter 0.2 mm. The disk was placed one meter into the measuring section to allow for probe calibration upstream of the disk. Previous experiments reported by Johansson *et al.* (2002) used four support wires instead of three, and a discussion about differences in the final result is found in Appendix B. There were none observed.

2.2. *Spatial resolution*

The arrays were used in the same manner as Glauser & George (1987) and Johansson *et al.* (2002) to obtain the two-point velocity cross-spectra for all combinations of locations shown in figure 1. The measurement grid of 7×7 was chosen following Glauser & George (1992), so as to provide the minimal resolution to apply the POD. This requires that in order to avoid spatial aliasing, the number of azimuthal measurement positions must be at least greater than the number of modes needed to describe the energy in the flow. Similar considerations apply in the azimuthal direction where the number of angular increments must be greater than twice the number of azimuthal modes required (since the eigenfunctions are in general complex); for this experiment estimated as 12.

The maximum radius of the rakes (R in equations 3.2 and 3.4) is also important, and must span enough of the flow so that the POD results are independent of it. Since the rake is fixed, but the wake grows, the relative coverage varies downstream. Appendix A contains an evaluation of the effects of varying coverage on the results reported below. The effect is very small for the range of variation in these experiments.

The upper array of probes was movable, and traversed from a 15° separation up to 180° with 15° increments in $\Delta\theta$, see figure 1. Each hot-wire probe is numbered and marked by a circle. The angle separation $\Delta\theta = 90^\circ$ could not be measured directly, since the movable probe rake caught the wake of the suspending wires. Instead, measurements at the opposite position 270° were used. In all, half the cross-section of the wake at a fixed downstream position was scanned, and pairs of instantaneous velocity cross-spectra

for a fixed angle separation computed. Note that the cross-spectra corresponding to the remaining half-plane were available from the azimuthal symmetry of the flow, verified through extensive tests reported in Part 1 of this paper.

3. Proper orthogonal decomposition

3.1. *An overview of the pod*

At the core of the theoretical and experimental application of the POD is the replacement by deterministic functions of the instantaneous random flow which have maximal projection on it. These deterministic functions (or eigenfunctions) are obtained either analytically or empirically from the resulting integral equation, the kernel of which is the two-point correlation of the velocity itself. The original field can be recovered by summing together (or integrating over) the contributions of each eigenfunction and its random coefficient, the latter determined by projecting each eigenfunction onto the instantaneous field (exactly like the determination of coefficients in ordinary Fourier analysis). Note that this projection and reconstruction requires that all points be measured simultaneously, which was not possible in this experiment. Thus only the eigenspectra and eigenvectors can be produced using rakes of probes as employed herein.

The turbulent axisymmetric wake is both stationary in time and homogeneous, periodic in the azimuthal direction. The POD integral equations can be immediately solved in these directions to yield Fourier modes, continuous in temporal frequency, f, and discrete in azimuthal mode number, m, (George, 1988). The streamwise direction is problematical, since it is neither homogenous nor of finite total energy. Hence in the absence of other considerations, the eigenfunctions will be determined by how the domain is truncated. This problem is avoided in this study by only applying the POD to cross-sections of the flow, and treating the streamwise position, x, as a parameter. This particular version of the POD is sometimes called the 'slice' POD.

In general it is easier to proceed if the field is first decomposed using the known eigenfunctions, then the POD applied to this transformed field in the remaining inhomogeneous variables. Thus the problem becomes to seek empirical eigenfunctions which optimally project a deterministic function, $\psi_i(m, f, x; r)$, onto the transformed random velocity field, $\hat{u}_i(m, f, x; r)$. The variables m, f, and x are essentially parameters. In general there are an infinite number of eigenfunctions, $\psi_i^{(n)}$, which are solutions to the integral equation:

$$\int_0^R B_{i,j}(m, f, x; r, r')\psi_j^{(n)}(m, f, x; r')\, r'\, dr' \tag{3.1}$$

$$= \lambda^{(n)}(m, f, x)\psi_i^{(n)}(m, f, x; r) \tag{3.2}$$

where $B_{i,j}$ is the cross-spectral tensor and R is the limit of the domain.

The decomposition is optimal in the sense that the lowest order eigenfunction contains the maximum possible amount of energy. Moreover the total "energy spectrum" at a cross-section is the sum of the eigenvalues; i.e.,

$$\tilde{E}(m, f, x) = \sum_{n=1}^{\infty} \lambda^{(n)}(m, f, x) \tag{3.3}$$

These can in turn be summed over all frequencies and azimuthal modes numbers to recover the total energy in a cross-section as shown below. In practice the number of eigenfunctions is limited by the finite number of resolved points of the kernel.

3.2. *This application*

If only the streamwise velocity component at a fixed downstream location is considered (i. e., $i = j = 1$), the following integral equation(s) must be solved:

$$\int_0^R B_{1,1}(m, f, r, r'; x)\psi^{(n)}(m, f, r'; x)r'\, dr' = \lambda^{(n)}(m, f; x)\psi^{(n)}(m, f, r; x) \tag{3.4}$$

where R is the limit of the domain, $B_{1,1}(m, f, r, r'; x)$ is the two-point velocity correlation Fourier transformed in time and expanded in Fourier series in the azimuthal direction, the $\psi^{(n)}(m, f, r; x)$ are the eigenfunctions, and $\lambda^{(n)}(m, f; x)$ the corresponding eigenspectra. (Note that the $\psi_1^{(n)}$ of equation 3.2 is not in general the same as $\psi^{(n)}$, since the latter is produced from a scalar decomposition.) The eigenspectra, $\lambda^{(n)}(m, f; x)$, are representations of how the energy is distributed as function of azimuthal mode number, m, and frequency, f, at a given downstream position, x. Therefore their downstream evolution shows how the main characteristics of the flow evolve.

It is important to first discuss what the variable f means, or more precisely, what it does *not* mean. Experimentally it is the frequency (or temporal variation) observed by the measuring apparatus. Unfortunately its interpretation as space or time is complicated by the fact the turbulence is being convected by the probes while it is also evolving in time. The so-called "Taylor's frozen field hypothesis" assumes that convection dominates the temporal evolution, so that temporal variations can be interpreted as spatial variations. For the wake where $u'/U < 10\%$, Taylor's hypothesis is certainly valid, at least for all but the very lowest frequencies. Thus the proper interpretation of the frequency in this experiment, for all but the very lowest frequencies, is as a wave number, $k = 2\pi f/U$, where U is the local mean velocity. Because of the interesting problem at very low frequencies of the eigenspectra presented later in this paper, and the questionable applicability of Taylor's hypothesis for them, the data have been left in terms of the primitive variable, f.

In practice, the following steps are taken to implement the POD in this experiment:

(a) Measure the instantaneous velocity at two points.

(b) Fourier transform in time and compute the cross-spectrum.

(c) Repeat step (a) and (b) for many pairs of points.

(d) Expand the cross-spectra obtained in (b) in a Fourier series in the azimuthal direction.

(e) Solve the remaining eigenvalue problem in the radial direction, equation 3.4, for each frequency and azimuthal mode number.

This is exactly the procedure used by Glauser & George (1987) in an earlier jet mixing layer study and in an earlier version of this investigation of the axiaymmetric wake by Johansson *et al.* (2002).

4. POD results

The distribution of the resolved energy in the POD modes are summarized in table 1. After $x/D \approx 50$, the first (radial) POD mode accounts for about 56 % of the total resolved energy, the second for about 19 %, the third about 10 %, and the rest the remainder. Clearly the lowest order POD mode dominates the energetics of the flow. This was expected from the Hilbert-Schmidt theory which applies to this direction, and produces order and proper results (the lowest order has the most energy, the next the next most, etc.). For most of the rest of this paper, it is this lowest order POD mode

	$\lambda^{(n)}$							Energy
x/D	$n=1$	$n=2$	$n=3$	$n=4$	$n=5$	$n=6$	$n=7$	(10^{-5} m^2.s^{-2})
30	63.1	17.6	10.4	5.6	2.3	0.68	0.3	22.649
50	59.6	17.2	10.1	6.0	3.8	2.2	1.1	16.114
70	57.4	17.5	10.2	6.2	4.3	2.9	1.6	12.694
90	55.9	18.4	10.3	6.3	4.4	3.0	1.6	11.020
110	55.9	18.8	10.5	6.1	4.3	2.8	1.6	9.4162
130	56.7	18.6	10.4	6.0	4.0	2.7	1.5	8.2688
150	56.7	19.1	10.2	6.0	4.0	2.6	1.3	7.1374

TABLE 1. Relative percentage per POD mode number, and total turbulent kinetic energy resolved.

($n = 1$) and its associated eigenspectrum, $\lambda^{(1)}(m, f)$, which will receive most of the attention.

4.1. *The eigenspectra as functions of m and f.*

Figure 2 shows three-dimensional plots of the first eigenspectrum, $\lambda^{(1)}(m, f, x)$, for the disk wake at $x/D = 30$, 50, 70, 90, 110, 130 and 150. The most striking feature is the clear separation of the frequency content of the various modes. Only mode-1 has a peak at a non-zero frequency. The other eigenspectra (of which mode-2 is predominant) all resemble the usual broadband one-dimensional spectra of turbulence which peak at zero frequency (usually due to aliasing from the unresolved directions). The eigenspectra have not been normalized, so their heights decay downstream as the wake itself decays. But even from just these seven plots it is obvious that mode-1 dies more quickly than the other modes, and especially mode-2. In fact, the reason for the behavior of the normalized azimuthal mode number plots below (figure 7) is clearly not that mode-2 is increasing its contribution, but that mode-1 is fading more rapidly.

This can be seen another was as illustrated in figure 3. The value of $\lambda^{(1)}(m, f)$ for which it has a local maximum is plotted as a function of downstream distance for each of azimuthal modes 0, 1, and 2. Clearly azimuthal mode-1 is dying off faster than the others, at least for the first 100 or so diameters downstream.

The downstream evolution of the azimuthal modes is even more clearly in figure 2. Here, slices of the surface plots in figure 2 are shown for fixed azimuthal mode numbers $m = 0$, 1, and 2 as a function of frequency. As in figure 2, the eigenspectra have not been normalized.

Figure 5 shows plots of the total energy and azimuthal mode-1 alone as a function of frequency for the same downstream positions. Most striking is that the peak frequency of the band which contains most of the energy for azimuthal mode-1 does not evolve downstream, but is fixed. Moreover its contribution to the total energy is clearly diminishing downstream, as noted above. Thus the primary contribution of azimuthal mode-1 clearly does not scale in local shear layer variables, but is instead determined only by the Strouhal number of the near wake. It seems apparent that the primary contribution to azimuthal mode-1 has been convected in from the near wake, and is virtually independent of the local shear layer of the wake.

By contrast, the behavior of azimuthal mode-2 is quite different. Figure 6 shows azimuthal mode-2 normalized by the energy remaining *after* the energy from azimuthal mode-1 is removed. These data have been plotted as wavenumber spectra using Taylor's frozen field hypothesis. Note the remarkable 'notch' in azimuthal mode-2 (all the way to zero!) for the position closest to the disk at exactly the frequency where azimuthal mode-

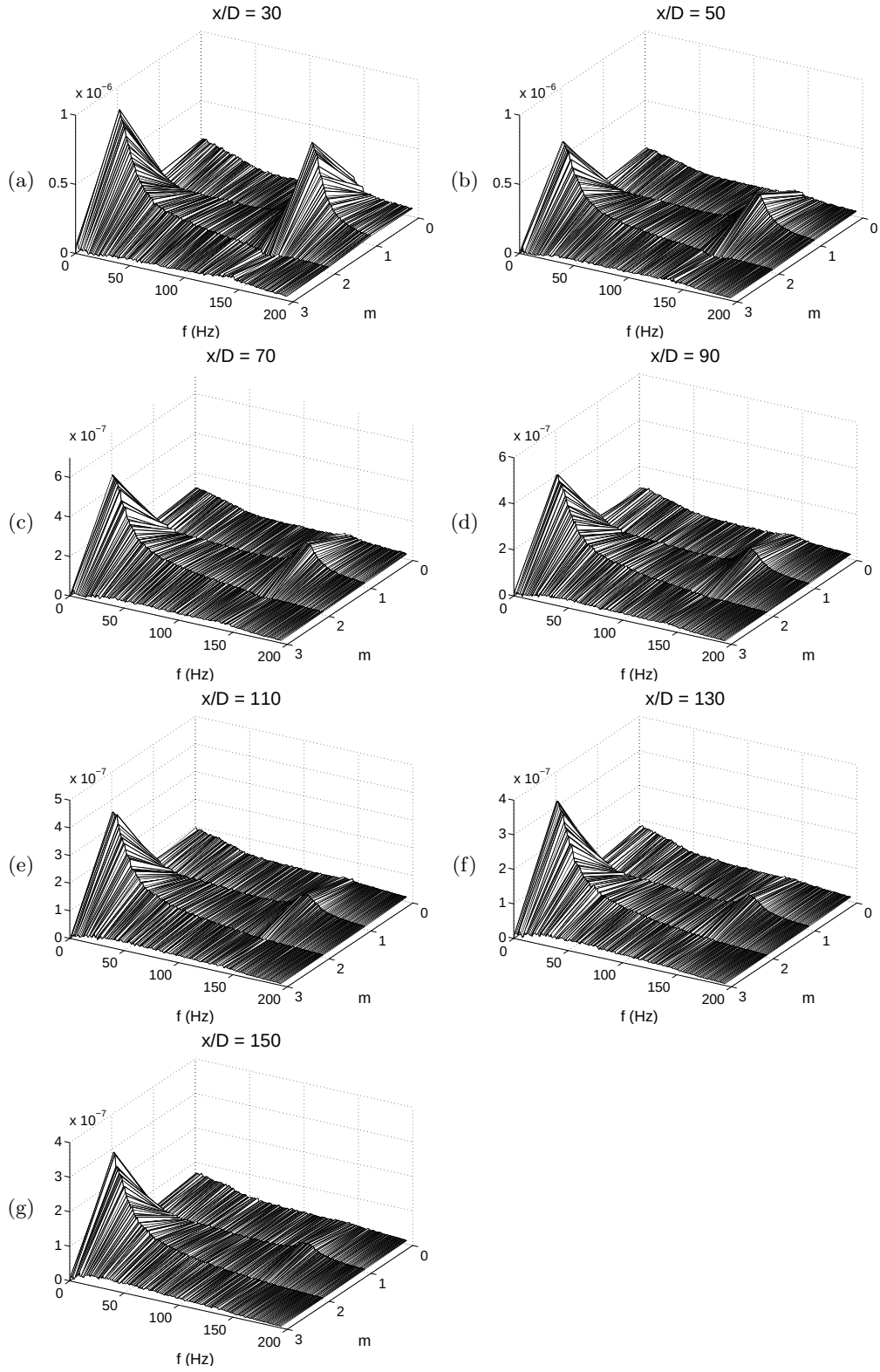

FIGURE 2. Eigenspectrum function of azimuthal mode number (m) and frequency (f) at different positions: (a) $x/D = 30$, (b) 50, (c) 70, (d) 90, (e) 110, (f) 130, and (g) 150.

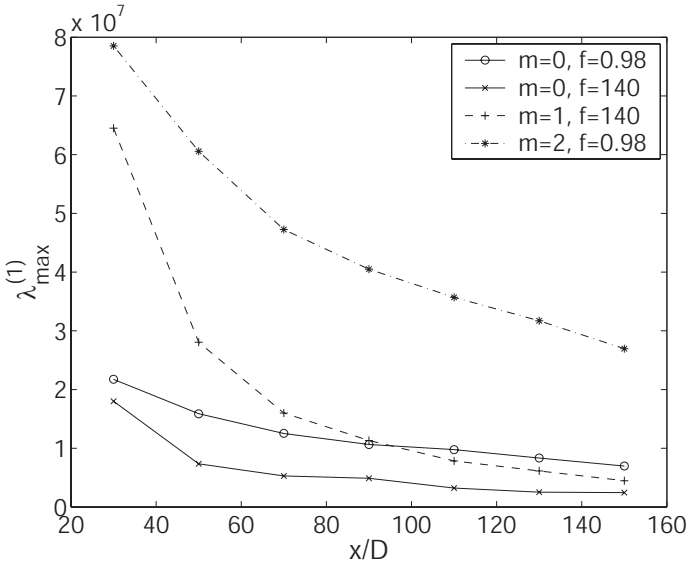

FIGURE 3. Maximum values of λ.

1 is dominant. Clearly azimuthal mode-1 is suppressing the development of azimuthal mode-2 at the dominant frequency. As the wake develops downstream, this notch fills in, and except for the very lowest wavenumbers (for which Taylor's hypothesis is of doubtful validity), these data collapse wonderfully in shear layer variables. Thus, once the contribution of azimuthal mode-1 has been removed, the rest of the turbulence behaves exactly as might be expected from an equilibrium similarity wake. This is certainly not the case if azimuthal mode-1 is not removed, which explains the frustrations of many authors in trying to explain their measurements for this flow.

4.2. *Eigenvalues integrated over frequency*

The eigenspectra can be integrated over frequency, f, to obtain the distribution of energy with only the azimuthal mode number, m. If this is normalized by the total energy at the cross-section the result is:

$$\xi^{(1)}(m) = \frac{\int_0^\infty \lambda^{(1)}(m,f)\,df}{\sum_{m=0}^{M}\int_0^\infty \lambda^{(1)}(m,f)\,df} \tag{4.1}$$

where M is the highest resolved azimuthal mode. Figure 7 shows the evolution of the eigenspectra integrated over frequency as a function of the azimuthal mode number. For the near wake, at $x/D = 10$, azimuthal mode-1 dominates, exactly as reported by others (Fuchs *et al.*, 1979, Berger *et al.*, 1990). But by $x/D = 30$, the energy in azimuthal mode-2 is nearly equal to that in azimuthal mode-1. By $x/D = 50$, azimuthal mode-2 dominates, as it does for all positions downstream. The difference between modes 0 and 1 far downstream is too small to be certain which is the largest, since the slight variation may be due to the differing areas covered by the probe arrays as the wake grows (as discussed in Appendix A).

5. Discussion

As presented above, the axisymmetric wake is dominated by two major features, azimuthal modes 1 and 2. Initially, azimuthal mode 1 clearly dominates the modal decom-

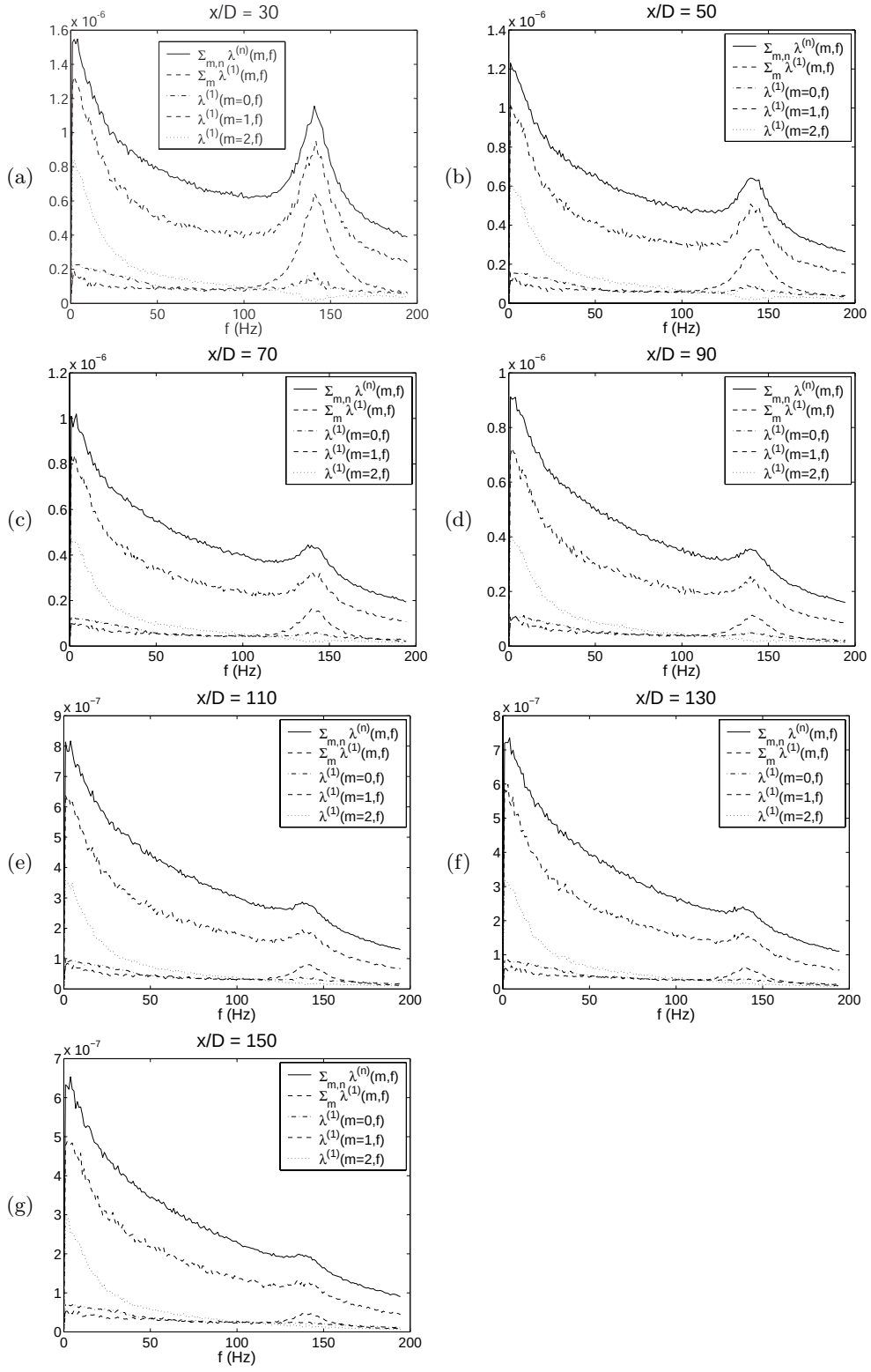

FIGURE 4. Slices of the eigenspectrum function of azimuthal mode number (m) and frequency (f) at different positions: (a) $x/D = 30$, (b) 50, (c) 70, (d) 90, (e) 110, (f) 130, and (g) 150.

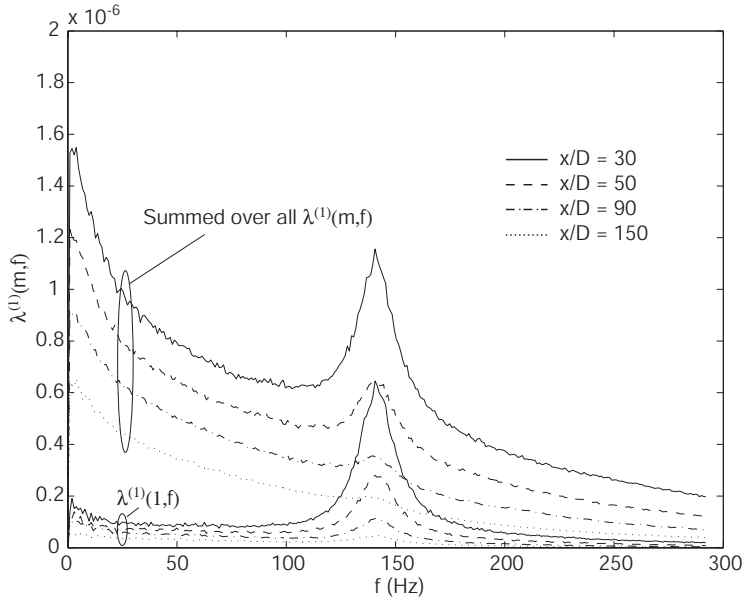

FIGURE 5. The total energy and mode-1 alone as a function of frequency at $x/D = 30$, 50, 90 and 150.

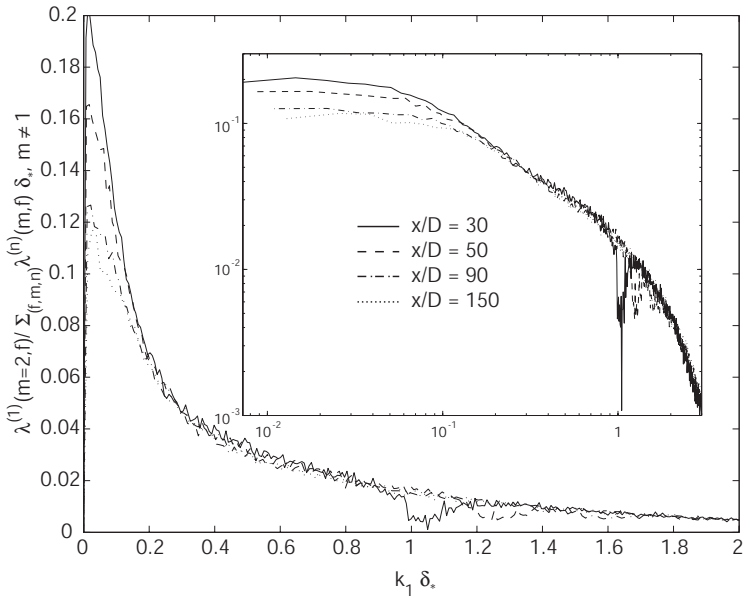

FIGURE 6. Mode-2 at x/D = 30, 50, 90 and 150, normalized by the energy remaining *after* the energy from mode-1 is removed. These data have been plotted as wavenumber spectra using Taylor's hypothesis.

position. This mode dies off rapidly and no longer dominates the flow after $x/D = 30$. Even so, it continues to be visible in the modal decomposition for all positions covered in this study. This is consistent with the power spectra presented in Part 1 of this paper, and also the findings of Cannon *et al.* (1993), who stated that this feature remains in the wake for very large downstream distances. In their azimuthal decomposition at

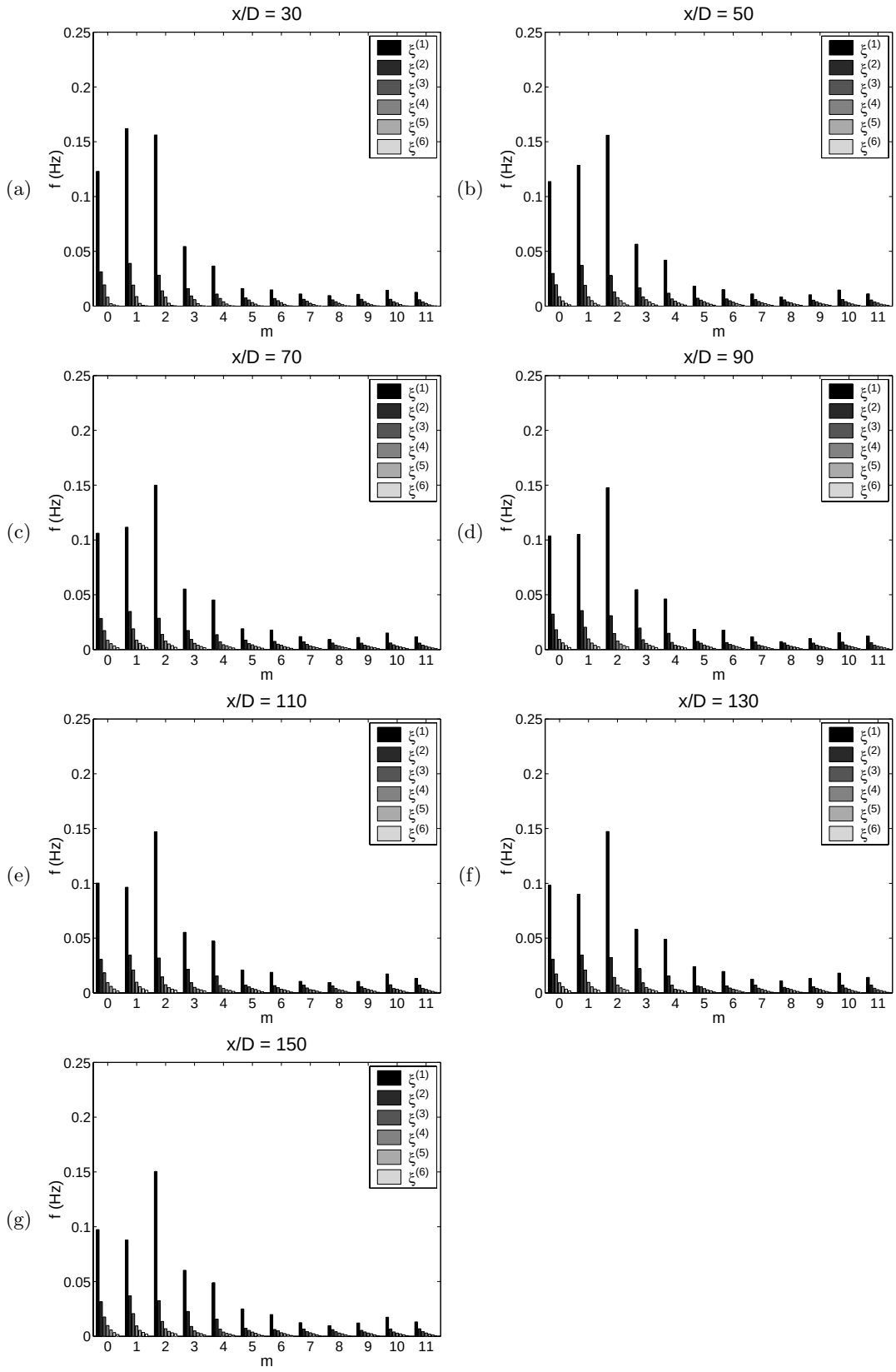

FIGURE 7. Eigenspectrum integrated over frequency (as defined in equation 4.1) as function of azimuthal mode number (m) at different positions: (a) $x/D = 30$, (b) 50, (c) 70, (d) 90, (e) 110, (f) 130, and (g) 150.

$x/\theta = 105$, they actually noticed mode 1 to be the most prominent mode. But it must be noted that this decomposition was made at a single radial position in the wake. Only the POD takes the whole cross-section of the flow under consideration.

One additional observation can also be made from figure 3. There is a very interesting problem presented by the lack of collapse of the spectra for azimuthal mode-2 at very low wavenumbers (or perhaps just low frequencies). These very large scales clearly satisfy Townsend's idea of the large eddies. They contain about 5 - 10 % of the energy and do not appear to interact with the main motion. Interestingly, if these data are NOT normalized as wavenumbers, but simply by the energy present at all mode numbers with mode-1 removed, they collapse without any scaling of the frequency axis at all. So what is their role, if any? This is not at all clear as of this writing. One possibility is that they simply slowly twist the mean flow. If so this could account for the remarkably high *local* turbulence intensity for this flow for which at the centerline $u'/(U_\infty - U_{CL}) \approx 110\%$. In effect, the mean profile is simply being moved around by this very large and slow modulation. There is some evidence for this in the flow visualizations of Taneda (1978) who observed wave-like behavior of the wake. Also, in the azimuthally averaged instantaneous DNS profiles of Gourlay (2001), some of the profiles appeared to be slightly off-center, consistent with both observations above.

It is also worth commenting on what the usual conditional sampling approaches to coherent structures would have (and have) focused on for this flow. The most coherent energetic motion is the transient azimuthal mode-1, and this is indeed what such studies have yielded. But this *is the least important part of the problem* for the far wake. Similar considerations apply to the jet as well where the most apparent coherent feature of the flow has seemingly nothing to do with the far jet's evolution, but is simply dying off.

Like the jet, the emergence of this mode-2 dominance corresponds also to the emergence of the similarity state, particularly evident in the normalized turbulence intensity which does not approach a constant until about $x/D = 30 - 50$. The implications of this for attempts to study axisymmetric wakes are profound, since most attempts seldom measured much beyond this point (e.g., Cannon, 1991, Uberoi and Freymuth, 1970) due to the extremely low turbulence intensities and limited wind tunnel lengths.

These results are also very interesting in view of the temporal linear parallel stability theory, since Gamard *et al.* (2002*a*) found that the conclusions of Batchelor & Gill (1962) that only azimuthal mode 1 can be unstable was much too restrictive. Indeed, the profile selected by Batchelor & Gill (1962) only allows mode 1 to be unstable, but the very same analysis applied on a more realistic profile for the far jet or wake reveals that azimuthal modes 0, 1, and 2 can be unstable.

6. Conclusions

The high Reynolds number axisymmetric wake behind a disk has been studied from $x/D = 30$ to $x/D = 150$ using the proper orthogonal decomposition (POD). It was found that the energetic structure of the axisymmetric wake can very efficiently be described in terms of a few POD modes with the first radial POD mode containing approximately 56 % of the energy. Two features dominated the eigenspectra, and these manifest themselves as major peaks. The first peak is an azimuthal mode 1 peak at a frequency corresponding to the Strouhal number of the wake. The second is an azimuthal mode-2 peak at near-zero frequency. The mode-1 peak dies off faster than the mode-2 peak, so that the far wake is dominated by the latter.

This evolution from azimuthal mode-1 dominance in the near wake to mode-2 dominance in the far wake corresponds closely to the approach to equilibrium similarity. Once

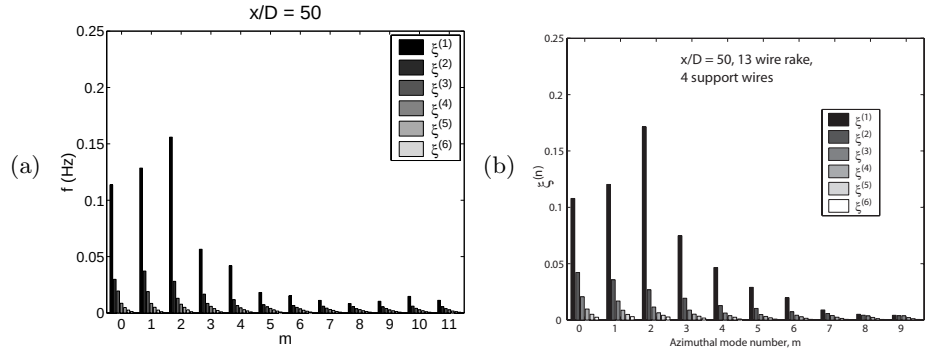

FIGURE 8. Eigenspectrum integrated over frequency as function of azimuthal mode number (m) at $x/D = 50$ for different configurations: (a) 15 hot-wires, (b) 13 hot-wires.

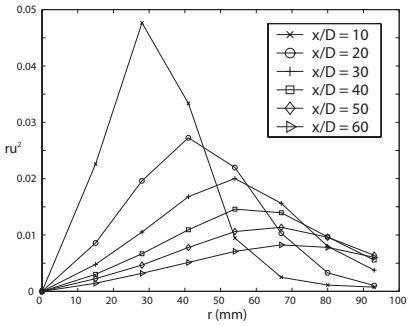

FIGURE 9.

mode-2 becomes equally important as mode-2 (after $x/D = 30$ or $x/\theta = 110$), the ratio of turbulence intensity to centerline velocity deficit is constant, the mean deficit and turbulence intensity collapse in similarity variables, and the wake grows as $x^{1/3}$.

7. Acknowledgements

The authors would like to thank Professor Henrik Alfredsson of the Swedish Royal Institute (KTH) for the use of the their MTL windtunnel. The first author would also especially like to thank Mr. Davide Medici for sharing the tunnel time and for the company during the experiment. This work was initially supported by Chalmers University of Technology. It continues with the support of the Swedish Research Council, grant number 2641.

Appendix A. Effect of array coverage

Figure 8 shows same wake at $x/D = 50$, but using the data obtained with the 13-wire rake presented in Johansson *et al.* (2002). There are only very small differences, one being that mode 0 is slightly larger for the 15-wire rake. This can be explained by the fact that this rake covers a larger portion of the wake. Certainly, this effect is very small.

Figure 9 shows plots of ru^2 versus r for all downstream positions. The total energy in the POD is the integral under these curves. Clearly as the rake is traversed downstream, progressively more and more of the total energy is not included in the decomposition (since the hot-wire rake is fixed). (This was one of the primary reasons for expanding from 13 to 15 wires.) The lost energy is less than 1% at $x/D = 10$ but perhaps as much

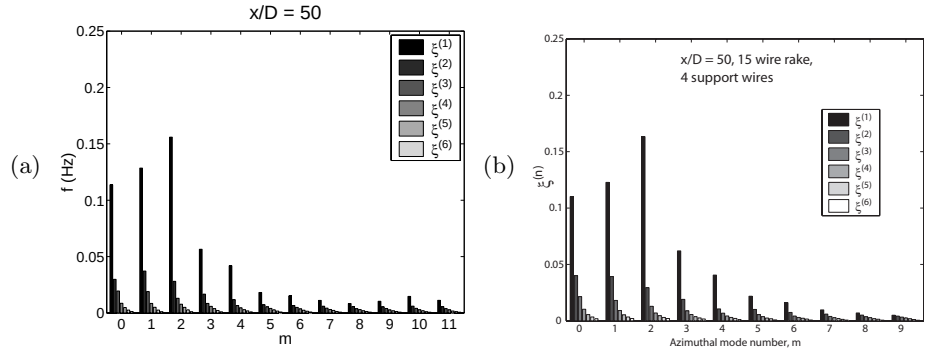

FIGURE 10. Eigenspectrum integrated over frequency as function of azimuthal mode number (m) at $x/D = 50$ for different configurations: (a) 3 pairs of support wires, (b) 4 pairs of support wires.

as 20% at $x/D = 60$. As figure 7 makes clear, the evolution from azimuthal mode-1 peak to a peak at mode-2 takes place between $x/D = 30$ and 40. Beyond $x/D = 40$ there is virtually no change in the eigenspectra, even though progressively more of the energy is lost. This suggests strongly that the outside energy does not affect the eigenspectra (at least in the lower modes). This is consistent with the lack of observed differences between the 13 and 15-wire arrays.

Appendix B. Effect of disk support wires

Figure 10 shows the same plots for the four and three wire supported rakes, also obtained using the 15 hot-wire rake at $x/D = 50$. The results are virtually indistinguishable, suggesting strongly that the whatever the physical cause of the observations, it is not a consequence of how the disk is supported in the wind tunnel.

REFERENCES

BATCHELOR, G. K. & GILL, E. A. 1962 Analysis of the instability of axisymmetic jets. *Journal of Fluid Mechanics* **14**, 529–551.

BERGER, E., SCHOLZ, D. & SCHUMM, M. 1990 Coherent vortex structures in the wake of a sphere and a circular disk at rest and under forced vibrations. *Journal of Fluids and Structures* **4**, 231–257.

BONNET, J. P., DELVILLE, J., GLAUSER, M. N., ANTONIA, R. A., BISSET, D. K., COLE, D. R., FIEDLER, H. E., GAREM, J. H., HILBERG, D., JEONG, J., KEVLAHAN, N. K. R., UKEILEY, L. S. & VINCENDEAU, E. 1998 Collaborative testing of eddy structure identification methods in free turbulent shear flows. *Experiments in Fluids* **25**, 197–225.

CANNON, S., CHAMPAGNE, F. & GLEZER, A. 1993 Observations of large-scale structures in wakes behind axisymmetric bodies. *Experiments in Fluids* **14**, 447–450.

CANNON, S. C. 1991 Large-scale structures and the spatial evolution of wakes behind axisymmetric bluff bodies. PhD thesis, Dept. of Aerosp. and Mech. Engr., Univ. of Arizona.

CITRINITI, J. H. & GEORGE, W. K. 2000 Reconstruction of the global velocity field in the axisymmetric mixing layer utilizing the proper orthogonal decomposition. *Journal of Fluid Mechanics* **418**, 137–166.

DELVILLE, J., UKEILEY, L., CORDIER, L., BONNET, J. P. & GLAUSER, M. 1999 Examination of large-scale structures in a turbulent plane mixing layer. part 1. proper orthogonal decomposition. *Journal of Fluid Mechanics* **391**, 91–122.

FUCHS, H. V., MERCKER, E. & MICHEL, U. 1979 Large scale coherent structures in the wake of axisymmetric bodies. *Journal of Fluid Mechanics* **93**, 189–211.

GAMARD, S., JOHANSSON, B. P. V. & GEORGE, W. K. 2002*a* Another look at the batchelor

and gill temporal stability analysis of parallel axisymmetric flows. *Submitted to Journal of Fluid Mechanics* .

Gamard, S., Jung, D., Woodward, S. & George, W. K. 2002*b* Application of a 'slice' POD to the far field of an axisymmetric turbulent jet. *Accepted for publication in Physics of Fluids* **14** (6).

George, W. K. 1988 Insight into the dynamics of coherent structures from a proper orthogonal decomposition. In *Symposium on Near Wall Turbulence*. Dubrovnik, Yugoslavia.

Ghidersa, B. & Dušek, J. 2000 Breaking of axisymmetry and onset of unsteadiness in the wake of a sphere. *Journal of Fluid Mechanics* **423**, 33–69.

Glauser, M. & George, W. 1987 Orthogonal decomposition of the axisymmetric jet mixing layer including azimuthal dependence. In *Advances in Turbulence* (ed. G. Comte-Bellot & J. Mathieu), pp. 357–366. Spring-Verlag.

Glauser, M. N. 1987 Coherent structures in the axisymmetric turbulent jet mixing layer. PhD thesis, State University of New York at Buffalo.

Glauser, M. N. & George, W. K. 1992 Application of multipoint measurements for flow characterization. *Experimental Thermal and Fluid Science* **5**, 617–632.

Gourlay, M. J., Arendt, S. C., Fritts, D. C. & Werne, J. 2001 Numerical modeling of initially turbulent wakes with net momentum. *Phys. Fluids* **13**, 3783–3802.

Johansson, A. V. 1992 A low speed wind-tunnel with extreme flow quality - design and tests. In *Prog. ICAS congress 1992*, pp. 1603–1611. ICAS-92-3.8.1.

Johansson, P. B. V. & George, W. K. 2002 Far downstream development of POD modes in a turbulent disk wake. In *Ninth European Turbulence Conference*. Southampton, July 2-5.

Johansson, P. B. V., George, W. K. & Woodward, S. H. 2002 Proper orthogonal decomposition of an axisymmetric turbulent wake behind a disk. *Physics of Fluids* **14** (6).

Johnson, T. A. & Patel, V. C. 1999 Flow past a sphere up to a reynolds number of 300. *Journal of Fluid Mechanics* **378**, 19–70.

Kim, I. & Pearlstein, A. J. 1990 Stability of the flow past a sphere. *Journal of Fluid Mechanics* **211**, 73–93.

Lee, S. I. & Bearman, P. W. 1992 An experimental investigation of the wake structure behind a disk. *Journal of Fluids and Structures* **6**, 437–450.

Lumley, J. L. 1967 The inertial subrange in nonequilibrium turbulence. In *Atmospheric Turbulence and Radio Wave Propagation* (ed. A. M. Yaglom & V. I. Tatarsky), pp. 157–164. Moscow, USSR: Nauka.

Magarvey, R. H. & Bishop, R. L. 1961 Transition ranges for three-dimensional wakes. *Canadian Journal of Physics* **39**, 1418–1422.

Magarvey, R. H. & MacLatchy, C. S. 1965 Vortices in sphere wakes. *Canadian Journal of Physics* **43**, 1649–1656.

Marshall, D. & Stanton, T. E. 1931 On the eddy system in the wake of flat circular plates in three dimensional flow. *Proc. Roy. Soc. London A* **130**, 295–301.

Miau, J. J., Leu, T. S., Liu, T. W. & Chou, J. H. 1997 On vortex shedding behind a circular disk. *Experiments in Fluids* **23**, 225–233.

Möller, W. 1938 Experimentelle untersuchengen zur hydrodynamik der kugel. *Phys. Z.* **39**, 57–80.

Monkewitz, P. A. 1988 A note on vortex shedding from axisymmetric bluff bodies. *Journal of Fluid Mechanics* **192**, 561–575.

Natarajan, R. & Acrivos, A. 1993 The instability of the steady flow past spheres and disks. *Journal of Fluid Mechanics* **254**, 323–344.

Pao, H.-P. & Kao, T. W. 1977 Vortex structure in the wake of a sphere. *The Physics of Fluids* **20** (2), 187–191.

Perry, A. E. & Lim, T. T. 1978 Coherent structures in coflowing jets and wakes. *Journal of Fluid Mechanics* **88**, 451–463.

Perry, A. E. & Watmuff, J. H. 1981 The phase-averaged large-scale structures in three-dimensional turbulent wakes. *Journal of Fluid Mechanics* **103**, 33–51.

Roberts, J. B. 1973 Coherence measurements in an axisymmetric wake. *AIAA Journal* **11, no. 1**, 1569–1571.

Sato, H. & Okada, O. 1966 The stability and transition of an axisymmetric wake. *Journal of Fluid Mechanics* **26**, 237–253.

Taneda, S. 1978 Visual observations of the flow past a sphere at reynolds numbers between 10^4 and 10^6. *Journal of Fluid Mechanics* **85** (1).

Tomboulides, A. G. & Orszag, S. A. 2000 Numerical investigation of transitional and weak turbulent flow past a sphere. *Journal of Fluid Mechanics* **416**, 45–73.

Uberoi, M. S. & Freymuth, P. 1970 Turbulent energy balance and spectra of the axisymmetric wake. *Phys. Fluids* **13** (9), 2205–2210.